

LIC-02-0147

Attachment Enclosures

LIC-91-0003L

LIC-01-0095

LIC-02-0007

Calculation Number FC006608

January 14, 1991
LIC-91-0003L

Omaha Public Power District
444 South 16th Street Mall
Omaha, Nebraska 68102-2247
402/636-2000

U. S. Nuclear Regulatory Commission
Attn: Document Control Desk
Mail Station P1-137
Washington, DC 20555

Reference: Docket No. 50-285

Gentlemen:

Subject: Licensee Event Report 90-28 for the Fort Calhoun
Station

Please find attached Licensee Event Report 90-28 dated January 14, 1991. This report is being submitted voluntarily due to potential NRC and industry interest.

Further inspections resulting from this event and other activities planned for the next refueling outage will be discussed at a meeting with NRC personnel to be scheduled later in 1991.

If you should have any questions, please contact me.

Sincerely,



W. G. Gates
Division Manager
Nuclear Operations

WGG/djm

Attachment

c: R. D. Martin, NRC Regional Administrator
W. C. Walker, NRC Project Manager
R. P. Mullikin, NRC Senior Resident Inspector
INPO Records Center

LICENSEE EVENT REPORT (LER)

ESTIMATED BURDEN PER RESPONSE TO COMPLY WITH THIS INFORMATION COLLECTION REQUEST: 500 HRS. FORWARD COMMENTS REGARDING BURDEN ESTIMATE TO THE RECORDS AND REPORTS MANAGEMENT BRANCH (P-530) U.S. NUCLEAR REGULATORY COMMISSION WASHINGTON DC 20555 AND TO THE PAPERWORK REDUCTION PROJECT (3150-0104) OFFICE OF MANAGEMENT AND BUDGET WASHINGTON DC 20503

FACILITY NAME (1) Fort Calhoun Station Unit No. 1 DOCKET NUMBER (2) 0 | 5 | 0 | 0 | 0 | 2 | 8 | 15 | 1 | of | 1 | 0 | PAGE (3)

TITLE (4) Leakage Through Control Element Drive Mechanism Housing

EVENT DATE (5)				LER NUMBER (6)		REPORT DATE (7)			OTHER FACILITIES INVOLVED (8)															
MONTH	DAY	YEAR	YEAR	SEQUENTIAL NUMBER	REVISION NUMBER	MONTH	DAY	YEAR	FACILITY NAMES	DOCKET NUMBER(S)														
1	2	1	4	9	0	9	0	0	2	8	0	1	1	4	9	1		0	5	0	0	0	1	1

THIS REPORT IS SUBMITTED PURSUANT TO THE REQUIREMENTS OF 10 CFR § (Check one or more of the following) (11)

OPERATING MODE (9) 2	20.402(b)	20.406(a)	50.73(a)(2)(iv)	73.71(b)
POWER LEVEL (10) 01012	20.406(a)(1)(i)	50.38(a)(1)	50.73(a)(2)(v)	73.71(c)
	20.406(a)(1)(ii)	50.38(a)(2)	50.73(a)(2)(vi)	<input checked="" type="checkbox"/> OTHER (Specify in Abstract below and in Test NRC Form 368A)
	20.406(a)(1)(iii)	50.73(a)(2)(i)	50.73(a)(2)(vii)(A)	Voluntary Report
	20.406(a)(1)(iv)	50.73(a)(2)(ii)	50.73(a)(2)(vii)(B)	
	20.406(a)(1)(v)	50.73(a)(2)(iii)	50.73(a)(2)(ix)	

LICENSEE CONTACT FOR THIS LER (12)

NAME: J. M. Cate, Special Services Engineer TELEPHONE NUMBER: 4 | 0 | 2 | 5 | 3 | 3 | - | 1 | 6 | 8 | 3 | 4

COMPLETE ONE LINE FOR EACH COMPONENT FAILURE DESCRIBED IN THIS REPORT (13)

CAUSE	SYSTEM	COMPONENT	MANUFACTURER	REPORTABLE TO NPROS	CAUSE	SYSTEM	COMPONENT	MANUFACTURER	REPORTABLE TO NPROS
X	A	B	P	S	X				
			G	4	9	0			Y

SUPPLEMENTAL REPORT EXPECTED (14)

YES (if you complete EXPECTED SUBMISSION DATE) NO

EXPECTED SUBMISSION DATE (15)

MONTH	DAY	YEAR

ABSTRACT (Limit to 1400 spaces or approximately fifteen single-space typewritten lines) (16)

On December 14, 1990, an investigation of unknown Reactor Coolant System (RCS) leakage identified the source as installed spare Control Element Drive Mechanism (CEDM) housing number 9. Subsequent removal and inspection identified two axial cracks in an inside diameter weld overlay region approximately two feet from the bottom flange of the housing. Similar installed spare CEDM housing number 13 was also removed and inspected, revealing two similar cracks in the weld overlay region.

The cause of this event was lack of venting, which created conditions conducive to transgranular stress corrosion cracking (TGSCC) in the spare housings. This report is submitted voluntarily due to potential NRC and industry interest.

Blank flanges were installed in place of CEDM housings 9 and 13. A procedure change has been implemented to assure complete venting of two other similar housings. Other appropriate CEDM housings have been examined with no cracks found. An enhanced RCS leakage monitoring program has been implemented.

LICENSEE EVENT REPORT (LER)
TEXT CONTINUATION

ESTIMATED BURDEN PER RESPONSE TO COMPLY WITH THIS INFORMATION COLLECTION REQUEST 500 HRS FORWARD COMMENTS REGARDING BURDEN ESTIMATE TO THE RECORDS AND REPORTS MANAGEMENT BRANCH (P 530) U.S. NUCLEAR REGULATORY COMMISSION WASHINGTON DC 20555 AND TO THE PAPERWORK REDUCTION PROJECT (3150-0104) OFFICE OF MANAGEMENT AND BUDGET WASHINGTON DC 20503

FACILITY NAME (1)	DOCKET NUMBER (2)	LER NUMBER (8)			PAGE (3)	
		YEAR (7)	SEQUENTIAL NUMBER	REVISION NUMBER		
Fort Calhoun Station Unit No. 1	0510101285910	-0	28	-0	0	02 OF 10

TEXT (If more space is required, use additional NRC Form 306A(1) (1/7))

At Fort Calhoun Station Unit No. 1, the Control Element Drive Mechanism (CEDM) housings are primary pressure boundary components. They were designed and fabricated to the requirements of the 1965 Edition, including the Winter 1967 Addenda, of the ASME Boiler and Pressure Vessel Code, Section III, for Class A vessels. Each CEDM housing is mounted on a nozzle flanged pipe that is welded to the reactor vessel closure head.

The reactor vessel head nozzle flange is made of SA-182 Grade 316 stainless steel. The CEDM housings are fabricated from SA-182 and SA-312 Grade 347 or Grade 348 stainless steel. Each CEDM housing is omega-seal welded to the nozzle flange and then bolted to the nozzle flange with eight (8) threaded studs. Each stud is torqued in place with a hex nut over a pair of spherical washers.

As originally constructed, there were a total of forty-one (41) CEDM housings attached to the reactor vessel head. These forty-one (41) housings were identical in design to each other but utilized in different ways. Thirty-seven (37) of these locations have always been considered "active" CEDM housings since they house Control Element Drive Mechanisms which attach to Control Element Assemblies (CEAs). The remaining four (4) CEDM housings were installed spares originally designed for future use. Two (2) of these spares, at location numbers 7 and 11 on the reactor vessel head, are now being used to house the Heated Junction Thermocouple (HJTC) probes. The other two (2) spare CEDM housings, at location numbers 9 and 13, contained only internal natural circulation spoiler assemblies and were essentially "passive" since initial plant startup. These two spare housings served no safety function other than maintaining the integrity of the primary pressure boundary.

On October 21, 1990, Reactor Coolant System (RCS) unknown leakage was identified and quantified at 0.1 to 0.2 gpm during operation at 100 percent power. Between October 21, 1990 and December 14, 1990, this leakage increased to and stabilized at approximately 0.4 gpm. During this period, extensive walkdowns of various plant systems including Reactor Coolant, Chemical and Volume Control, Safety Injection, Containment Spray, Sampling, and Waste Disposal Systems were performed. The source of the leakage, however, was not identified. The leak rate was verified by hand calculations using tank curves and verifying that the amount of water added to the RCS equaled the leak rate. Several possible leakage collection points were eliminated and it was determined that the leak was most likely an uncollected reactor coolant leak in containment.

LICENSEE EVENT REPORT (LER)
TEXT CONTINUATION

ESTIMATED BURDEN PER RESPONSE TO COMPLY WITH THIS INFORMATION COLLECTION REQUEST 500 HRS. FORWARD COMMENTS REGARDING BURDEN ESTIMATE TO THE RECORDS AND REPORTS MANAGEMENT BRANCH, IP 5301 U.S. NUCLEAR REGULATORY COMMISSION, WASHINGTON, DC 20555 AND TO THE PAPERWORK REDUCTION PROJECT (3150-0104) OFFICE OF MANAGEMENT AND BUDGET, WASHINGTON, DC 20503

FACILITY NAME (1)	DOCKET NUMBER (2)	LER NUMBER (6)			PAGE (3)
		YEAR (4)	SEQUENTIAL NUMBER	REVISION NUMBER	
Fort Calhoun Station Unit No. 1	0 15 0 0 0 2 8 5	9 0	— 0 2 8	— 0 0	0 3 OF 10

TEXT (If more space is required, use additional NRC Form 306A's) (17)

On December 14, 1990, the reactor was placed in hot standby mode to look for the RCS leak on or around the Reactor Vessel head. An investigation team looking for the source of the unknown RCS leakage had narrowed the possibility for the leakage path to the Reactor Vessel head area. The receipt of alarms from fire detection instruments in the reactor vessel head area due to borated spray was further confirmation of the leakage location. The inspection of the head revealed a leak coming from the spare CEDM number 9 housing. The reactor was then placed in cold shutdown mode to allow further investigation and corrective actions.

On December 19, 1990, spare CEDM housing number 9 was removed, and a visual inspection was performed by ABB-Combustion Engineering (ABB-CE) personnel. Axially oriented cracks were identified on the inside diameter of the pressure housing, one of which had penetrated through-wall. The cracking was localized in a weld overlay area of the housing which exists on all the CEDM housings to provide positive positioning of applicable housing internals. On December 20, 1990, a 2.5 foot section of the housing containing the cracks was cut out and sent to ABB-CE facilities for metallurgical analysis.

On December 20, 1990, ABB-CE personnel performed an external visual inspection of CEDM housing numbers 1 and 4 for possible steam impingement damage, as these housings were located in the area where steam was leaking from CEDM housing number 9. No damage was found. The inspection team also completed an external visual inspection of CEDM numbers 7, 11, 14, 15, 17, 32, 34, and 38 to determine if any cracking was apparent on these housings. No defects were found on any of the housings that were inspected. Further investigation revealed that no damage was present on any other systems, the head, seismic skirt, CEDM housing externals, or fasteners.

As a result of the cracking found on CEDM housing number 9, the decision was made to remove CEDM housing number 13 from the reactor vessel head for a detailed examination, since it had been subject to the same conditions as housing number 9. On December 21, 1990, CEDM housing number 13 was removed and ABB-CE personnel performed an on-site visual inspection of the housing. The visual inspection of the number 13 housing also revealed axially oriented cracks in the area of the weld overlay, similar to those found on number 9. A 2.5 foot section of the number 13 housing containing the cracks was then cut out and sent to ABB-CE facilities for analysis.

LICENSEE EVENT REPORT (LER)
TEXT CONTINUATION

ESTIMATED BURDEN PER RESPONSE TO COMPLY WITH THIS INFORMATION COLLECTION REQUEST 500 HRS FORWARD COMMENTS REGARDING BURDEN ESTIMATE TO THE RECORDS AND REPORTS MANAGEMENT BRANCH (P 530) U.S. NUCLEAR REGULATORY COMMISSION WASHINGTON DC 20555 AND TO THE PAPERWORK REDUCTION PROJECT (3150-0104) OFFICE OF MANAGEMENT AND BUDGET WASHINGTON DC 20503

FACILITY NAME (1) Fort Calhoun Station Unit No. 1	DOCKET NUMBER (2) 0 5 0 0 0 2 8 5 9 0 - 0 2 8 - 0 0	LER NUMBER (6)			PAGE (3)	
		YEAR	SEQUENTIAL NUMBER	REVISION NUMBER		
					0 4	OF 1 10

EXT (If more space is required, use additional NRC Form 306A's) (17)

CEDM blind flange assemblies were designed and fabricated by ABB-CE to replace the numbers 9 and 13 housings that had been removed. The blind flange assemblies were installed by ABB-CE personnel on December 27, 1990. The modification involved a change to the sealing mechanism from the original omega-seal welded design to a metal O-ring design. The CEDM flanges on the Reactor Vessel head have existing O-ring grooves which were originally used for the installation of blind flanges and O-rings used in initial hydrostatic testing of the head by Combustion Engineering. ABB-CE and Omaha Public Power District (OPPD) determined the acceptability of this modification for the remainder of Cycle 13 since there is no difference in the probability of occurrence or the consequences of primary coolant leakage from an omega-seal compared to an O-ring. Furthermore, in both sealing arrangements, the integrity of the joint is maintained by eight studs, spherical washer pairs, and nuts.

Upon receipt at the ABB-CE facilities in Windsor, CT, the sections of CEDM housings 9 and 13 were re-examined to verify the locations of the through-wall crack and the indications on the inside diameter of the housings. Two crack-like indications were identified in each of the housings. The housings were then sectioned to perform a more detailed visual inspection of the inside diameter surfaces. Visual exams were performed both with the naked eye and with low power magnification using a stereo microscope.

When short sections of the housings containing the indications were removed and cut longitudinally, the outside diameters decreased by 0.020 inches on number 9 and 0.023 inches on number 13. The nominal outside diameter is 8.627 inches and the nominal inside diameter is 7.189 inches. This decrease in diameter is attributable to residual stresses in the housing resulting from the weld overlay. The corresponding stress associated with the decrease in diameter was calculated to be on the order of 10 ksi. The tensile hoop stress introduced by an operational pressure of 2100 psi would be an additional 10.4 ksi which results in a total tensile stress in the weld overlay area of greater than 20 ksi. Under stagnant oxygenated conditions, this tensile stress level would be sufficient to result in transgranular stress corrosion cracking in the SA 312 Type 348 stainless steel pressure housing material. When a similar longitudinal cut was made on a section of the housing that did not contain the weld overlay, the measured diametrical change was only 0.0015 inches. This diametrical change indicates that the residual stresses in the housing material alone are quite low.

LICENSEE EVENT REPORT (LER)
TEXT CONTINUATION

ESTIMATED BURDEN PER RESPONSE TO COMPLY WITH THIS INFORMATION COLLECTION REQUEST 500 HRS. FORWARD COMMENTS REGARDING BURDEN ESTIMATE TO THE RECORDS AND REPORTS MANAGEMENT BRANCH (F-9301) U.S. NUCLEAR REGULATORY COMMISSION WASHINGTON DC 20555 AND TO THE PAPERWORK REDUCTION PROJECT (3150-0104) OFFICE OF MANAGEMENT AND BUDGET WASHINGTON DC 20503

FACILITY NAME (1)	DOCKET NUMBER (2)	LER NUMBER (8)			PAGE (3)	
		YEAR	SEQUENTIAL NUMBER	REVISION NUMBER		
Fort Calhoun Station Unit No. 1	0 5 0 0 0 0 2 1 8 5 9 0	- 0	2 1 8	-	0 0	0 5 OF 1 0

TEXT If more space is required, use additional NRC Form 366A's (11)

The portions of the housings containing the reducer section and the two full penetration butt welds were also sectioned longitudinally to establish whether there were any additional indications in other areas of the housings. The reducer sections were examined visually and a dye penetrant examination was performed on the reducer section from CEDM housing number 9. There were no indications revealed by these examinations in any location other than those previously found in the weld overlay.

Based on these examinations, only two (2) axially oriented cracks were confirmed in each housing. Number 9 had one (1) through-wall crack and one (1) crack which was approximately 85 percent through-wall. The through-wall crack had a length of approximately 2-7/8 inches on the inside diameter and 3/4 inch on the outside diameter. The two (2) cracks in the number 13 housing were determined to be approximately 95 percent and 70 percent through-wall. All four (4) cracks had aspect ratios (length on the inside diameter surface to depth of penetration) in the range of 3.7 to 3.9.

Fractographic examination of the cracks revealed all were initiated from the inside diameter of the housings. The initiation sites were all near the upper edge of the weld overlay region. The cracks then propagated outward into the wall of the pressure housing, extending nearly symmetrically downward through the weld overlay region and upward into the base metal of the pressure housing. The cracks were found to be nominally axial, but some of the cracks and portions of cracks were skewed off axial by approximately 15 degrees. The fracture surfaces of two (2) of the cracks had a clearly defined "ring" pattern that indicates that crack initiation occurred between 1981 and 1984. These dates were obtained by counting the number of rings observed on photographs of the fracture surfaces and then correlating each ring with one cycle of cold shutdown (with RCS drained down) and heat-up.

Scanning Electron Microscopy (SEM) of the crack surfaces and metallographic analysis of cross sections of the cracks were performed to identify the mode of cracking. The evaluations found all the cracking to be transgranular stress corrosion cracking (TGSCC). No impurity elements were found on the fracture surfaces. The types of austenitic stainless steels from which the CEDM housings are fabricated are known to be susceptible to TGSCC when exposed to adverse environmental conditions in the presence of tensile stress in the material. As discussed previously, it was found that the weld overlay in the CEDM housing introduced a significant residual tensile stress in the material.

LICENSEE EVENT REPORT (LER)
TEXT CONTINUATION

ESTIMATED BURDEN PER RESPONSE TO COMPLY WITH THIS INFORMATION COLLECTION REQUEST 500 HRS FORWARD COMMENTS REGARDING BURDEN ESTIMATE TO THE RECORDS AND REPORTS MANAGEMENT BRANCH (P 530) U.S. NUCLEAR REGULATORY COMMISSION WASHINGTON DC 20555 AND TO THE PAPERWORK REDUCTION PROJECT '3150-0104' OFFICE OF MANAGEMENT AND BUDGET WASHINGTON DC 20503

FACILITY NAME (1)	DOCKET NUMBER (2)	LER NUMBER (6)			PAGE (3)	
		YEAR	SEQUENTIAL NUMBER	REVISION NUMBER		
Fort Calhoun Station Unit No. 1	0 5 0 0 0 2 8 5	9 0	- 0 2 8	- 0 0	0 6	OF 1 0

TEXT (If more space is required, use additional NRC Form 305A's) (17)

To create the corrosive environment necessary for TGSCC to occur in the CEDM housings, high oxygen levels and some halogens (e.g., chlorides) must be present. Very low concentrations of chlorides can produce TGSCC when the oxygen content is high enough. However, the water chemistry at Fort Calhoun Station has been consistently controlled within Technical Specification limits. It was determined that with the chloride level within Technical Specification limits of less than 0.15 ppm, the oxygen level required to cause TGSCC is about 4 to 8 ppm. It was also determined that the installed spare CEDM housings, numbers 9 and 13, were not routinely vented during startup procedures during the previous operating life of the plant. It could not be positively determined why venting of these housings was not included in plant operating procedures or instructions. The estimated oxygen level in the spare CEDM housings without venting was calculated to be between 300 and 1300 ppm, which provided the conditions conducive to TGSCC.

To summarize, the cracks in the spare CEDM housings resulted from prolonged unvented operation which created conditions conducive to TGSCC. This report is submitted voluntarily due to potential NRC and industry interest.

The other two (2) spare CEDM housings with the HJTC probes, numbers 7 and 11, have been manually vented during startup since the HJTC probes were installed in 1984. Discussions between OPPD and ABB-CE revealed, however, that the venting procedures employed may not have ensured that these housings were free of air bubbles. The procedures did not ensure that venting would take place after the starting of the reactor coolant pumps during heatup. It was postulated that, if the HJTC housings were vented prior to starting the reactor coolant pumps, air bubbles from the steam generator tubes could become trapped in the HJTC housings when the pumps were started. Based on this information, it was decided that housings 7 and 11 would be examined by ultrasonic testing (UT) to determine the presence of cracks. This UT examination, utilizing both shear wave and refracted L-wave techniques, was performed by EBASCO Services personnel on December 29, 30, and 31, 1990. No crack indications were found.

The remaining 37 active CEDM housings are self venting through the rotating mechanical seals in the CEDM seal housing. Also, when the CEDMs are operated, there is an interchange of coolant water between the housing and the bulk RCS coolant inventory. As a result of the venting and the interchange of coolant during CEDM operation, the oxygen levels in the active housings should closely reflect the low oxygen levels of the bulk RCS inventory. Therefore, TGSCC in active CEDM housings is not considered credible.

LICENSEE EVENT REPORT (LER)
TEXT CONTINUATION

ESTIMATED BURDEN PER RESPONSE TO COMPLY WITH THIS INFORMATION COLLECTION REQUEST 500 HRS. FORWARD COMMENTS REGARDING BURDEN ESTIMATE TO THE RECORDS AND REPORTS MANAGEMENT BRANCH IF 5301 U.S. NUCLEAR REGULATORY COMMISSION WASHINGTON DC 20555 AND TO THE PAPERWORK REDUCTION PROJECT 3150-0104 OFFICE OF MANAGEMENT AND BUDGET WASHINGTON DC 20503

FACILITY NAME (1)	DOCKET NUMBER (2)	LER NUMBER (8)			PAGE (3)		
		YEAR	SEQUENTIAL NUMBER	REVISION NUMBER			
		Fort Calhoun Station Unit No. 1	0 5 10 0 0 2 8 5	9 0	0 2 8	0 0	0 7

TEXT (If more space is required, use additional NRC Form 306A's) (17)

In addition to the forty-one (41) CEDM housings, there are six (6) In-Core Instrumentation (ICI) housings located on the reactor vessel closure head. These housings have also not been vented since initial startup in 1973. Despite this fact, the ICI housings are not considered to be susceptible to the same kind of stress corrosion cracking observed on the spare CEDM housings because the ICI housings do not have a weld overlay region. As a result, there are lower residual stresses to assist in the initiation of stress corrosion cracking. Additionally, the ICI housing diameter is approximately a factor of 2 larger than the CEDM penetration diameter. This promotes more naturally convective coolant circulation so that internal oxygen content is closer to that of the bulk RCS coolant inventory. Thus, the ICI housings are not considered to be subject to TGSCC.

OPPD determined that there was minimal safety significance associated with the cracks in the number 9 spare CEDM housing. This determination was based on the individual assessments noted below of (1) reactor coolant system leakage, (2) potential for catastrophic rupture, (3) steam impingement, and (4) boric acid corrosion.

(1) Reactor Coolant System Leakage

The spare CEDM housings (numbers 9 and 13) did not have a safety function other than maintaining the integrity of the primary pressure boundary. Since there is no means during operation of detecting leakage as being specifically from a CEDM housing, any leakage from a CEDM housing would be categorized as from an unknown source.

To assure safe reactor operation, the reactor coolant system leakage limit from an unidentified source is limited to 1 gpm by Technical Specification 2.1.4. If the unidentified leakage exceeds 1 gpm, the reactor must be in hot shutdown within 12 hours and cold shutdown within 24 hours. Reactor coolant leakage indicates the possibility of a breach in the primary pressure boundary. The basis for the low leakage limits is to minimize the chance of a crack progressing to an unsafe condition without detection and proper evaluation. When the source of the leakage is unknown, placing the reactor in hot shutdown within 12 hours provides adequate time for an orderly reduction of plant power level. The hot shutdown condition also allows personnel to enter the containment and inspect the pressure boundary for leaks. The 24 hours allowed prior to going to cold shutdown allows reasonable time to correct small deficiencies. If major repairs are needed, a cold shutdown condition would be in order.

LICENSEE EVENT REPORT (LER)
TEXT CONTINUATION

ESTIMATED BURDEN PER RESPONSE TO COMPLY WITH THIS INFORMATION COLLECTION REQUEST 500 HRS. FORWARD COMMENTS REGARDING BURDEN ESTIMATE TO THE RECORDS AND REPORTS MANAGEMENT BRANCH (F 530) U.S. NUCLEAR REGULATORY COMMISSION WASHINGTON DC 20555 AND TO THE PAPERWORK REDUCTION PROJECT (3150-0104) OFFICE OF MANAGEMENT AND BUDGET WASHINGTON DC 20503

FACILITY NAME (1)	DOCKET NUMBER (2)	LER NUMBER (8)			PAGE (3)
		YEAR (7)	SEQUENTIAL NUMBER	REVISION NUMBER	
Fort Calhoun Station Unit No. 1	05100021815910	—0	218	—010	018 OF 110

TEXT (If more space is required, use additional NRC Form 306A's) (17)

During this event, the reactor was shut down and eventually placed in a cold shutdown condition with RCS leakage well below the Technical Specification limit. The axial orientation of the cracks on the housing resulted in a slowly increasing rate of primary coolant leakage which was monitored and also provided sufficient time to place the reactor in a safe shutdown condition. Thus, the consequences of the RCS leak were well within the licensed design basis of the plant.

(2) Potential for Catastrophic Rupture

The potential for a catastrophic rupture from the stress corrosion cracking was evaluated. The stress corrosion cracks were oriented axially along the housing. This crack growth orientation does not readily lend itself to sudden crack growth and rupture. Austenitic stainless steel is sufficiently ductile such that rapid crack propagation would not be likely before the reactor could be shut down in an orderly manner due to excess leakage.

(3) Steam Impingement

Steam sprayed from the through-wall crack in the number 9 CEDM housing onto adjacent active CEDM housings numbers 1 and 4, potentially causing impingement damage to these active CEDM housings. The active CEDM housings have mechanisms with CEAs that control the reactivity in the reactor during normal operation, postulated accidents or other potential malfunctions. These active CEDM housings thus include equipment that is important to safety.

The adjacent CEDM housings, including numbers 1 and 4, were visually inspected for indications of steam impingement damage. No impingement damage was detected.

(4) Boric Acid Corrosion

A potential problem for reactor equipment is corrosion wastage which can result from the leakage of boric acid primary coolant water. Evaporation of this water leaves dry crystalline boric acid residue which is essentially non-corrosive. However, any subsequent re-wetting of this residue creates a boric acid slurry that causes corrosion wastage.

The CEDMs adjacent to the through-wall crack and a few locations on the reactor vessel head were visually inspected for damage from the boric acid residue. No damage was detected. A large amount of boric acid residue was cleaned up from accessible areas during this inspection.

LICENSEE EVENT REPORT (LER)
TEXT CONTINUATION

ESTIMATED BURDEN PER RESPONSE TO COMPLY WITH THIS INFORMATION COLLECTION REQUEST: 500 HRS. FORWARD COMMENTS REGARDING BURDEN ESTIMATE TO THE RECORDS AND REPORTS MANAGEMENT BRANCH (P-5301) U.S. NUCLEAR REGULATORY COMMISSION WASHINGTON DC 20555 AND TO THE PAPERWORK REDUCTION PROJECT (3150-0104) OFFICE OF MANAGEMENT AND BUDGET WASHINGTON DC 20503

FACILITY NAME (1)	DOCKET NUMBER (2)	LER NUMBER (8)			PAGE (3)	
		YEAR (7)	SEQUENTIAL NUMBER	REVISION NUMBER		
Fort Calhoun Station Unit No. 1	0 15 10 10 10 1 2 18 15	9 10	- 0 12 18	- 0 10	0 19	OF 1 10 1

TEXT (If more space is required, use additional NRC Form 306A's) (17)

A review of the Radiation Work Permits written as a result of this event indicated that approximately 13.3 man-rem of whole body gamma radiation exposure and approximately 0.5 man-rem of assigned skin dose were received by personnel involved with inspection and repairs at the site. There were no internal doses recorded. Workers receiving doses included personnel from OPPD's Pressure Equipment, Electrical Maintenance, Mechanical Maintenance, Operations, Radiation Protection, Chemistry, Engineering, General Maintenance, Quality Control, and Training departments, as well as contractor personnel.

Completed corrective actions for this event include:

- (1) CEDM housings 9 and 13 were removed from the reactor vessel head per Maintenance Work Orders (MWOs) 904996 and 904997 respectively. They were visually inspected and sectioned per MWOs 905030, 905048 and 905069. ABB-Combustion Engineering was contracted to perform detailed destructive and metallurgical examinations of the cracked housings.

Reactor vessel head locations numbers 9 and 13 were capped by CEDM blind flange assemblies under Modification MR-FC-90-74. These assemblies have been analyzed for material compatibility and structural strength in accordance with applicable sections of the ASME Boiler and Pressure Vessel Code. The blind flange assemblies were leak tested during the RCS leak test on January 6, 1991, per Surveillance Test Procedure OP-ST-RC-3007, prior to startup and power operation. No leakage was identified.

- (2) Visual inspections of CEDMs 1 and 4 were performed per MWO 905048 to determine if any damage due to steam impingement had occurred. No damage was found. Visual inspections of CEDMs 7, 11, 14, 15, 17, 32, 34, and 38 were performed per MWO 905051 to determine if any cracking was apparent on those housings. No defects were found. A UT examination was then performed on CEDM housings 7 and 11 to detect any cracks that may have been present. No cracking was identified in these housings. An evaluation determined that, due to their self venting feature through mechanical seals, the remaining 37 active CEDM housings are not susceptible to TGSCC.

- (3) Operating Instruction Procedure OI-RC-3, "Reactor Coolant System (RCS) Startup" was revised to add a step to vent the HJTC housings after the reactor coolant pumps are started and the reactor coolant pump seals are vented. This will ensure the venting of any air bubbles that may become trapped in the HJTC housings when the reactor coolant pumps are started.

LICENSEE EVENT REPORT (LER)
TEXT CONTINUATION

ESTIMATED BURDEN PER RESPONSE TO COMPLY WITH THIS INFORMATION COLLECTION REQUEST 500 HRS. FORWARD COMMENTS REGARDING BURDEN ESTIMATE TO THE RECORDS AND REPORTS MANAGEMENT BRANCH (P 530) U.S. NUCLEAR REGULATORY COMMISSION WASHINGTON DC 20555 AND TO THE PAPERWORK REDUCTION PROJECT (3150-0104) OFFICE OF MANAGEMENT AND BUDGET WASHINGTON DC 20503

FACILITY NAME (1)	DOCKET NUMBER (2)	LER NUMBER (6)			PAGE (3)		
		YEAR (4)	SEQUENTIAL NUMBER	REVISION NUMBER			
Fort Calhoun Station Unit No. 1	0 5 0 0 0 2 8 5	9 0	— 0 12 8	— 0 0	1 0	OF	1 0

TEXT (If more space is required, use additional NRC Form 366A's) (17)

- (4) An enhanced Reactor Coolant System leakage action plan has been implemented to provide direction in the event of any future increases in the RCS leakage rate.

The following corrective action will be completed:

An evaluation supporting the unvented blind flange modification for the life of the plant will be completed and provided as backup documentation to the existing analysis which allows use of the unvented blind flange assemblies for the remainder of Cycle 13. The scheduled completion date for this evaluation is June 30, 1991.

There have been no other LERs concerning RCS leakage due to transgranular stress corrosion cracking. LER 84-08 concerned a steam generator tube rupture which was the result of secondary side intergranular stress corrosion cracking, a different mechanism.

OPPD will discuss with Region IV personnel the scope of future inspections deemed necessary. This discussion will occur prior to the 1991 refueling outage.



144 South 16th Street Mall
Omaha NE 68102-2247

October 15, 2001
LIC-01-0095

U. S. Nuclear Regulatory Commission
Attn: Document Control Desk
Washington, D.C. 20555-0001

- References:
1. Docket No. 50-285
 2. NRC Bulletin 2001-01, "Circumferential Cracking of Reactor Pressure Vessel Head Penetration Nozzles"

SUBJECT: Fort Calhoun Station (FCS) Control Element Drive Mechanism (CEDM) Housing Reliability Management

As a result of control rod drive mechanism housing cracks experienced by the nuclear industry, Omaha Public Power District (OPPD) and NRC have had several telephone conferences discussing the reliability of CEDM housings at FCS. In order to support these conferences, FCS has telecopied materials to NRC which describe the programmatic actions being taken by FCS to assure reliability and integrity of the CEDM housings. The purpose of this submittal is to summarize and docket the technical information previously telecopied and presented during the telephone conferences.

The attachment contains only the information and conclusions previously presented during the telephone conferences and does not constitute any new commitments.

FCS technical staff has been in communication with Palisades plant personnel and industry leaders in this field and is participating/leading in Electric Power Research Institute meetings and Combustion Engineering Owner's Group meetings. FCS will continue to use industry experience to stay informed of the developments associated with the control rod drive mechanism housing cracking problems as noted at Palisades and elsewhere in the industry. Lessons learned from the industry experience are being evaluated and appropriately included in the Fort Calhoun CEDM Material Reliability Management Program. OPPD encourages this continuing dialog with the NRC on this important issue.

Please contact me if you have any questions.

U. S. Nuclear Regulatory Commission
LIC-01-0095
Page 2

Sincerely,



R. L. Phelps
Division Manager
Nuclear Engineering

RLP/RLJ/rlj

Attachment

- c: E. W. Merschoff, NRC Regional Administrator, Region IV
- A. B. Wang, NRC Project Manager
- W. C. Walker, NRC Senior Resident Inspector
- Winston & Straw

Table of Contents

i	Executive Summary	2
1.0	Introduction	3
1.1	Self-Identified Material Reliability Issue	3
1.2	Corrective Actions Taken	3
2.0	'Program Plan for FCS CEDM Seal Housing' Basis and Content	4
2.1	TGSCC Root Cause	4
2.2	Environment Condition	5
2.3	Program Plan's Content Summary	5
3.0	Program Plan's Broader View of Operating Experience	5
3.1	CEDM Seal Housing Assembly	6
3.1.1	Active Housing Stagnant Area Defined	6
3.1.2	Environment/Material Condition Evaluated	6
3.1.3	Risk Evaluated/Validated	7
3.2	CEDM Upper Housing Assembly	7
3.2.1	Non-Active Housing Stagnant Area Defined	7
3.2.2	Vented Versus Non-Vented Housing	8
3.3	Reactor Vessel Head Penetration Nozzle	8
3.3.1	Industry Concerns	8
3.3.2	FCS Response	9
4.0	Conclusion	9

i Executive Summary

During the past ten years the nuclear industry worldwide has focused on addressing stress corrosion cracking in control rod drive mechanism (CRDM) assemblies, and thereby maintaining the material integrity of the reactor coolant system. From a material perspective each CRDM, referred to as Control Element Drive Mechanism (CEDM) assembly at the Fort Calhoun Station (FCS), consists of three separate components: a CEDM seal housing, a CEDM upper housing, and a reactor vessel head nozzle. In the industry, stress corrosion cracking has been found in each of these three material components. In 1990 at FCS, stress corrosion cracking was found in two spare unvented CEDM upper housings. This lack of venting, which produced completely stagnant conditions no longer exists at FCS.

Likewise, FCS's responses to nuclear industry events and experiences have been consistent in developing corrective actions that are focused on safe and event free operations. FCS has demonstrated responsiveness to industry/operation experiences by establishing corrective actions, increasing inspections, developing a program plan, and performing self assessments and independent evaluations using input from other sources in and outside of the nuclear industry. FCS continues to learn from industry (nuclear and non-nuclear) issues in order to provide a reasonable assurance of a low risk probability of rupture and/or excessive leakage in the primary system.

At FCS, a corrosion model has been developed into a program plan for CEDM seal housings. This program plan is a living document that discusses the mechanism of stress corrosion cracking, contains results of non-destructive examinations and gives contingencies for repair and replacement of seal housings. It is the position of FCS that a key element in the cracking of the CEDM seal housings is the stagnant environmental condition that exists in the CEDM seal housings. The CEDM seal housings contain the highest degree of stagnancy, and a chronic, highly oxygenated environment, which makes the seal housings the most susceptible of the three material CEDM components to transgranular stress corrosion cracking (TGSCC). The CEDM seal housings will be the first to crack and act as a precursor to ensuing cracking in the CEDM upper housings and reactor vessel head penetration nozzles. Therefore, by monitoring the condition of the CEDM seal housings with non-destructive examinations, FCS has a predictive tool to anticipate when the cracking in the CEDM upper housings and reactor vessel head penetration nozzles will occur. Based on this approach, FCS has performed non-destructive examinations of the CEDM seal housings in the past two refueling outages, and is continuing to develop a corrosion model by incorporating empirical experimental data.

The FCS CEDM program plan will incorporate, and address any new nuclear industry stress corrosion cracking events. FCS is actively pursuing greater understanding of the corrosion mechanism in the CEDM seal housings. FCS has self-identified the material reliability issue throughout the CEDM housing assemblies, and has instituted corrective actions and contingencies to address the concerns. The management of the material reliability of the FCS CEDM housings is proactive and innovative in assessing the risk, and ensuring the safe material health of each material component of the CEDM assemblies.

In the future, FCS plans to monitor nuclear industry stress corrosion cracking events and to participate in, and when necessary lead nuclear industry activities relating to stress corrosion cracking. During the 2002 refueling outage non-destructive examinations are being planned for the CEDM housings (in accordance with the FCS program plan) and effective visual examinations for the reactor vessel head. It is because of these activities and inspections in conjunction with a comprehensive FCS CEDM program plan that FCS concludes it is effectively managing its risk of stress corrosion cracking and maintaining reactor coolant system integrity by increasing the reliability of the CEDM assemblies

1.0 Introduction

At FCS, a corrosion model has been developed into a program plan for CEDM seal housings. This program plan is a living document that discusses the mechanism of stress corrosion cracking, contains results of non-destructive examinations and gives contingencies for repair and replacement of seal housings. It is the position of FCS that a key element in the cracking of the CEDM seal housings is the stagnant environmental condition that exists in the CEDM seal housings. The CEDM seal housings contain the highest degree of stagnancy, and a chronic, highly oxygenated environment, which makes the seal housings the most susceptible of the three material CEDM components to transgranular stress corrosion cracking (TGSCC). The CEDM seal housings will be the first to crack and act as a precursor to ensuing cracking in the CEDM upper housings and reactor vessel head penetration nozzles. Therefore, by monitoring the condition of the CEDM seal housings with non-destructive examinations, FCS staff and management have a predictive tool to assess the risk of cracking in the CEDM upper housings and reactor vessel head penetration nozzles. Therefore, FCS has self identified the material reliability issue of the CEDM housing and has instituted corrective actions that are described and/or elaborated in the following discussion.

1.1 Self-Identified Material Reliability Issue

In the last decade FCS and the Industry have experienced unscheduled outages, which were directly the result of transgranular stress corrosion cracking (TGSCC). This condition is a challenge to the material reliability for the CEDM housing assemblies. The kind of environment to subject the material condition into an accelerated corrosion attack is present at the FCS CEDM housing assemblies.

1.2 Corrective Actions Taken

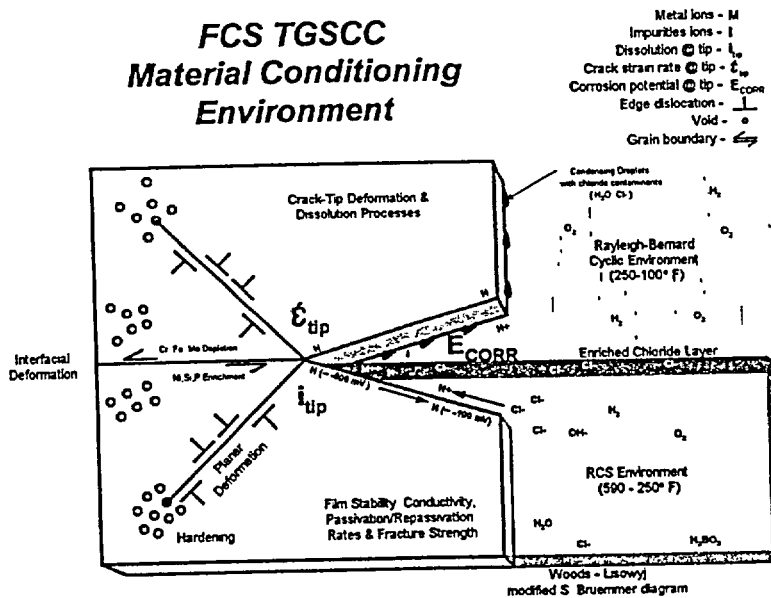
The possibility of TGSCC precipitated development of the Program Plan for FCS CEDM Seal Housings which applies critical self assessment of information, experience and techniques that support the goal of reliable plant material conditions. This program plan presents the basis of the inspection process with a discussion of the environmental conditions in relationship to the two phases of stress corrosion cracking (SCC), which are the incubation and cracking periods. The incubation and/or environmental conditioning period can be described with the industry's most current model diagram as a point of reference. The cracking period is based on the industry's use of Weibull curves, and both FCS and Palisades data resulting in a prediction of cracked housings during

the 1999 refueling outage at Palisades. However, the nuclear industry's prediction model's crack rate has shown to be an unreliable gage in the industry for predicting size and/or locating occurrences. This is due to the material conditioning rate (i.e., incubation period). Material conditioning is affected by many material factors, such as initial fabrication and localized environmental conditions, which make it difficult to quantify. Finally, FCS has a unique opportunity to utilize the information from our previous experience and future non-destructive examination signatures to develop a material conditioning model that will determine TGSCC occurrences for FCS components.

2.0 Program Plan for FCS CEDM Seal Housing Basis and Content

The basis for this program plan has been derived from elements that define TGSCC and the environmental effects that would elevate an early retirement of a component considered resistant to this kind of corrosive condition. These definitions help to define the risk, inspection focus and possible remediation/repair/replacement plan. A systematic inspection plan has been developed in conjunction with support from the Electric Power Research Institute and Westinghouse. In addition, FCS continues to interact with these institutes and other resources to enhance the reliability of this plan.

2.1 TGSCC Root Cause



Crack Model
Figure No. 1

The evolution of TGSCC is started from a process in which an electrochemically oxidizing corrosion environment removes surface metal ions. This chemical reaction attacks the steel's surface structure if not arrested by passivation of material surface (protective film layer). However, repassivation does not occur when the surface is being washed by an acidic solution contaminated by chlorides (leached from: Graphitar, O-ring and Flexitallic gasket). Therefore, this condition tends to deplete iron (Fe), chromium (Cr) and molybdenum (Mo) ions from the crack tip, which in turn are replaced by impurities resulting in a corrosion potential that is referred to as transpassive region (E_{CORR}), see Figure

No. 1 showing the corrosion mechanism.

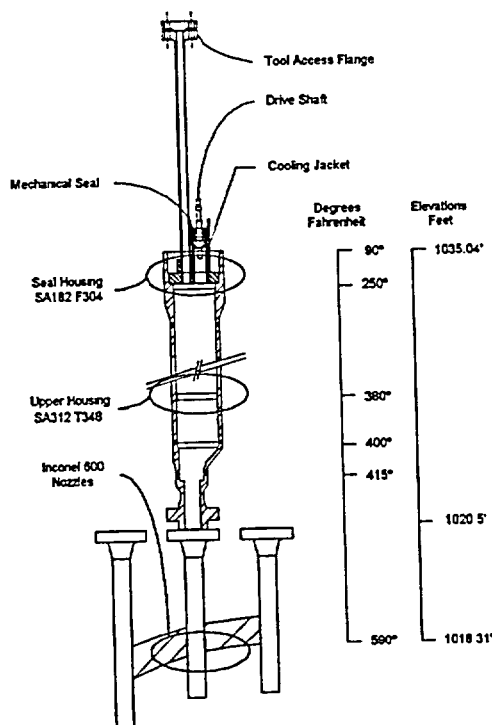
2.2 Environment Condition

The environment conditioning in the CEDM housings is considered to be accelerated by the process that is characterized by the Rayleigh-Bernard cycle. This condition assumes a void develops in a stagnant leg, and a cycle of wetting and drying develops, which removes the film layer and prevents repassivation. This condition would result in an aggressive electrochemical attack of the surface boundary in a corrosive resistant material. This offers a possible explanation for the industry's experience of premature failures of corrosive resistant materials such as stainless steel and Inconel 600 alloys.

2.3 Program Plan's Content Summary

This program plan's content has considered a selection, inspection, evaluation, remediation and repair of the CEDM seal housing assemblies at FCS. This information is based on the most current industry information on the principles, process and techniques for assessing SCC. In addition, the plan also describes in detail the history of gas bubble events that has prompted FCS's concerns for the CEDM housing assemblies material reliability based on TGSCC events of stainless steel material.

3.0 Program Plan's Broader View of Operating Experience

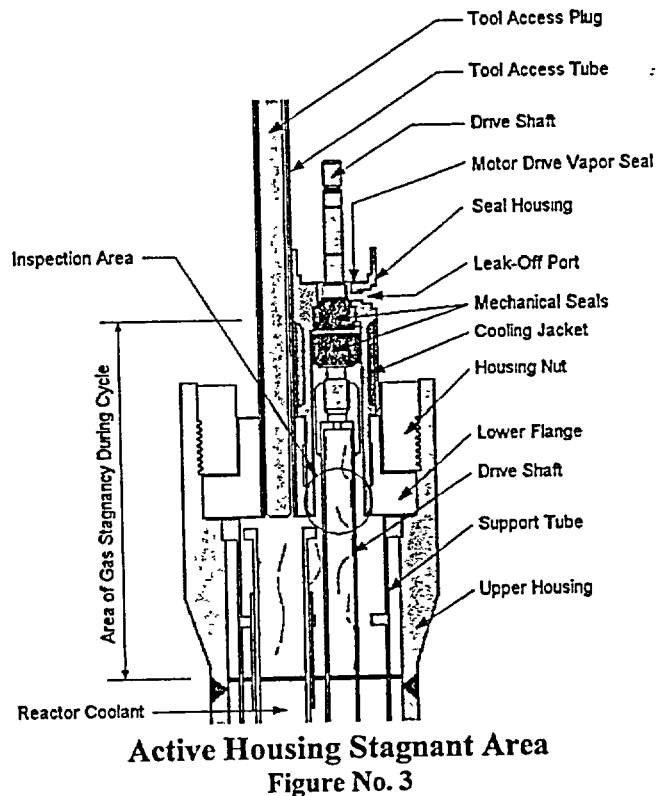


Broader View
Figure No. 2

At FCS as at other plants, the prime areas of concern are the reactor vessel head penetration (RVHP) nozzles. The nuclear industry has labeled these failures as primary water stress corrosion cracking (PWSCC), which has been generalized as a susceptible material under a tensile stress in an environment containing some oxygen and a chloride ion catalyst. A more specific corrosive model developed at FCS depicts the development of a low electrochemical potential (~500 mv) near a cold worked and/or tensile stressed area in contact with the primary system, which can initiate a Transgranular and/or Intergranular Stress Corrosion Crack (TGSCC/IGSCC). In this consideration, the focus of FCS has been to take a broader view of TGSCC versus reacting to single events. This broader view has included the RV head penetration nozzles, CEDM upper and seal housing assemblies (see Figure No. 2). Even though the CEDM upper and seal housing assemblies are made of stainless steel, the environmental conditioning that causes PWSCC is similar to the Inconel 600, head penetration nozzles. Understanding this conditioning or incubation period that is due to stagnancy is paramount to understanding SCC in the CEDM housings and RVHP nozzles.

3.1 CEDM Seal Housing Assembly

The CEDM Seal Housing Assembly is made of ASME SA 182 Type F304 material. The assembly consists of three principal elements: the drive housing, the tool access tube and the autoclave flange (see Figure No. 3). The drive housing has an inside diameter (ID) of 2.0625" with a wall thickness of 312 mils and functions as a boundary between the RCS and motor drive. The tool access tube has an ID of 1.240" with wall thickness of 120 mils and provides access for decoupling the control element assembly prior to removal of the reactor head. These two components are sleeve fitted and seal welded to the autoclave flange (outside diameter of 8.825") that is bolted to the upper CEDM housing assembly.



3.1.1 Active Housing Stagnant Area Defined

The stagnant legs of the reactor coolant system have shown signs of localized corrosion in which the metal loss has been exacerbated by the presence of oxygen, chloride and a tensile stress. The industry's and FCS's experiences with TGSCC of CRDM/CEDM assemblies including the seal housings at Palisades (1986 thru 1990, and 1999 events) and the upper assembly spares at FCS (1990 event) suggest similarities in environmental condition. These experiences have demonstrated a significant reduction in the components' life cycle, increased risk for unscheduled outages and reduced reliability of the reactor coolant system's integrity.

3.1.2 Environment/Material Condition Evaluated

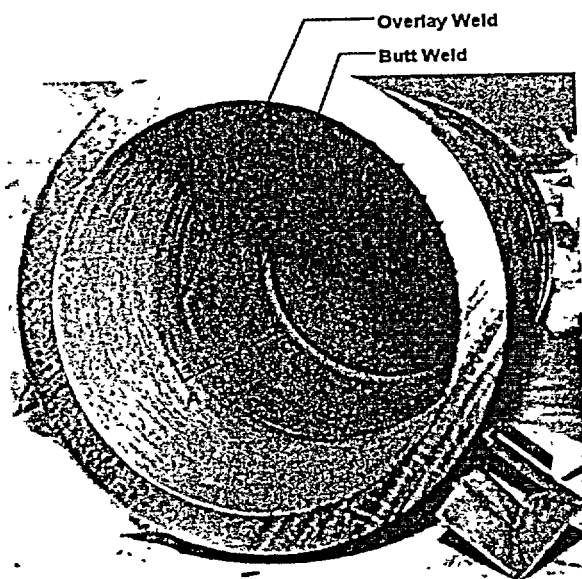
The longest stagnant period is at or near the top of the upper housing assembly's autoclave connection to the seal housing assembly (see sketch in section 3.1). The CEDM seal housing is considered as a precursor and/or corrosion history definition for the reactor vessel head CEDM assemblies. It should be noted that each CEDM has a different degree of stagnancy relative to its length, operational function and mechanical venting efficiency. The FCS staff has assessed the CEDM assemblies by evaluating fabrication and inspection records, re-inspecting, considering operating experience, industry data and inspection results to identify areas of concern. This model is continually being validated by operating experience and FCS investigation activities into the definition of material conditioning for the reactor vessel head assemblies.

3.1.3 Risk Evaluated/Validated

Finally, the industry's experience on seal housings and upper housing assemblies defines a sequence of events that should be anticipated for the FCS reactor vessel head assemblies. These events should begin at FCS with a through-wall crack near the J-Weld of the CEDM seal housing assembly and about fifteen years later another through-wall crack should develop near the overlay weld for an active CEDM housing assembly. This scenario supports FCS's basis for the Program Plan for FCS CEDM Seal Housing, which has been in continual development since March 4, 1999. The program plan ensures ongoing monitoring of the CEDM seal housings with non-destructive examinations.

3.2 CEDM Upper Housing Assembly

The CEDM Upper Housing Assembly consists of an upper flange, lower flange and a modified eccentric reducer that is made of ASTM SA182 Type F348, and a pipe that is made of ASTM SA312 Type F348 material. This upper flange supports the seal housing assembly and is secured by a housing nut. The lower flange is secured to reactor vessel head penetration nozzle and is sealed by an omega seal. These flanges are attached to a 8", schedule 120 pipe and a 5"x8", schedule 120 eccentric reducer by butt welds and the internals support ring formed from an overlay weld. The assembly consists of five principal internals, which are: the support tube assembly, piston tube guide assembly, rack assembly, drive shaft, and bevel gear housing. The spare CEDM Upper Housing Assemblies were supplied with a spoiler to enhance circulation in these assemblies.



**Non-Active Housing
Stagnant Area**
Figure No. 4

3.2.1 Non-Active Housing Stagnant Area Defined

The through-wall crack event at FCS in 1990 defines the maximum level of stagnancy in non-vented housings (spares). During the destructive examinations, a discoloration on the inside diameter surface was observed just below the overlay weld (Line 'B' on Figure No. 4). The importance of this information is the presentation of an oxygenated, chloride environment in the vicinity of a known tensile field relative to a through-wall TGSCC event. This environmental condition is a classic TGSCC model as presented in the FCS 'Program Plan for FCS CEDM Seal Housings'.

3.2.2 Vented Versus Non-Vented Housing

The discoloration level (refer to section 3.2.1) is not a definition for an active/vented housing assembly, which will have a varying level of stagnancy that is dependent on operational activities and mechanical seal performance. This event does provide a real life predictive model based on environmental condition and residual stress conditions that induce TGSCC. The information provided by this event has been utilized in implementing a method in assessing material risk and management of the material condition of the reactor vessel head assemblies.

3.3 Reactor Vessel Head Penetration Nozzle

There are 48 RVHP nozzles of which 37 are used for active CEDMs, two of these are spares, two are heated junction thermocouples, six are incore instrumentation and one vent line. The majority of the nozzles are constructed with a stainless steel SA-183 type F316 safe-end and an Inconel SB-167 pipe connected by a full penetration butt weld and attached to the reactor head with partial penetration J-weld.

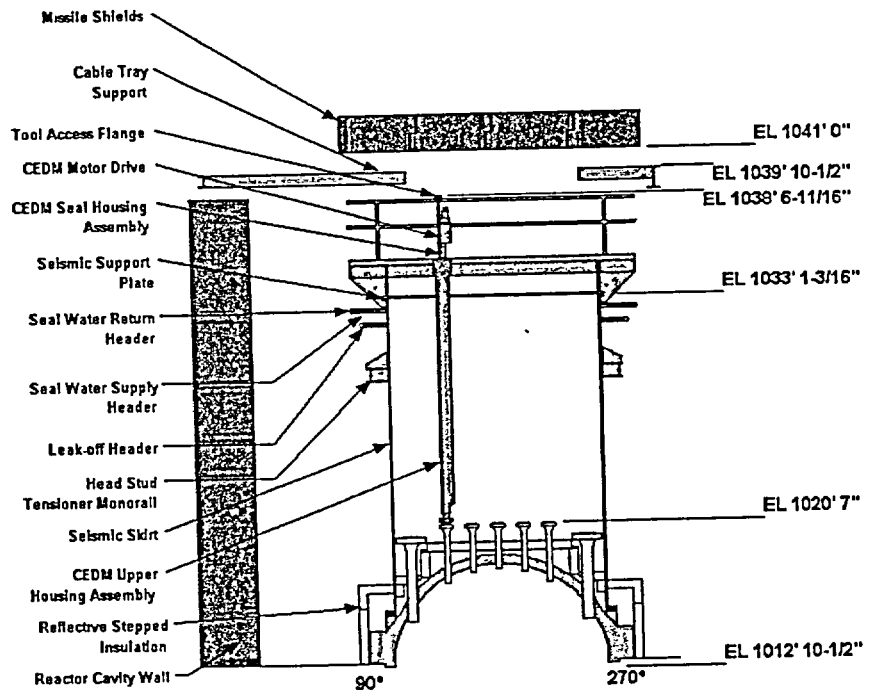
3.3.1 Industry Concerns

The most recent events that have raised concerns about material reliability for the primary water system occurred at V.C. Summer (NRC Information Notice 2000-17) and Oconee Unit 3 Nuclear Station (NRC Information Notice 2001-5). These two events have challenged the industry's predictability and degree of severity assessment on the effects of PWSCC of Alloy 600 in stagnant areas and/or stratified flows that produce a low corrosive potential. The safety concerns are the numbers, orientation, locations and coalescence of cracks in the areas of the reactor vessel hot/cold legs and CEDM nozzles above and below the interface J-weld. The incidence of circumferential secondary cracking at Oconee Unit No. 3 is a major current industry concern.

Fort Calhoun Station
 Managing the Material Reliability of the
 Reactor Vessel Head Assemblies

3.3.2 FCS Response

The NRC has issued Bulletin 2001-01 on RVHP nozzle cracking on August 3, 2001. The commission has grouped the primary water reactors into four categories based on the initial industry RV head time-at-temperature histogram in which FCS is assessed at 17.9 Effective Full Power Years (EFPY) from Oconee Unit 3 conditions. FCS has responded to this bulletin by demonstrating regulatory compliance, supplying requested information, and planning an effective visual examination of the reactor head surface during the 2002 refueling outage (see Figure No. 5).



RVHP and Associated Equipment
 Figure No. 5

4.0 Conclusion

Management of the material reliability issues for the reactor vessel head assemblies has been addressed and actions taken based on the operating experience of the industry. These actions have considered the root cause of TGSCC by defining a crack model in relationship to the environmental and operational conditions that focus on a broader view perspective. In addition, a comprehensive FCS contingency plan is in place for the possible remediation/repair/replacement of the CEDM assemblies based on a theme of safe and reliable operation to reach end of life. Finally, FCS is continuing this effort in reassessing this concern based on the new information from on-going evaluation, inspection results and industry information and/or events. By performing this continuing assessment FCS is effectively managing its risk of TGSCC and increasing the reliability of the reactor vessel head CEDM assemblies.



444 South 16th Street Mall
Omaha NE 68102-2247

January 25, 2002
LIC-02-0007

U. S. Nuclear Regulatory Commission
ATTN: Document Control Desk
Washington, DC 20555

- References:
1. Docket No. 50-285
 2. Letter from OPPD (R. L. Phelps) to NRC (Document Control Desk), dated October 15, 2001, "Fort Calhoun Station (FCS) Control Element Drive Mechanism (CEDM) Housing Reliability Management" (LIC-01-0095)
 3. Letter from NRC (A. B. Wang) to OPPD (S. K. Gambhir), dated November 16, 2001, "Fort Calhoun Station, Unit No. 1 - Control Element Drive Mechanism Housing Cracking" (NRC-01-104)

SUBJECT: Fort Calhoun Station (FCS) Discussion of Control Element Drive Mechanism (CEDM) Housing Reliability

In response to Reference 3, Omaha Public Power District (OPPD) is providing additional information on the factors affecting material reliability management of the CEDM housings as presented to the NRC in Reference 2. The primary factors considered are welding and cold working tensile residual stresses and temperature, two components of the triad that define the transgranular stress corrosion cracking (TGSCC) phenomena. OPPD has prepared an interpretation of the possible stress magnitudes and distribution and temperature variation that is inherently used in defining the Fort Calhoun Station (FCS) inspection criteria and frequency. This interpretation concludes that: 1) the highest risk component is the j-groove weld on the CEDM seal housing assemblies, and 2) the primary driving force is the environmental condition for TGSCC.

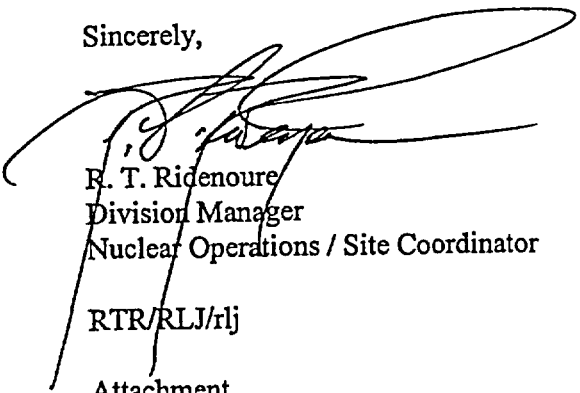
OPPD continues to pursue all available information related to the material reliability of the CEDM housing assemblies. The scope of the inspections planned during the FCS spring 2002 refueling outage has been expanded by: 1) increasing the number of CEDM seal housing assemblies to be inspected from six to eight, and 2) adding volumetric examination of six CEDM upper housing assemblies. Increasing the number of inspected seal housing assemblies allows OPPD to complete the baseline inspection of CEDM seal housings assemblies by 2006. A semi-remote ultrasonic technique will be applied to the In-Service Inspection (ISI) program's examination of the CEDM upper housing assemblies to minimize personnel radiation exposure and to improve the examination process reliability.

U. S. Nuclear Regulatory Commission
LIC-02-0007
Page 2

These inspections and this perspective on TGSCC contributing factors do not constitute new commitments. OPPD encourages continuing dialog with the NRC on this important inspection planning issue.

Please contact me if you have any questions.

Sincerely,



R. T. Ridenoure
Division Manager
Nuclear Operations / Site Coordinator

RTR/RLJ/rlj

Attachment

c: E. W. Merschoff, NRC Regional Administrator, Region IV
A. B. Wang, NRC Project Manager
W. C. Walker, NRC Senior Resident Inspector
Winston & Strawn

Fort Calhoun Station
Discussion of Control Element Drive Mechanism Housing
Reliability

TABLE OF CONTENTS

i.	Executive Summary:	2
1.0	Introduction:	3
2.0	Review of the NRC's Questions:	3
3.0	Overview of OPPD Letter LIC-01-0095:	3
4.0	Response to NRC Questions:	5
4.1	Residual Stress:	5
4.1.1	Weld Residual Stress:	5
4.1.2	Pre-Cold Working (Weld Joint Prep):	8
4.1.3	Post-Cold Working (Blending):	9
4.2	Temperature:	9
4.2.1	Temperature Distribution:	9
4.2.2	Crack Rate Versus Temperature Distribution:	9
5.0	Summary:	10
6.0	Figures:	12
1	- CEDM Seal Housing Assembly J-Weld Geometry	12
2	- CEDM Seal Housing Assembly J-Weld Circumferential Stress	13
3	- CEDM Seal Housing Assembly J-Weld Longitudinal Stress	14
4	- CEDM Upper Housing Assembly Overlay & Butt Weld Geometry	15
5	- CEDM Upper Housing Assembly Overlay Weld Circumferential Stress	16
6	- CEDM Upper Housing Assembly Overlay Weld Longitudinal Stress	17
7	- CEDM Upper Housing Assembly Butt Weld Through-Wall Stress	18
8	- CEDM Upper Housing Assembly Circumferential Butt Weld Stress	19
9	- CEDM Upper Housing Assembly Longitudinal Butt Weld Stress	20
10	- CEDM Assembly Temperature Gradient	21
11	- CEDM Sensitized 304 Stainless Steel Bathtub Curve	22

**Fort Calhoun Station
Discussion of Control Element Drive Mechanism Housing
Reliability**

i. Executive Summary:

In response to the NRC request for additional information to Omaha Public Power District (OPPD) letter LIC-01-0095¹, OPPD has addressed residual welding stresses and the effects of cold working and temperature on the material reliability of the control element drive mechanism (CEDM) housing. This request has been bundled as an interpretation of the magnitude of the welding and cold working tensile residual stress and the range of temperature conditions that would be significant in predicting transgranular stress corrosion cracking (TGSCC) occurrences. In addition, OPPD has presented the macro assessment of welding and cold working residual stress as having limitations in determining possible occurrences of TGSCC.

The most favorable condition for TGSCC is confirmed to be located in the CEDM seal housing assemblies' j-groove weld due to stagnancy, temperatures, and transverse weld shrinkage. The CEDM upper housing assemblies' weld overlay area and double v-groove (butt welds) are shown to be of lesser significance as candidates for TGSCC occurrence, based on the same quantitative interpretations. The cold working applied in fabricating these housings is not significant enough from weld to weld to provide a measurable difference as a predictive tool. Finally, OPPD has shown that the crack rate variation with temperature is also an insignificant variable compared to operating experience.

The conclusion is the CEDM seal housing operating conditions of temperature, stagnancy, and residual tensile stresses generated by j-groove welds is the optimal area for inspection for TGSCC. However, OPPD continues to investigate and refine its model based on a micro-structural stress concept in combination with a stagnant environment. Understanding this TGSCC mechanism will assist OPPD in assuring safe operation of the Fort Calhoun Station (FCS).

1

Letter from OPPD (R. L. Phelps) to NRC (Document Control Desk), dated October 15, 2001, "Fort Calhoun Station (FCS) Control Element Drive Mechanism (CEDM) Housing Reliability Management" (LIC-01-0095)

Fort Calhoun Station
Discussion of Control Element Drive Mechanism Housing
Reliability

1.0 Introduction:

This discussion is in response to an NRC request for additional information regarding the material reliability of the FCS CEDM housings. This discussion presents the corrective actions taken and methodology used in managing the industry's concerns on transgranular stress corrosion cracking (TGSCC) in CEDM housing assemblies. The NRC has requested additional information on OPPD's perspective of the importance on residual stress and temperature as a primary driving force for determining inspection criteria and frequency. The discussion that follows will elaborate on the basis of OPPD's methodology for managing the material reliability of the CEDM housing assemblies and the depth of actions taken for maintaining a reasonable assurance of safe operation of FCS.

2.0 Review of the NRC's Questions:

The NRC's questions suggest that OPPD's efforts are based on a "limited area" of inspections for TGSCC. The areas that have been inspected are based on concerns as presented in OPPD letter LIC-01-0095 for all weld areas in the CEDM housing assembly with an emphasis on the J-weld and overlay weld geometries based on operating experiences and OPPD's inspections. The NRC staff questions suggest the primary driving force for TGSCC to be from the tensile stress generated possibly from welding, pre-cold working (weld joint prep), or post-cold working (finish blending) conditions. In conjunction with a notion of the housing operating temperatures decreasing significantly with increasing elevation, this variation could change the incubation/cracking rate significantly. The scope and frequency of CEDM housing inspections have been evaluated based on a "broader view" that considered the CEDM assemblies as a system. The methodology used at FCS has considered the same factors as questioned by the NRC and more in determining frequencies, inspection types, risks, and contingencies that defined the actions taken in order to manage the material reliability of the FCS CEDM housing assemblies.

3.0 Overview of OPPD Letter LIC-01-0095:

OPPD letter LIC-01-0095 discussed OPPD's corrective actions and self identification of the concerns as a result of industry experience with TGSCC. These actions were formulated into a comprehensive assessment of the potential cause and risk, and a review of previous inspections, fabrication records, inspection plans, and possible contingencies that are documented in the OPPD's program plan.

This program plan is the basis and guidance for selection, inspection, evaluation, remediation, or repair of the CEDM seal housing assemblies at FCS. This plan proposes an inspection criteria and frequency, which is based on the environmental conditions (stagnancy, tensile stress, and temperature) in relationship with the two phases of stress corrosion cracking period which is defined by the incubation and cracking duration. In

Fort Calhoun Station
Discussion of Control Element Drive Mechanism Housing
Reliability

addition, the evaluation of non-destructive examination techniques was reviewed for their possible limitation in detecting tight cracks and surface geometry challenges in the areas of concern. The eddy current technique that was selected is based on a pilot study performed on the spare CEDM seal housings provided by FCS and Palisades on May 7, 1999. The enhanced eddy current technique, based on the pilot inspection, was then applied during the 1999 and 2001 refueling outages (RFO) with promising results. These results suggested the potential for predicting the incubation period, which is being investigated as a possible barometer for determining changes in the material properties and subsequently the threshold limits.

It should be noted the selection criteria for the 1999 RFO inspection were based on higher potential residual stress and temperature conditions. However, the results from this inspection were in contrast with the prediction model that suggested 2 of 6 housings would have positive indications. This information suggested the prediction model was inaccurate as a selection criteria and frequency definition for future inspections. OPPD's re-assessment of the possible environmental conditions resulted in the 2001 RFO selection criteria being focused on stagnancy, residual stress, and temperature.

In summary, OPPD's initial efforts were focused on the industry's perception in the form of a macro residual stress condition, which has been deemed as a poor prediction model for TGSCC condition. The current path being taken by OPPD emphasizes micro-stresses, or sometimes referred to as textural stresses², that better explain the known failure mechanism that defines TGSCC. This mechanism is believed to be more in line with the phenomena known as mechanical cleavage that is predominantly an environmental effect that lowers the material stress threshold³. Therefore, this approach has currently shown to be more reliable as a selection and frequency definition for FCS's CEDM housing assembly inspection criteria. The sections that follow will provide the foundation for this logic.

²

"Mechanical Metallurgy," by George E. Dieter, Jr., published by McGraw-Hill Book Company, copyright©1961

³

"Fundamentals of Electrochemical Corrosion," by E.E. Stransbury & R.A. Buchanan, published by ASM International®, copyright©2000

4.0 Response to NRC Questions:

The following sections will present OPPD's understanding of the possible residual stress conditions introduced by the fabrication process such as welding, machining, weld joint preparation, and finishing work and the operating temperature variation in the FCS's CEDM housing assemblies.

4.1 Residual Stress:

This section will focus on residual stress that can drive the alignment of slip planes, reduce dislocation energy, change grain texture, cluster voids, etc., that could increase the potential for stress corrosion cracking. These changes can occur during high tensile stresses that are introduced with the fabrication process through forming, machining, welding, abrupt geometry changes, etc., that approach or exceed the yield strength of the material into the plastic deformation range.

4.1.1 Weld Residual Stress:

The weld process inherently introduces residual stress in the weld area that could be considered to be an energy source for crack propagation in weakened grain structures. The resulting residual stress distribution varies widely with weld volume, joint geometry, and process. There were three weld geometry types used to construct the CEDM housing assemblies: the j-groove weld, overlay weld, and double v-groove weld.

The j-groove weld type is used for the CEDM seal housing's connection between the autoclave flange and drive housing (see Figure No. 1) as well as the reactor head nozzle penetration that is attached to the vessel head. This weld geometry type can generate tensile stress on the inside diameter surface in the longitudinal and circumferential directions as the result of weld transverse shrinkage. This residual stress can be approximated⁴ from an estimated deformation for the longitudinal, circumferential, and radial stress magnitude in the cylinder⁵ (see Figure No. 2) wall. This estimate reflects the fabrication records that document deformation up to a maximum of 75 mils exceeds the material yield strength. Therefore, in order to estimate the residual stress magnitude, a yield strain calculated at 2 mils will be applied to assess the longitudinal and circumferential

⁴

"Aluminum Welding Practice," by L. Capel, published by British Welding Journal, Vol 8 (No. 5), 961, pg. 245-248

⁵

"Formulas For Stress and Strain," by Raymond J. Roark, published by McGraw-Hill Book Company, fourth edition copyright©1965

Fort Calhoun Station
Discussion of Control Element Drive Mechanism Housing
Reliability

stress distribution. This results in circumferential tapered stress distributions through the wall thickness that denote a maximum tensile stress condition on the inside diameter near the weld root toe (see Figure No. 3). The corresponding longitudinal stress distribution also has a maximum tensile stress at the weld root toe throughout the heat affected zone (HAZ), but is only about one-third of the circumferential stress (see Figures No. 2 & 3). This magnitude and stress distribution is similar to the test report on heater sleeve nozzle mockups that exhibit maximum circumferential stress⁶ at 520 MPa (75.4 ksi) and longitudinal stress at 320 MPa (46.4 ksi) that also exceeds the material yield strength. However, it should be noted the reactor vessel penetration nozzles and head were heat treated. Therefore, the reactor head penetration welds should anticipate a considerable reduction in residual stress in contrast to the CEDM seal housing's j-groove weld geometry.

In general the CEDM seal housing's j-groove weld has the potential to generate higher circumferential stress than longitudinal stress, specifically, near the tool access tube that is less rigid compared to the support provided by the autoclave flange. This residual stress condition plus the unbalanced stress condition on the inside diameter surface suggest a potential energy source to initiate crack propagation in a corrosive environment.

The overlay weld type is in the form of cladding or built-up material and is applied on the inside diameter face of the CEDM upper housing (see Figure No. 4), which provides a support for the tube and gear assembly housing's internals. This weld type can also generate tensile stresses on the inside diameter face in the longitudinal and circumferential directions due to transverse and longitudinal weld shrinkage, respectively. The radial and longitudinal deformation can be estimated based on studies on fillet welds⁷ that provide a reasonable approximation of the longitudinal and circumferential stress distribution that could represent a general definition of magnitude. The resulting circumferential stress based on longitudinal shrinkage provides a nominal residual tensile stress condition on the inside diameter that is diminishing to the outside diameter face (see Figure No. 5). The longitudinal stress distribution can also be approximated based on the hot weldment concept, where the thermal contraction on cooler edges causes a mismatch between the

6

"Measurement of Residual Stresses in Alloy 600 Pressurizer Penetration Nozzles," J.F. Hall, J.P. Molkenthin (ABB-CE), P.S. Prev y (Lambda Research) & R.S. Pathania (EPRI), Conference on Contribution of Materials Investigation to the Resolution of Problems Encountered in Pressurizer Reactor Vessels, dated Sept.12-16, 1994

7

"Control of Distortion and Shrinkage Welding," by W. Spraragen and W.G. Ettinger, published by American Welding Society, Welding Journal , Vol 29 (No. 6 and 7) Research Supplement, 1950, pg 292s-294s and 323s-325s

Fort Calhoun Station
Discussion of Control Element Drive Mechanism Housing
Reliability

edges and center⁸. The expected result is a peak longitudinal tensile stress at the center of the overlay weld, but transition into compressive stress within the weld and HAZ (see Figure No. 6). Therefore, when considering this distribution in conjunction with circumferential stress distribution, these magnitudes are reasonable in comparison to the destructive examination on the spare CEDM upper housing assemblies, which reported a 9.5 ksi to 10.9 ksi residual stress⁹ condition.

The overlay weld is capable of generating longitudinal and circumferential tensile stress. However, the early through-wall longitudinal crack experience in 1990 on the spare CEDM upper housing (S/N 23866-9 & 13) in the overlay weld area was from a relatively low circumferential stress field estimated to be at one-third of the yield strength.

The double v-groove weld is also referred to as a butt weld and is based on a standardized weld end preparation detail¹⁰, specific to a plain bevel end detail without a contour taper (see Figure No. 4). This type of weld geometry generates longitudinal tensile stress and circumferential compressive stress on the inside diameter surface, in contrast to the j-groove and overlay weld configurations. The circumferential residual stress can be estimated by evaluating longitudinal weld shrinkage deformation¹¹. This assessment of residual stress magnitude for the butt weld joint is more complex since the initial weld root pass puts a tensile stress on the inside diameter, and each subsequent weld pass acts as compression jacket on the previous weldment. Therefore, each weld pass adds compressive stress to the previous weldment in the form of jacketing. This fabrication sequence stress summation results in a circumferential compression on the inside diameter with a transition to tensile stress on the outside diameter (see Figure No. 7). This circumferential distribution is confirmed by destructive examination on butt weld

8

"Corrosion and Corrosion Control and Introduction to Corrosion Science and Engineering," by H.H. Uhlig, published by John Wiley and Sons, copyright©1963

9

"Metallurgical Evaluation of Cracking in Fort Calhoun Spare CEDM Upper Pressure Housings Serial Nos. 9 and 13," Report No. TR-M.C.-169, prepared by Combustion Engineering, Inc. Materials & Chemical Technology, dated January 1991

10

"Buttwelding Ends," ASA B16.25-1964, published by The American Society of Mechanical Engineers

11

"Transactions of the Institute of Engineers and Shipbuilders in Scotland," Vol 87 pages 238-255, by C.W.R. King, dated 1944

Fort Calhoun Station
Discussion of Control Element Drive Mechanism Housing
Reliability

mockups for a 10-inch diameter, schedule 40 pipe¹² (see Figure No. 8) that is deemed to be relevant to the CEDM upper housing assembly. Therefore, the longitudinal stress presented in the Electric Power Research Institute (EPRI) report¹² appears to be a reasonable assessment of the magnitude anticipated in the FCS CEDM upper housing assembly (see Figure No. 9). In addition, the in-service condition was included in both the circumferential and longitudinal EPRI plots to determine the potential impact of the modified eccentric reducer stress concentration factor that could increase the stress by a factor of two due to the dimensional changes in pipe diameter¹³. In addition, the classical longitudinal distribution was applied to consider the difference in the fabrication jig setup that suggests a non-uniform distribution as presented in the EPRI report¹².

The double v-groove weld generated compression circumferential residual stress that is considered an enhancement in resisting in-service loading and stress corrosion cracking conditions. The longitudinal stress typically has a peak tensile stress at the weld root centerline that quickly transitions into compression stresses before extending past the weld joint and/or the HAZ. In addition, the magnitude of this tensile stress is only about two-thirds of the pipe material yield strength in contrast to typical higher weld yield strength, generally twice the strength of the base material.

In conclusion, the j-groove weld generates the highest circumferential and longitudinal residual stress that could support inside diameter surface cracking in a corrosion environment. The overlay weld, though demonstrating a nominal residual stress condition, has shown to be subject to the TGSCC condition from FCS's 1990 event of the spare CEDM housing assemblies. Finally, the double v-groove weld is the least susceptible to weld-induced residual stress based on this magnitude comparison of the different types of weld joints used in the CEDM assembly.

4.1.2 Pre-Cold Working (Weld Joint Prep):

The process of preparing a pipe or fitting end for a weld joint, as well as the prep work done after each weld pass, falls into the residual stress category of cold working. The CEDM housing assemblies' weld joint preparations were all machined except for the overlay weld. However, during the process of welding these initial residual stresses

¹²

"Studies on AISI Type-304 Stainless Steel Piping Weldments for Use in BWR Application," EPRI NP-944 Project 449-2 Final Report, prepared by Electric Power Research Institute, dated December 1978

¹³

"Finite Element Analysis of Eccentric Reducers and Comparisons with Concentric Reducers," by R.R. Avent, M.H. Sadd, and E.C. Rodabaugh, Bulletin 285, published by Welding Research Council, dated July 1983, ISSN 0043-2326

introduced by machining or grinding should have been reformed by the fusion process. The weld joint preparation step generally is a generic process used throughout the CEDM housing assembly and therefore has no measurable significance in determining potential risk.

4.1.3 Post-Cold Working (Blending):

The finished machining or blending also falls into the residual stress category of cold working. The areas of machining are the seal housing assembly's drive housing, upper housing assembly's upper and lower flange, and modified eccentric reducer, which were all cut to a minimum of 125 micro finish^{14&15}. In addition, the formed weld joints and fabrication blemishes were blended by a grinder to reduce stress risers from abrupt surface changes. The residual stresses are also generic through the assembly and again have no measurable significance in determining a magnitude difference in assessing potential risk.

4.2 Temperature:

4.2.1 Temperature Distribution:

The CEDM housing assembly temperature distribution has been previously evaluated for the possibility of loss-of-offsite power in relation to assessing the CEDM seal assemblies' o-ring failure mechanism¹⁶. However, this report was inconclusive in determining a specific temperature distribution and, in general, presented a linear variation from the reactor vessel head to the CEDM seal housing assembly's autoclave flange. Therefore, with the reactor head temperature at about 590° F and assuming the CEDM seal housing assembly's autoclave flange is around 250° F provides a relative temperature distribution (see Figure No. 10). The significant change between the CEDM seal housing assembly's autoclave flange to the leak-off chamber is due to a cooling water jacket that was provided to maintain a controlled temperature for the protection of the o-rings that are employed as part of the mechanical seal assembly.

4.2.2 Crack Rate Versus Temperature Distribution:

¹⁴

"Seal Housing Assembly Detail," Drawing CND-E-2935, File 21591, Rev. 7

¹⁵

"Upper Housing Assembly," Drawing CND-E-2927, File 1324, Rev. 5

¹⁶

"CRDM Seal Leak Testing-October 1989," Prepared for Omaha Public Power District and Consumers Power Corporation, prepared by Combustion Engineering's Operations Services and Mechanical Engineering & Technology

Fort Calhoun Station
Discussion of Control Element Drive Mechanism Housing
Reliability

There are several studies on the effects of temperature on the relationship with stress corrosion cracking that generally depict an inverted bathtub curve of temperature versus crack growth rate¹⁷ (see Figure No. 11). In an attempt to determine the temperature variation, a base temperature is selected from the operational experience from the control rod drive mechanism (CRDM) seal housing assemblies' through-wall cracking event at Palisades Nuclear Plant in 1999. This information suggests a temperature of 250° F at the j-groove weld location as discussed in section 4.2.1 and was applied in the previous section to determine a linear temperature variation throughout the assembly. In addition, FCS's similar experience in the spare CEDM upper housing assembly through-wall crack at the overlay weld location in 1990 suggests a variation from the linear interpolation previously presented. This difference is based on similar crack rates from operating experience at different locations and temperatures but suggests a delta of +50° F at the overlay weld locations from linear interpolation. However, this condition of temperature variation was proposed by the station blackout study for higher heat loads in the CEDM stack due to the internal assemblies acting as a heat escalator.

5.0 Summary:

The previous sections describe in detail OPPD's perceptions on the possible effects of residual stress generated by welding and surface cold working during the fabrication process of the CEDM housing assembly and operating temperature distribution during normal operation as suggested by the NRC. In addition, it should be noted that these factors were considered and implemented at FCS in response to the operating experience of Palisades in 1999 and are part of the current methodology and were the basis of the 1999 and 2001 RFO inspections. However, OPPD has not been satisfied with the inconsistencies of industry inspection results, the operating experience, and industry data as compared to the failure mechanisms in the industry. The CEDM seal housing assembly j-groove weld is shown to have the highest longitudinal and circumferential tensile residual stress at the weld root. The Palisades experience from 1986 through 1999 has reported that circumferential and longitudinal cracks in the area of the CRDM seal drive housing are more prevalent approximately one inch above the autoclave face. This information proposes the in-service stress, nicks, and scratches are more predominant than the fabrication tensile stresses generated from welding residual stresses. The FCS experience in 1990 with a through-wall crack at the overlay weld area had relatively low circumferential tensile residual stress and no reported cold working conditions to promote a longitudinal crack in this area. The current Palisades event of through-wall cracks at the double v-groove weld has circumferential compressive residual stress and surface blending that should reduce stress in this transition area. In addition, the circumferential cracks found

17

"BWR Water Chemistry Guidelines - 2000 Revision," Final Report No. TR-103515-R2, published by Electric Power Research Institute, February 2000

Fort Calhoun Station
Discussion of Control Element Drive Mechanism Housing
Reliability

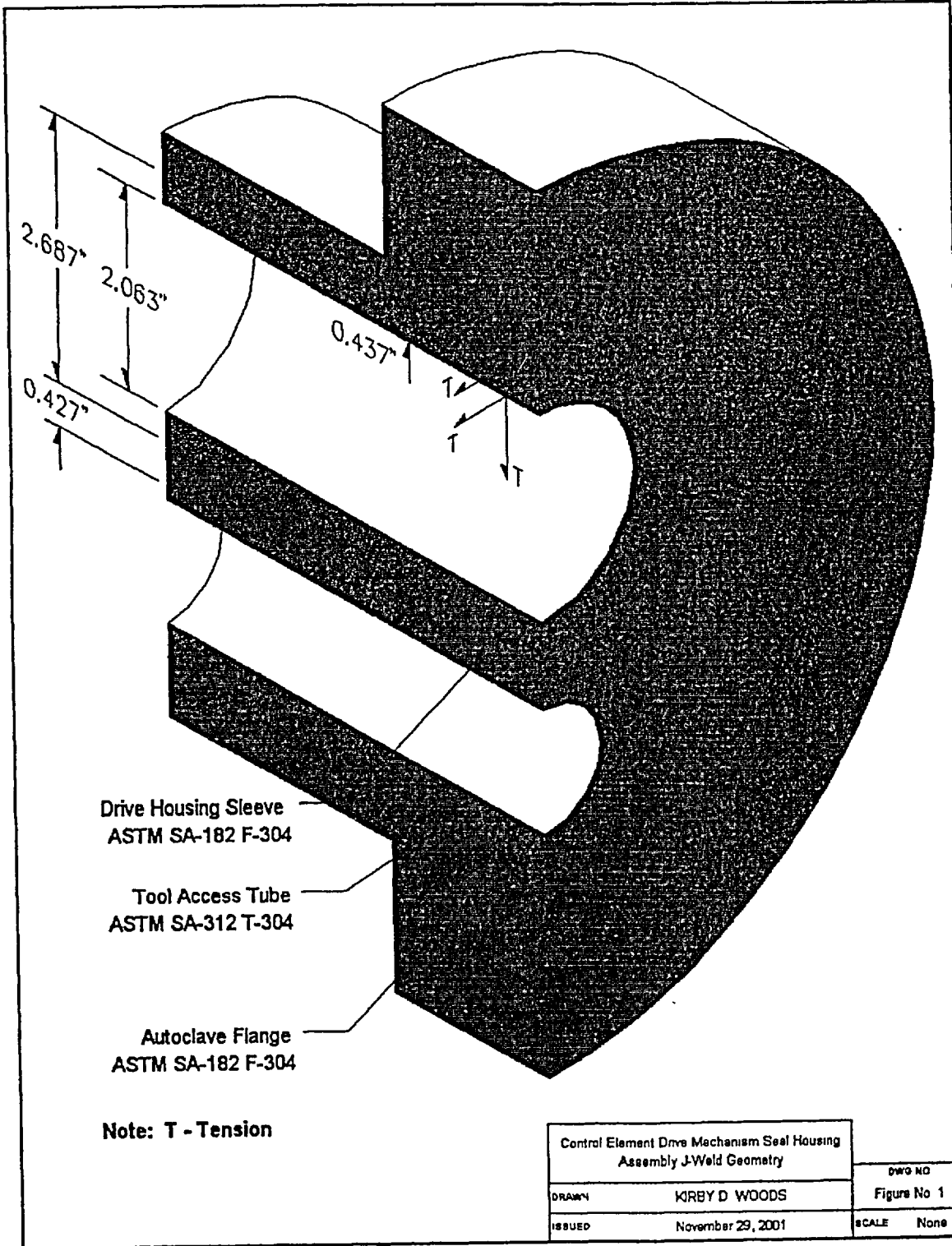
in the counterbore area of the modified eccentric reducer has no significant weld residual stress or cold working stress that could have promoted stress corrosion cracking in these areas. These conditions and their discrepancies suggest the focus on macro residual stresses from welding and cold working normal fabrication processes have significant limitations in determining an inspection and frequency criteria. However, OPPD recognizes these limitations and has implemented a more complete model by considering the stagnant condition of these assemblies in an effort to assess the material micro-stresses condition. This approach is more in line with current studies that propose the material properties are in the process of change from the installed condition. This electrochemical model¹⁸ proposes a chemical reaction of the metal surface with the environment that introduces contaminants in exchange of good metal ions such as carbon, iron, and molybdenum in the vicinity of crack morphology.

OPPD has aggressively pursued the industry concerns for TGSCC in the CEDM housing assemblies. This task has focused on all of the available information that also included operationally difficult inspections to assess component material reliability. This effort was based on the industry's current analysis and inspection techniques to achieve a corporate goal of excellence in material condition of the plant. Finally, the operating experience and failure mechanism experience at FCS and Palisades and information provided in this discussion indicate the highest level of component risk is with the CEDM seal housing assembly, based on the temperature, residual stresses, and the environment.

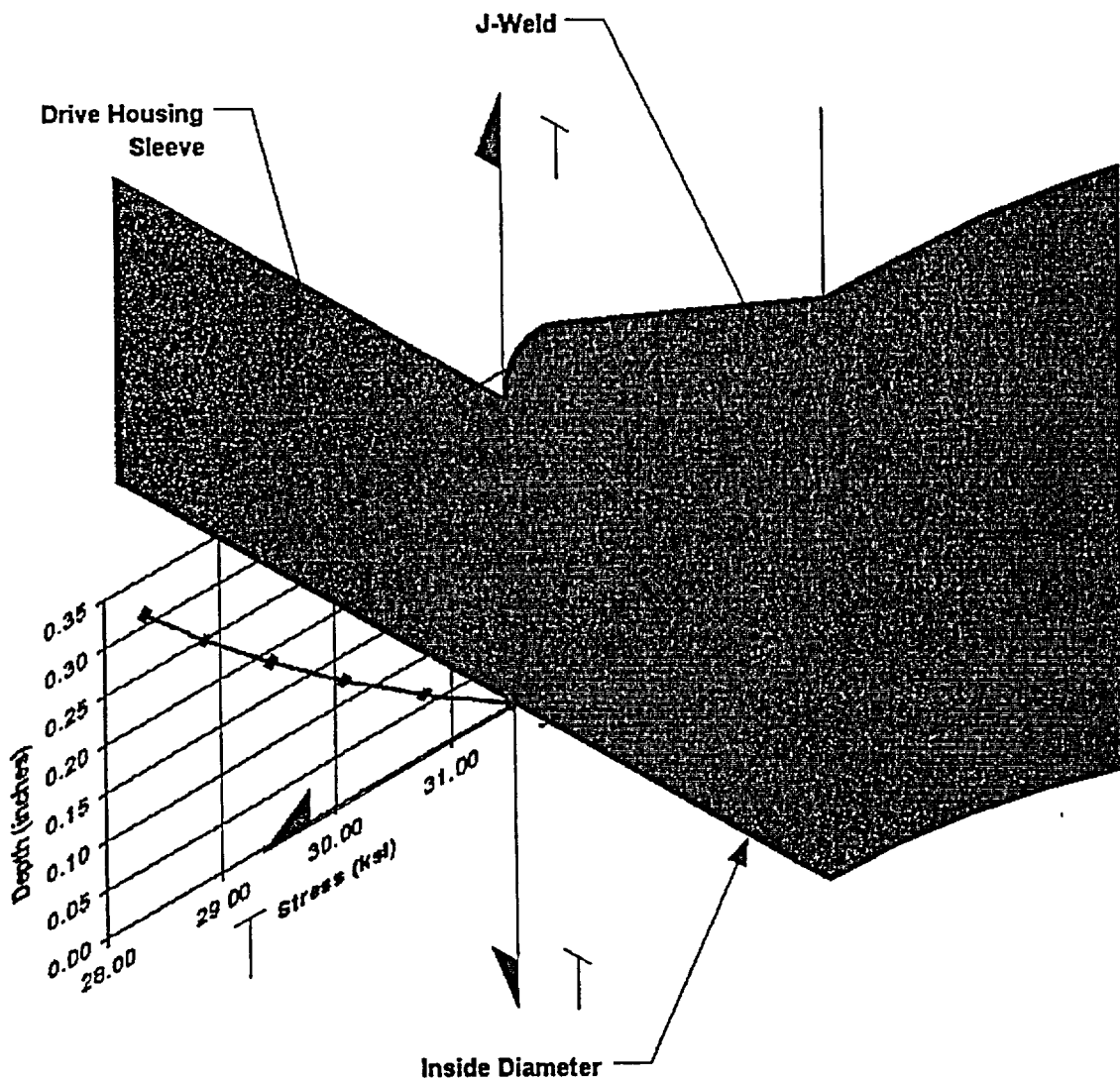
18

"S. Bruemmer Model," presented by Larry Nelson at the Nuclear Regulatory Commission's Workshop on Environmentally Assisted Cracking, Chaired by Mike McNeil, Thursday, April 20, 2000

Fort Calhoun Station
 Discussion of Control Element Drive Mechanism Housing
 Reliability



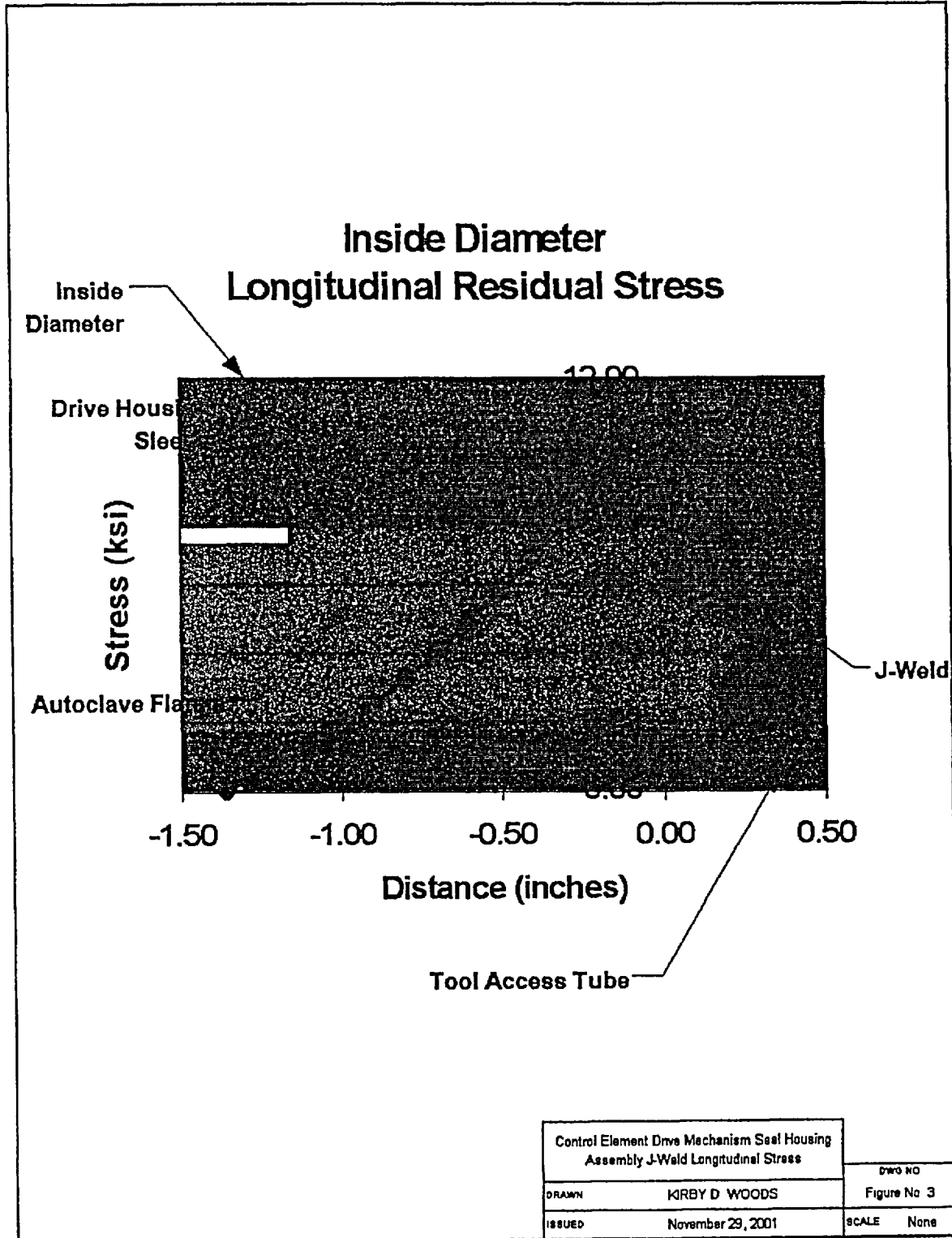
J-Weld Through-Wall Circumferential Residual Stress



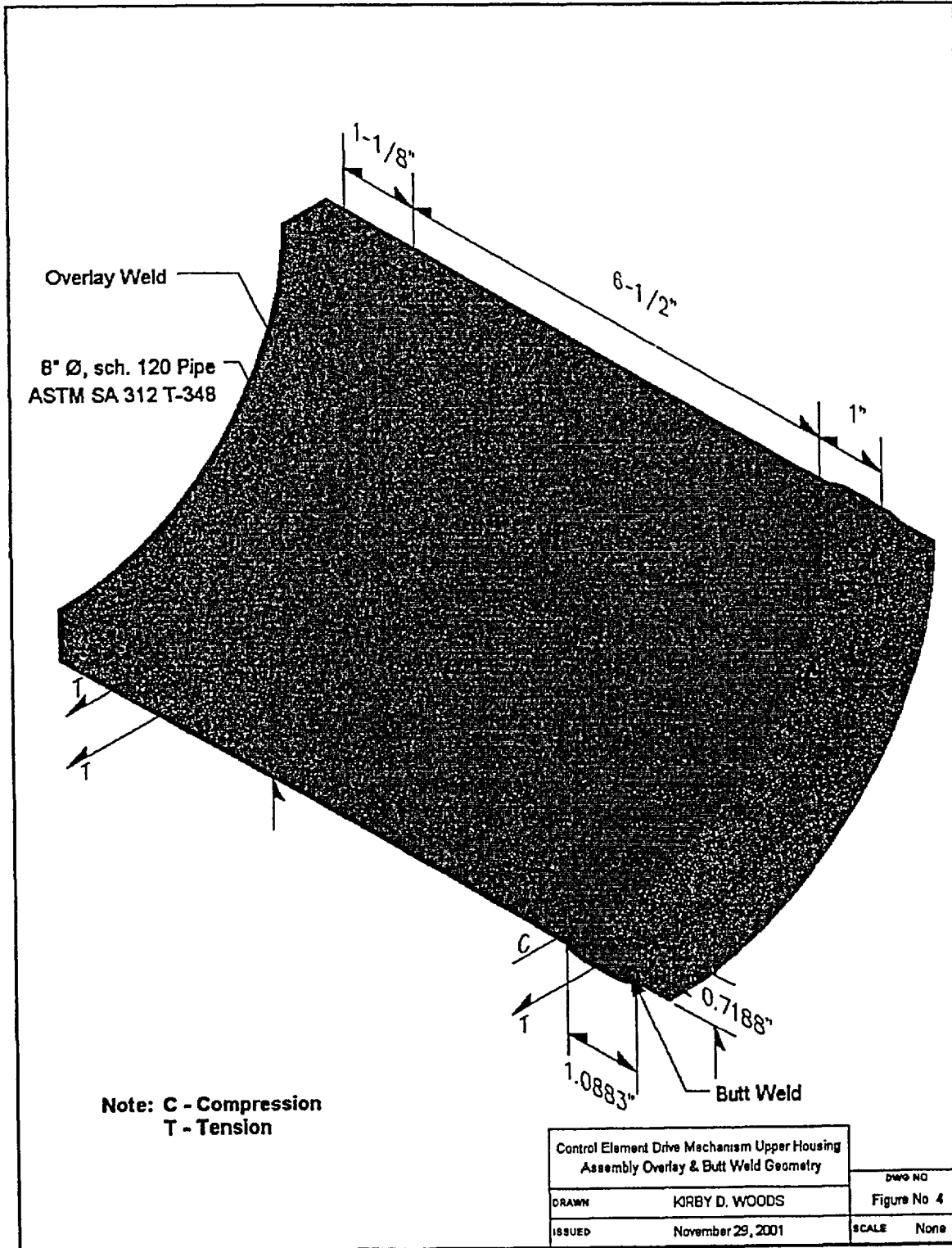
Note: T - Tension

Control Element Drive Mechanism Seal Housing Assembly J-Weld Circumferential Stress		DWG NO
DRAWN	KIRBY D WOODS	Figure No 2
ISSUED	November 29, 2001	SCALE None

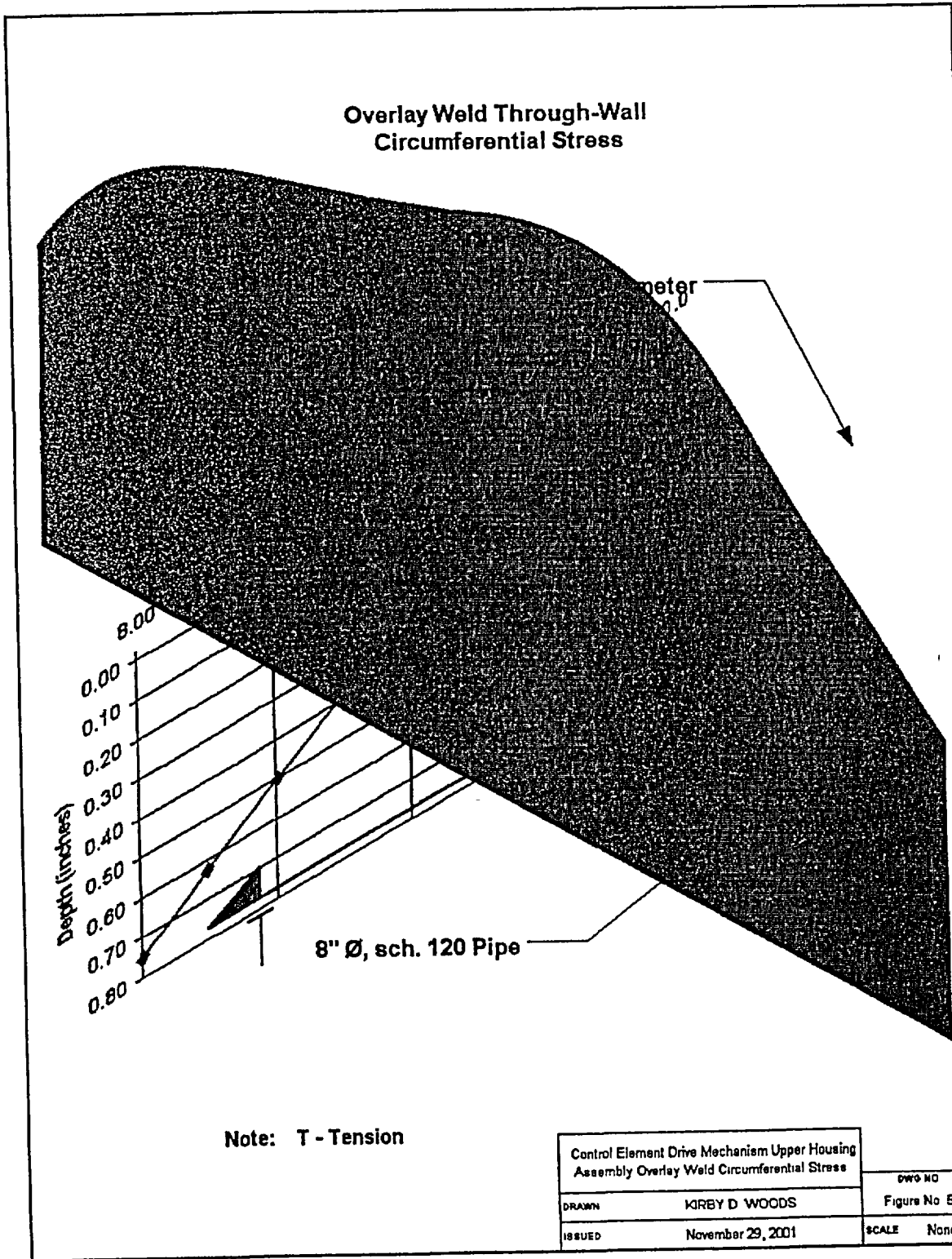
Fort Calhoun Station
 Discussion of Control Element Drive Mechanism Housing
 Reliability



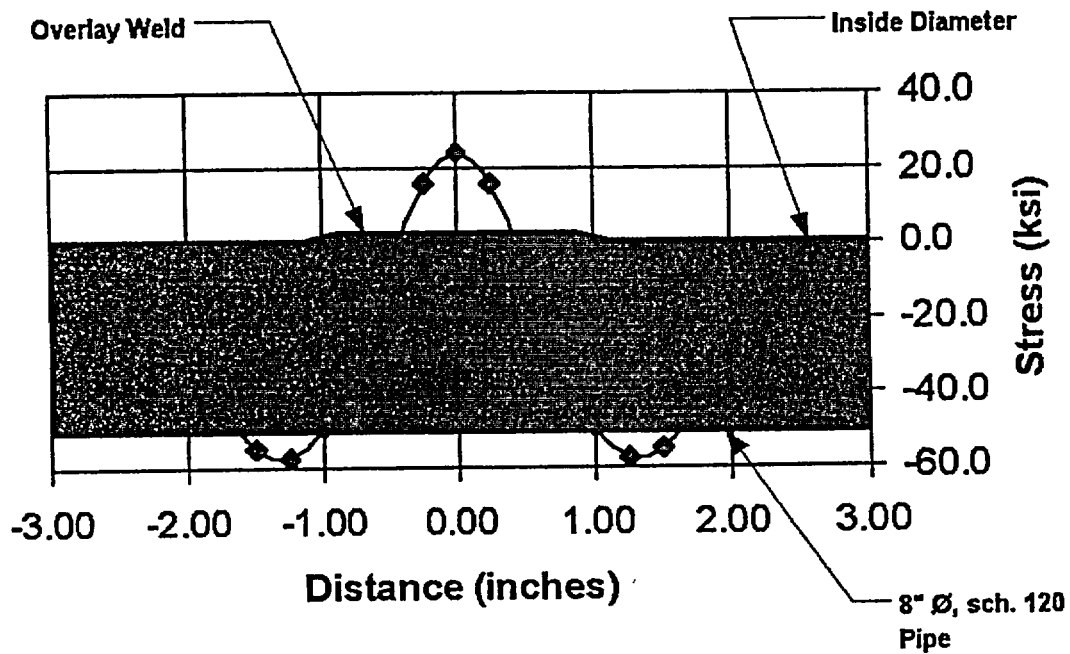
Fort Calhoun Station
 Discussion of Control Element Drive Mechanism Housing
 Reliability



Fort Calhoun Station
 Discussion of Control Element Drive Mechanism Housing
 Reliability



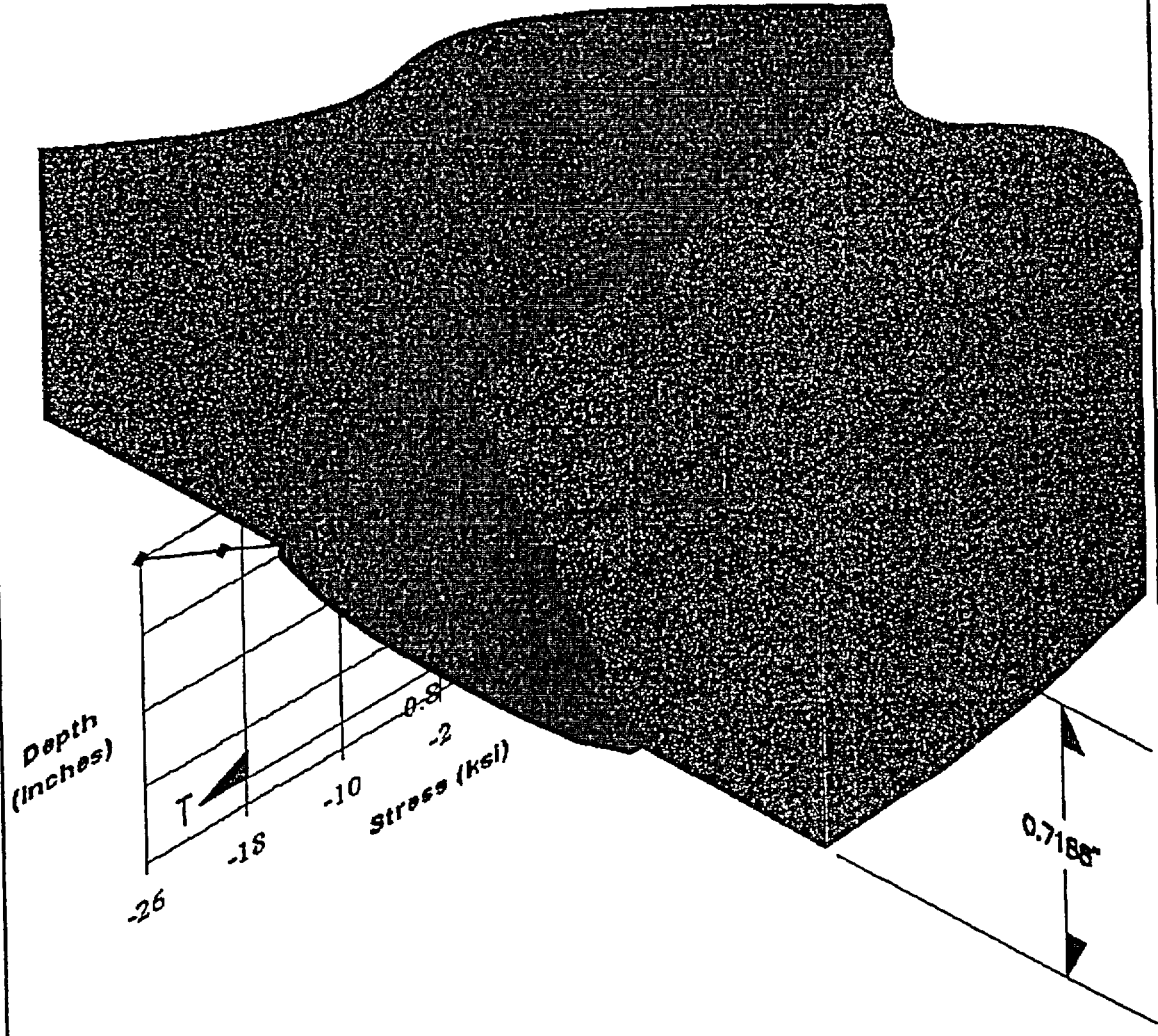
Inside Diameter Longitudinal Residual Stress



Control Element Drive Mechanism Upper Housing Assembly Overlay Weld Longitudinal Stress		DWG NO
DRAWN	KIRBY D. WOODS	Figure No 6
ISSUED	November 29, 2001	SCALE None

Fort Calhoun Station
Discussion of Control Element Drive Mechanism Housing
Reliability

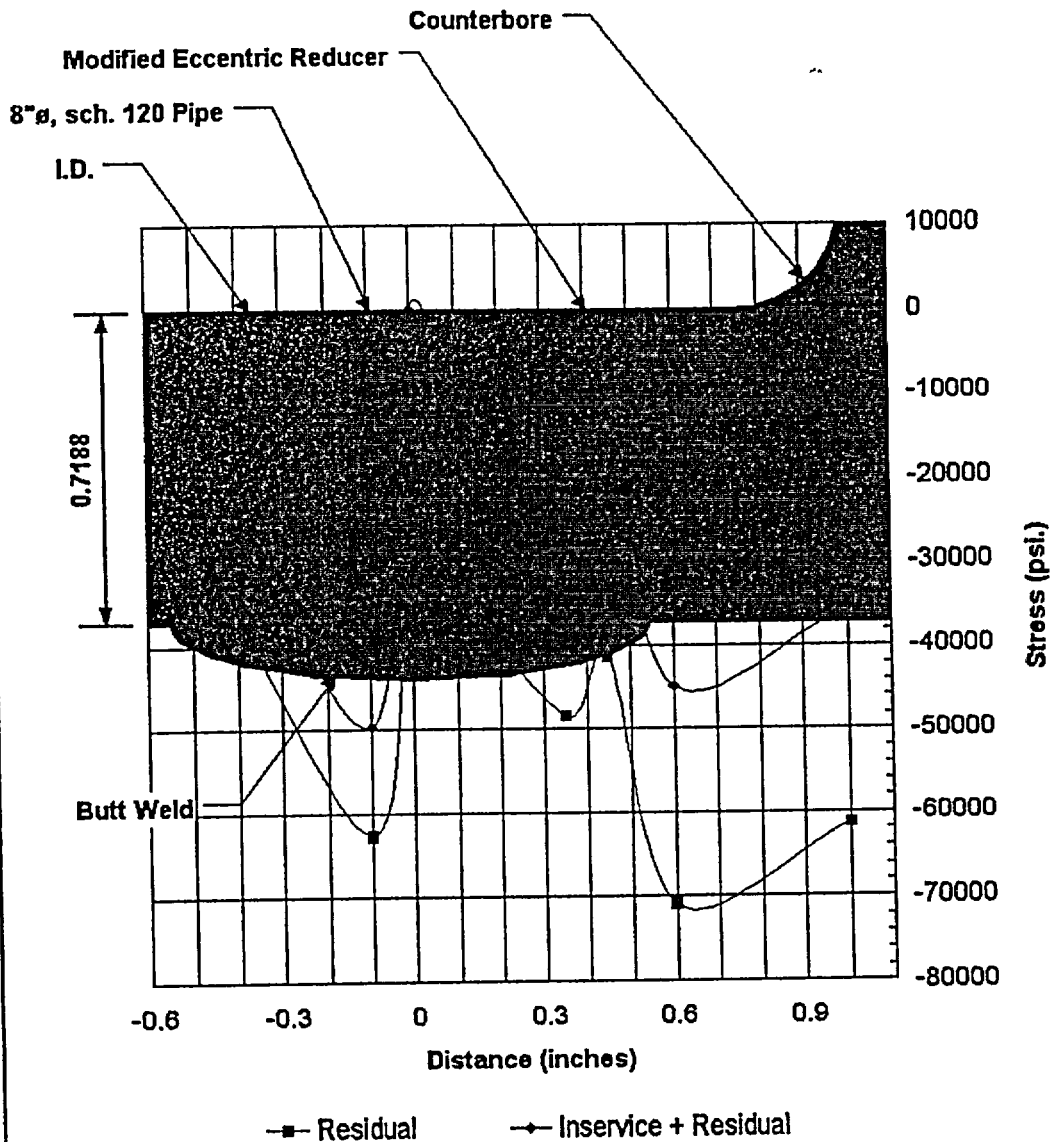
Butt Weld Through-Wall
Circumferential Stress



Note: C - Compression
T - Tension

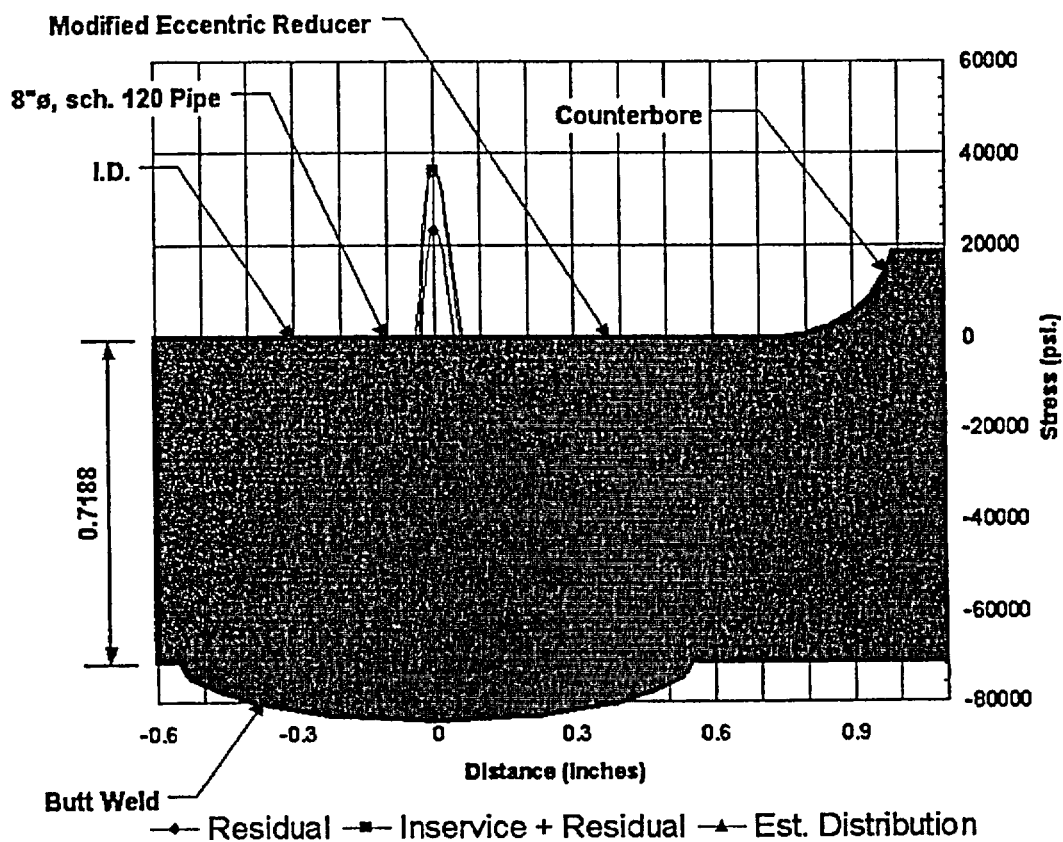
Control Element Drive Mechanism Upper Housing Assembly Butt Weld Through-Wall Stress		DWG NO
DRAWN	KIRBY D WOODS	Figure No 7
ISSUED	November 29, 2001	SCALE 1:1

Inside Diameter Circumferential Residual Stress



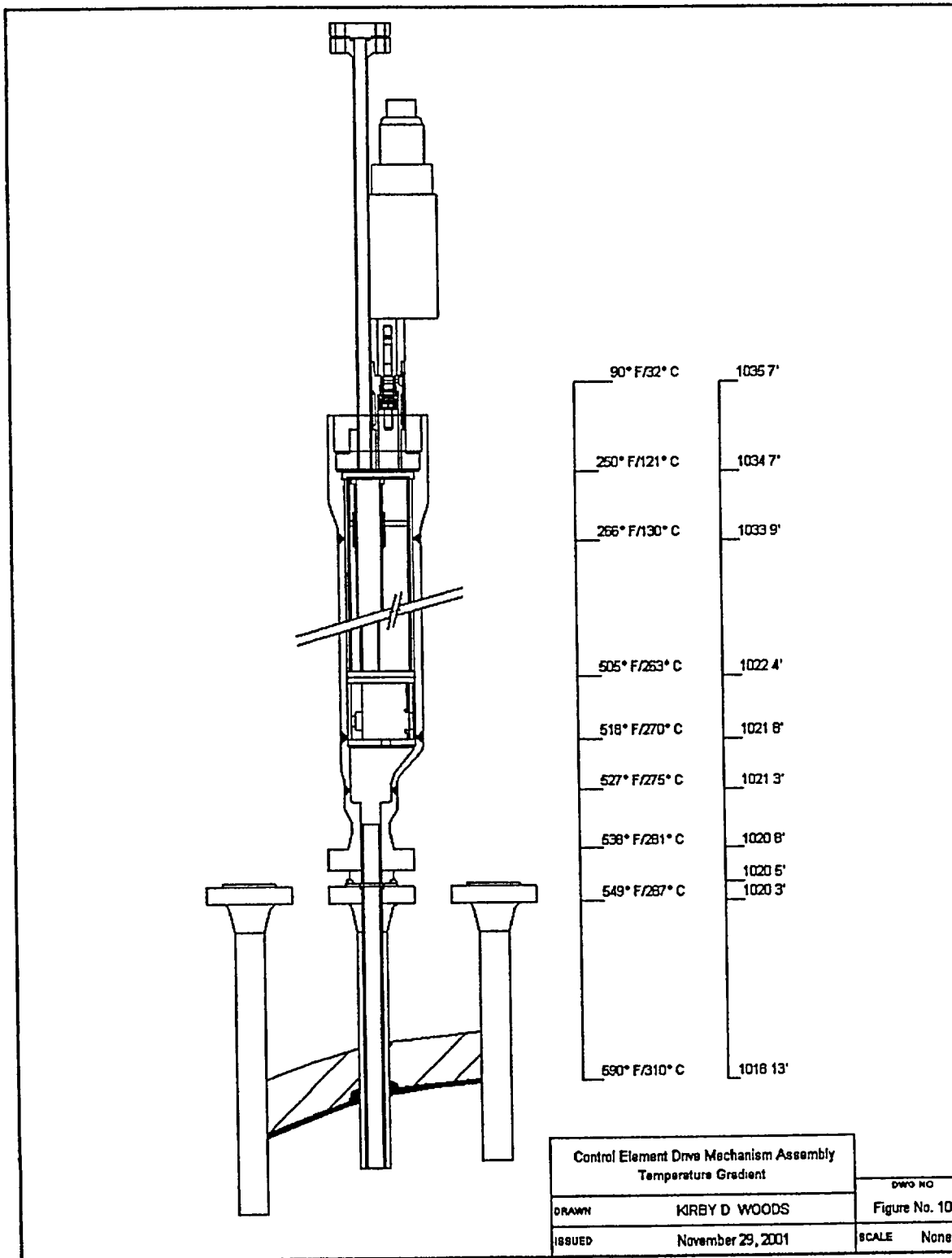
Control Element Drive Mechanism Upper Housing Assembly Circumferential Butt Weld Stress		DWG NO
DRAWN	KIRBY D WOODS	Figure No. B
ISSUED	November 29, 2001	SCALE None

Inside Diameter Longitudinal Residual Stress

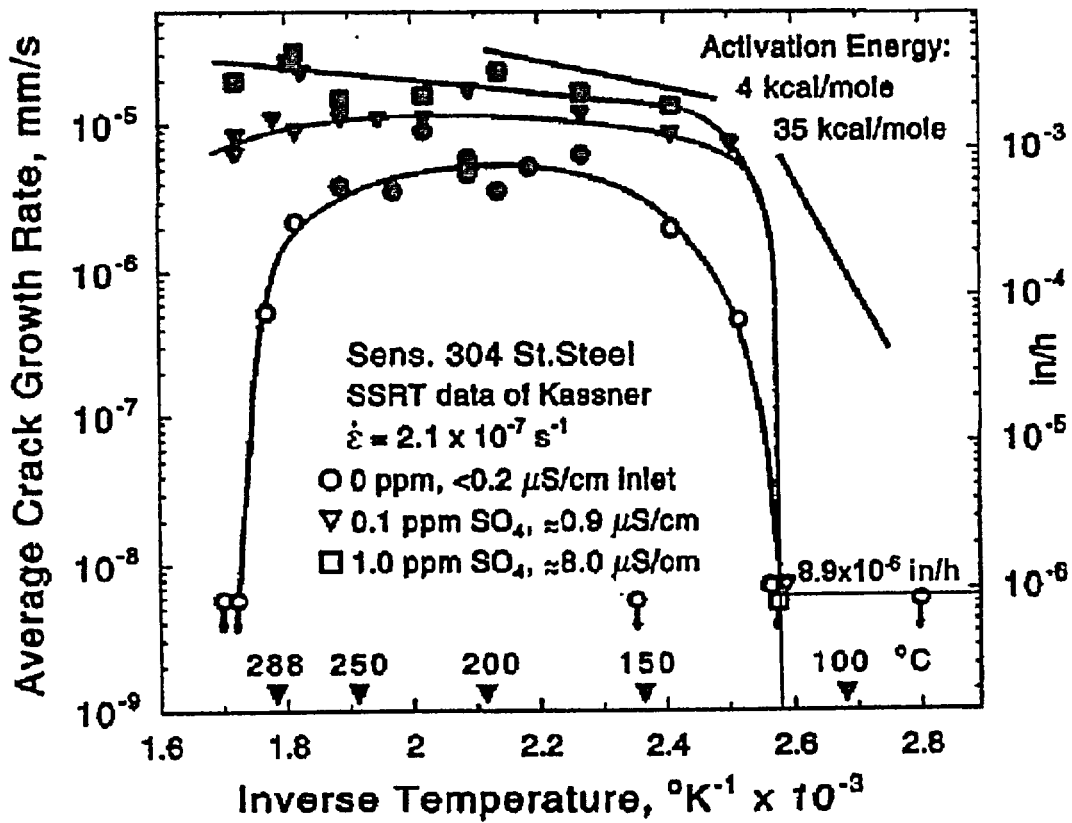


Control Element Drive Mechanism Upper Housing Assembly Longitudinal Butt Weld Stress		DWG NO Figure No 9
DRAWN	KIRBY D WOODS	SCALE None
ISSUED	November 29, 2001	

Fort Calhoun Station
Discussion of Control Element Drive Mechanism Housing
Reliability



Fort Calhoun Station
 Discussion of Control Element Drive Mechanism Housing
 Reliability



Control Element Drive Mechanism Assembly Sensitized 304 Stainless Steel Bathtub Curve		DWG NO
DRAWN	KIRBY D WOODS	Figure No 11
ISSUED	November 29, 2001	SCALE None

CALCULATION COVER SHEET

Calc Number: FC06608		CQE IDV Required: <input checked="" type="checkbox"/> Yes <input type="checkbox"/> No PED Department: 357		Calc Page No.: - Total Pages: 5 ⁶ +13			
Calculation Title: Flywheel Strength Analysis - Operating, Seismic and Fracture Conditions			Short Term Calc: <input type="checkbox"/> Yes <input checked="" type="checkbox"/> No VENDOR CALC NO.: HTAM622595, Rev. C <input checked="" type="checkbox"/> MR No.: FC-95-022 <input type="checkbox"/> ECN No.: <input type="checkbox"/> Engr Analysis: <input type="checkbox"/> Other: <input type="checkbox"/> DBD No.:				
APPROVALS - SIGNATURE AND DATE				Rev No.	Supersedes Calc No.	Confirmation Required (✓)	
Preparer(s)/ Date(s)	Reviewer(s)/ Date(s)	Independent Reviewer(s)/ Date(s)	Yes			No	
Meckel, 9-9-96 (ABB Industries)	Seidler, 9-9-96 (ABB Industries)	EGS Motor Dedication Report SAIC-TR-751.200-02	C			✓	
Meckel, 10-18-96 (ABB Industries)	Meckel, 10-18-96 (ABB Industries)	Di Fazio, 10-18-96 (ABB Industries)	D			✓	
As-Build (No changes) EJT 1-22-97			O			✓	
EXTERNAL ORGANIZATION DISTRIBUTION							
Name and Location		Copy Sent (✓)	Name and Location		Copy Sent (✓)		



Flywheel Strength Analysis 1
Operating, Seismic and Fracture Conditions

Natural Frequencies of the Rotor.Housing System 2
Rotor Critical Speed and Reed Frequency

3

4

5

6



Copy to

OPPD / Fort Calhoun Power Stn
Nuclear Licensing Dept.
P.O. Box 550
Fort Calhoun
NE 68 023

Dealt with by

Date
10/04/02

Our reference
G0599

For the attention of Tom C. Matthews

Your date

Your reference

Subject: Reactor Coolant Pump Motor / Report HTAM 622595

Dear Sirs,

We hereby permit your submission of subject report to the Nuclear Regulatory Commission for their review required for your licence renewal application.

Yours truly

Jan-Anders Bergman
V.P. Electrical Machines

Postal address
ABB Inc
16250 W Glendale Drive
New Berlin
WI 53 151. USA

Telephone
1 262 785 3200
Telefax
1 262 785 8828

Internet address
www.abb.com

ABB	ABB Industrie AG			HTAM 622595
Responsible department: CH-IMVP	Take over department: OPPD	Revision: D 96-10-18	Doc-type Report	File no.: 622595_H.DOC
Prepared: 96-10-18 Meckel <i>Me</i>	Checked: 96-10-18 Meckel <i>Me</i>	Approved: 96-10-18 Di Fazio <i>Di</i>	Language	Page: 0/54
Valid for:	Derived from:	Replaces	Classify no	Data set:

Fort Calhoun

REACTOR COOLANT PUMP MOTOR

QOVG 900 fa6

Fort Calhoun Power Station

Omaha Public Power District
Omaha, Nebraska

FLYWHEEL STRENGTH ANALYSIS

OPERATING, SEISMIC AND FRACTURE CONDITIONS

P.O. 1977

Table of Revision

No.	Reason	Revised Pages	By
A	Original Issue	None	Meckel 96-01-26
B	New Measured Material Data from Sidenor	0,1,4,6,23	Meckel 96-07-17
C	Data from fracture toughness test delivered by Sidenor	0,1,4,6,20,21,23,24	Meckel 96-09-09
D	Comments from OPPD, crack growth calculation added	0,1,2,3,4,20,54,55,56	Meckel 96-10-18

Supplement 1, Revision B, dated 96-10-18 is still valid for HTAM 622595, Revision D.

For updated results of the stress analysis and analysis of transmissible torque see Supplement 1, Revision B.

ABB-CE HTAM 622595

551833

860 731 6540

FRANK FERRACIO

0 Table of Contents

1 Purpose _____ 3

2 Results and Conclusions _____ 4

3 Design Inputs _____ 5

 3.1 Assumptions _____ 5

 3.2 Input Data _____ 6

4 Methodology _____ 7

 4.1 Stress analysis _____ 7

 4.1.1 Standstill _____ 7

 4.1.2 Normal operating speed _____ 9

 4.1.3 Test overspeed _____ 11

 4.2 Seismic analysis _____ 13

 4.2.1 Normal Loading Conditions _____ 14

 4.2.2 Vertical Seismic Load (OBE and DBE) _____ 15

 4.2.3 Horizontal Seismic Load (OBE) _____ 16

 4.2.4 Horizontal Seismic Load (DBE) _____ 17

 4.2.5 Synchronous Speed and OBE _____ 18

 4.2.6 Synchronous Speed and DBE _____ 19

 4.3 Non-Ductile Fracture Analysis _____ 20

 4.4 Ductile Fracture Analysis _____ 22

5 References _____ 24

APPENDIX A: SYSTEM OF UNITS _____ 25

APPENDIX B: LIST OF SYMBOLS _____ 26

APPENDIX C: FIGURES _____ 27

APPENDIX D: CRACK GROWTH CALCULATION _____ 54

ABB	Revision: D 96-10-18	Language: en	Page: 3 / 58	HTAM 622595
------------	-------------------------	-----------------	-----------------	-------------

1 Purpose

ABB INDUSTRIE AG In Birr, Switzerland, is building a motor QOVG 900 fa 6 for a reactor coolant pump in the nuclear power station „Fort Calhoun“ in Nebraska, USA.

The motor will be used to drive a vertical single stage centrifugal pump. The motor is a vertical, ripped-shaft, squirrel cage, self ventilated air cooled induction motor.

According to the flywheel specification an analysis shall be performed to insure that the flywheel assembly will maintain its structural integrity during

- Design Loading Condition
- Normal Loading Condition
- Upset Loading Condition
- Faulted Loading Condition

and to predict critical speeds for ductile and non-ductile fracture of the flywheel. Additional a crack growth prediction calculation is carried out.

All calculations are made in SI-Units, in the result summary tables also the American Units are given. A conversion table to American Units is given in Appendix A.

2 Results and Conclusions

The results of the Finite Element Analysis are summarized in the following tables:

Stress Analysis (® see Supplement 1)

Stress analysis	Calculated Von Mises stress N/mm ² (ksi)	Admissible Von Mises stress N/mm ² (ksi)	Safety margin
Synchronous speed (1200 rpm)	® 192.0 [*] (27.9)	® 195 (28.3)	® 1.02
Test overspeed (1500 rpm)	® 196.3 ^{**} (28.5)	® 390 (56.6)	® 1.99
Synchronous speed and OBE	200.4 (29.1)	526 (76.3)	2.62
Synchronous speed and DBE	203.8 (29.6)	526 (76.3)	2.58

The stresses in the flywheel are admissible for all load cases prescribed and in all these cases the flywheel will maintain its structural integrity.

Transmissible Torque (® see Supplement 1)

Transmissible torque	Calculated minimum transmissible torque Nmm (ft lbf)	Rated motor torque Nmm (ft lbf)	Safety margin
Synchronous speed (1200 rpm)	® 7.936E+08 (5.853E+05)	® 2.166E+07 (1.597E+04)	® 36.64
Test overspeed (1500 rpm)	® 2.547E+08 (1.878E+05)	® 2.166E+07 (1.597E+04)	® 11.76

The flywheel will not become loose at test overspeed.

Non-Ductile Analysis, Ductile Analysis and Crack Grow Prediction

Critical fracture speed	Critical fracture speed rpm	Predicted LOCA overspeed rpm	Safety margin
Non-ductile Fracture	4700	3697	1.27
Ductile fracture	3910	3697	1.05

The results show that the specification demand is fulfilled. The Crack Grow Prediction calculation shows that the critical crack size is not reached within 10000 cycles from zero to overspeed.

* The plane stress problem delivers in this case 160.3 N/mm². The difference is given by consideration of notch stresses and edge pressure in the FE-calculation.

** The plane stress problem delivers in this case 177.7 N/mm². The difference is given by consideration of notch stresses and edge pressure in the FE-calculation.

3 Design Inputs

3.1 Assumptions

The following assumptions are made:

- A 2D axially symmetric model for the flywheel will be used for normal operating conditions and design overspeed.
- A 2D axially symmetric model will be used for the vertical seismic load.
- A 3D model will be used for the horizontal seismic load.
- Only a segment of the flywheel and the shaft will be modelled. The results for operating and seismic load can be superposed.
- The crack size is determined from the minimum detectable single failure in ultrasonic inspection. Due to conservatism a crack with double size is considered. The crack shall be semi-penny-shaped.
- The crack will be located in the most dangerous position at the inner cylindrical surface of the flywheel. Because of the stress distribution in a rotating disc the normal of the crack plane will be in the circumferential direction, means that the maximum stress, the circumferential stress, will open the crack.
- Stress intensities resulting from the diameter step of the flywheel bore will be analysed separately and taken into account for the critical fracture speed analysis.

3.2 Input Data

The analysis is based on the following input data:

Material Specification

The material properties of the steel used for the flywheel are as follows:

Steel ASTM A508 Class 4/5 (forged)	Symbol	Value	Unit	Value	Unit
Elastic modulus	E	210000	N/mm ²	30479	ksi
Shear modulus	G	80000	N/mm ²	11611	ksi
Poisson`s ratio	ν	0.30	---	0.30	---
Mass density	ρ	7.85E-06	kg/mm ³	0.284	lb/in ²
Yield strength (min.) specified	R _{p0.2}	585	N/mm ²	85	ksi
Yield strength (min.) measured	R _{p0.2}	735	N/mm ²	106	ksi
Ultimate tensile strength specified	R _m	725 - 895	N/mm ²	105 - 130	ksi
Ultimate tensile strength measured	R _m	863	N/mm ²	125	ksi
Critical stress intensity factor specified	K _{IC}	3470	[N/mm ²]*mm ^{1/2}	100	ksi * in ^{1/2}
Critical stress intensity factor measured	K _{IC}	7148	[N/mm ²]*mm ^{1/2}	206	ksi * in ^{1/2}

Dimensions

The flywheel dimensions are taken from the drawing HTAM125306.

Loadings

The shrink stresses are calculated for the interferences as given in the drawing HTAM125307. Seismic loading is given in the Technical Specification Section H, Article 7.01:

Seismic loading	Horizontal	Vertical
Operating Basis Earthquake (OBE):	± 2.0 g	± 3.0 g
Design Basis Earthquake (DBE):	± 3.0 g	± 3.0 g

Speed definitions

The following speed rates are defined in the Technical Specification:

Normal operating speed :	1193 rpm	ABB calculation
Synchronous speed :	1200 rpm	Section H, (1.02)
Design overspeed (120 % of synchronous speed) :	1440 rpm	Section H, (10.03)
Test overspeed (125 % of synchronous speed) :	1500 rpm	Section H, (11.04)

4 Methodology

4.1 Stress analysis

4.1.1 Standstill

The analysis gives the maximum Von Mises stress along the shrink fit width at standstill (shaft / flywheel bore).

The FE-mesh for the 2D model is shown in Fig.1. It consists of 2D axially symmetric solid elements for the shaft and the flywheel. The shrink fit problem is solved by defining contact regions between the shaft and the flywheel.

The constraints imposed on flywheel and shaft are shown in Fig.1. The symbols indicate the suppressed displacement direction which are shown as marked squares. The constraints are necessary to make the calculation possible.

For the calculation of the maximum shrink stress the maximum shrinkage, according to the drawing HTAM125307, is taken into account.

Ø 790 mm:	R = 395 mm	ΔR = 0.34 mm
Ø 750 mm:	R = 375 mm	ΔR = 0.35 mm

For the calculation of the minimum transferable torque the minimum shrinkage must be considered:

Ø 790 mm:	R = 395 mm	ΔR = 0.30 mm
Ø 750 mm:	R = 375 mm	ΔR = 0.31 mm

Result: Maximum Von Mises Stress

The Von Mises stress distribution in the flywheel is shown as a fringe plot in Fig.2 and Fig.4 and as a graph plot along the width of the flywheel bore diameter in Fig.3 and Fig. 5.

Maximum stress at standstill	Unit	Maximum shrinkage	Minimum shrinkage
Standstill	rpm	0	0
Maximum Von Mises stress in the shaft	N/mm ²	313	283
Maximum Von Mises stress at the shrink fit R=395 mm	N/mm ²	180	159
Maximum Von Mises stress at the shrink fit R=375 mm	N/mm ²	188	166

The maximum value of Von Mises stress in the shaft is 313 N/mm². The maximum value of Von Mises stress in the flywheel is 188 N/mm² at the shrink fit.

Result: Minimum Transferable Torque

The radial stress as a graph plot along the shrink fit width is shown in Fig.3 and Fig. 5. From the medium radial stress in the contact region the transferable torque is calculated with the assumption for the coefficient of friction $\mu = 0.12$.

Minimum transmissible torque at standstill	Unit	Maximum shrinkage	Minimum shrinkage
Standstill	rpm	0	0
Medium radial stress at the shrink fit R=395 mm	N/mm ²	-85	-70
Medium radial stress at the shrink fit R=375 mm	N/mm ²	-90	-85
Minimum transmissible torque	Nm	2.052E+06	1.811E+06

The minimum transmissible torque is 1.811E+06 Nm. This is 83.6 times higher than the rated motor torque of 2.166E+04 Nm.

4.1.2 Normal operating speed

The analysis should show that the maximum Von Mises stress occurring at normal operating conditions is less than the admissible stress of 195 N/mm²

$$\sigma_{\text{Von Mises}} \leq R_{p0.2} / 3 = 195 \text{ N/mm}^2$$

✓ The stress distribution in the flywheel is determined by the shrink fit (shaft / flywheel bore) and the centrifugal forces at synchronous speed.

The FE-mesh for the 2D model is shown in Fig.1. It consists of 2D axially symmetric solid elements for the shaft and the flywheel. The shrink fit problem is solved by defining contact regions between the shaft and the flywheel.

The constraints imposed on flywheel and shaft are shown in Fig.1. The symbols indicate the suppressed displacement directions which are shown as marked squares. The constraints are necessary to make the calculation possible.

Result: Maximum Von Mises Stress

The Von Mises stress distribution in the flywheel is shown as a fringe plot in Fig.6 and Fig.8 and as a graph plot along the width of the flywheel bore diameter in Fig.7 and Fig. 9.

Maximum Stress at normal operating speed	Unit	Maximum shrinkage	Minimum shrinkage
Normal operating speed	rpm	1200	1200
Maximum Von Mises stress in the flywheel	N/mm ²	192	172
Maximum Von Mises stress at the shrink fit R=395 mm	N/mm ²	177	157
Maximum Von Mises stress at the shrink fit R=375 mm	N/mm ²	(192)	172

The maximum value of the Von Mises stress is 192 N/mm². This is lower than the maximum admissible Von Mises stress of 195 N/mm².

Result: Minimum Transmissible Torque

The radial stress as a graph plot along the shrink fit width is shown in Fig.7 and Fig. 9. From the medium radial stress in the contact region the transmissible torque is calculated with the assumption for the coefficient of friction $\mu = 0.12$.

Minimum Transmissible Torque at normal operating speed	Unit	Maximum shrinkage	Minimum shrinkage
Normal operating speed	rpm	1200	1200
Medium radial stress at the shrink fit R=395 mm	N/mm ²	- 40	-30
Medium radial stress at the shrink fit R=375 mm	N/mm ²	- 45	-38
Minimum transmissible torque	Nm	9.951E+05	7.936E+05

The minimum transmissible torque is 7.936E+05 Nm. This is 36.64 times higher than the rated motor torque of 2.166E+04 Nm.

4.1.3 Test overspeed

The analysis should show that the maximum Von Mises stress occurring at test overspeed is less than the admissible stress of 390 N/mm².

$$\sigma_{\text{Von Mises}} \leq R_{p0.2} \cdot 2/3 = 390 \text{ N/mm}^2.$$

The stress distribution in the flywheel is determined by the shrink fit (shaft / flywheel bore) and the centrifugal forces at test overspeed.

The FE-mesh for the 2D model is shown in Fig.1. It consists of 2D axially symmetric solid elements for the shaft and the flywheel. The shrink fit problem is solved by defining contact regions between the shaft and the flywheel.

The constraints imposed on flywheel and shaft are shown in Fig.1. The symbols indicate the suppressed displacement direction which are shown as marked squares. The constraints are necessary to make the calculation possible.

Result: Maximum Von Mises stress

The Von Mises stress distribution in the flywheel is shown as a fringe plot in Fig.10 and Fig.12 and as a graph plot along the width of the flywheel bore diameter in Fig.11 and Fig. 13.

Maximum Stress at test overspeed	Unit	Maximum shrinkage	Minimum shrinkage
Test overspeed	rpm	1500	1500
Maximum Von Mises stress in the flywheel	N/mm ²	196	177
Maximum Von Mises stress at the shrink fit R=395 mm	N/mm ²	181	162
Maximum Von Mises stress at the shrink fit R=375 mm	N/mm ²	196	177

The maximum value of the Von Mises stress is 196 N/mm². This is lower than the maximum admissible Von Mises stress of 390 N/mm².

Result: Minimum Transmissible Torque

The radial stress as a graph plot along the shrink fit width is shown in Fig.11 and Fig. 13. From the medium radial stress in the contact region the transmissible torque is calculated with the assumption for the coefficient of friction $\mu = 0.12$.

Minimum Transmissible Torque at test overspeed	Unit	Maximum shrinkage	Minimum shrinkage
Test overspeed	rpm	1500	1500
Medium radial stress at the shrink fit R=395 mm	N/mm ²	- 18	-8
Medium radial stress at the shrink fit R=375 mm	N/mm ²	- 22	-14
Minimum transmissible torque	Nm	4.673E+05	2.547E+05

The minimum transmissible torque is 2.547E+05 Nm. This is 11.76 times higher than the rated motor torque of 2.166E+04 Nm.

4.2 Seismic analysis

The analysis should show that the maximum Von Mises stress occurring at Upset Loading Conditions and Faulted Loading Conditions defined in Section H (7.01) is less than the admissible stress of 526 N/mm².

$$\sigma_{\text{Von Mises}} \leq 0.9 * R_{p0.2} = 526 \text{ N/mm}^2$$

Stresses under Normal Loading Conditions, vertical seismic load and horizontal seismic load can be superposed to calculate the combined stress in the flywheel. The equivalent Von Mises stress is defined e.g. in J.A.Collins, „Failure of Materials in Mechanical Design“ or Robert C. Juvinall, „Stress Strain Strength“ as follows:

$$\sigma_{\text{Von Mises}} = \sqrt{\sigma_x^2 + \sigma_y^2 + \sigma_z^2 - \sigma_x * \sigma_y - \sigma_x * \sigma_z - \sigma_y * \sigma_z + 3 * (\tau_{xy}^2 + \tau_{xz}^2 + \tau_{yz}^2)} \quad \text{Equation 1}$$

with $\sigma_x, \sigma_y, \sigma_z$ main tensions
 $\tau_{xy}, \tau_{xz}, \tau_{yz}$ shear tensions

Therefore the vertical seismic load and the horizontal seismic load are calculated separately and superposed later.

To obtain the maximum stresses under Normal Loading Conditions the stresses are calculated with maximum shrinkage.

4.2.1 Normal Loading Conditions

The stress distribution in the flywheel is determined for the maximum shrink fit and for the centrifugal forces at synchronous speed (1200 rpm).

In Fig.14 to Fig.17 the fringe plot of the von Mises stress and the graph plots of the stress distributions along the shrink fit width under Normal Loading Conditions are shown. The maximum stress values are listed in the following table.

Stresses under Normal Loading Conditions	Symbol	Unit	Value
Maximum Von Mises stress	$\sigma_{\text{Von Mises}}$	N/mm ²	192
Maximum Von Mises stress at the shrink fit R=395 mm	$\sigma_{\text{Von Mises}}$	N/mm ²	177
Maximum Von Mises stress at the shrink fit R=375 mm	$\sigma_{\text{Von Mises}}$	N/mm ²	192
Maximum radial stress at the shrink fit R=395 mm	σ_{xx}	N/mm ²	-52
Maximum radial stress at the shrink fit R=375 mm	σ_{xx}	N/mm ²	-55
Maximum shear stress at the shrink fit R=395 mm	τ_{xy}	N/mm ²	10
Maximum shear stress at the shrink fit R=375 mm	τ_{xy}	N/mm ²	13
Maximum axial stress at the shrink fit R=395 mm	σ_{yy}	N/mm ²	15
Maximum axial stress at the shrink fit R=375 mm	σ_{yy}	N/mm ²	17
Maximum tangential stress at the shrink fit R=395 mm	σ_{zz}	N/mm ²	155
Maximum tangential stress at the shrink fit R=375 mm	σ_{zz}	N/mm ²	171

4.2.2 Vertical Seismic Load (OBE and DBE)

The maximum vertical seismic load for the Operating Basis Earthquake (OBE) and for the Design Basis Earthquake (DBE) are equal. The stress distribution in the flywheel under vertical seismic load is determined for $\pm 3g$ vertical acceleration and the dead weight.

The FE-mesh for the 2D vertical seismic load model is shown in [Fig.18](#). It consists of 2D axially symmetric solid elements for the shaft and the flywheel, which are rigidly connected to each other. The constraints imposed on flywheel and shaft are shown in [Fig.18](#). They are necessary to make the calculation possible.

The Von Mises stress is shown in [Fig.19](#). The maximum stress values are listed in the following table, the corresponding graph plots are shown in [Fig.20](#) to [Fig.22](#).

Stresses under Vertical Seismic Load (OBE and DBE)	Symbol	Unit	Value
Maximum Von Mises stress	$\sigma_{\text{Von Mises}}$	N/mm ²	59
Maximum Von Mises stress at the shrink fit R=395 mm	$\sigma_{\text{Von Mises}}$	N/mm ²	17
Maximum Von Mises stress at the shrink fit R=375 mm	$\sigma_{\text{Von Mises}}$	N/mm ²	15
Maximum radial stress at the shrink fit R=395 mm	σ_{xx}	N/mm ²	17
Maximum radial stress at the shrink fit R=375 mm	σ_{xx}	N/mm ²	-16
Maximum shear stress at the shrink fit R=395 mm	τ_{xy}	N/mm ²	-4
Maximum shear stress at the shrink fit R=375 mm	τ_{xy}	N/mm ²	-4
Maximum axial stress at the shrink fit R=395 mm	σ_{yy}	N/mm ²	11
Maximum axial stress at the shrink fit R=375 mm	σ_{yy}	N/mm ²	4
Maximum tangential stress at the shrink fit R=395 mm	σ_{zz}	N/mm ²	15
Maximum tangential stress at the shrink fit R=375 mm	σ_{zz}	N/mm ²	-14

The maximum value of Von Mises stress in the shaft is 59 N/mm². The maximum value of Von Mises stress in the flywheel is 17 N/mm² at the shrink fit.

4.2.3 Horizontal Seismic Load (OBE)

The stress distribution in the flywheel during an Operating Basis Earthquake (OBE) is determined by $\pm 2g$ horizontal acceleration.

The FE-mesh of the 3D horizontal seismic load model is shown in Fig.23. It consists of 3D solid elements for the shaft and the flywheel, which are rigidly connected to each other. Only half of the flywheel and a quarter of the shaft are modelled. Equivalent boundary conditions at the cutting planes are introduced. The constraints imposed on flywheel and shaft are shown in Fig.23. They are necessary to make the calculation possible.

To avoid an unnecessary increase of model size, the flywheel bore is simplified. Only the smaller shrink fit radius $R = 375 \text{ mm}$ is considered.

The maximum stress values are listed in the following table, the corresponding fringe plots are shown in Fig.24 and Fig.25.

Stresses under Seismic Load Horizontal (OBE)	Symbol	Unit	Value
Maximum Von Mises stress	$\sigma_{\text{Von Mises}}$	N/mm^2	2.4
Maximum radial stress	σ_{xx}	N/mm^2	0.5
Maximum shear stress	τ_{xy}	N/mm^2	1.1
Maximum axial stress	σ_{yy}	N/mm^2	0.9
Maximum tangential stress	σ_{zz}	N/mm^2	2.5

Due to conservatism the maximum calculated stresses for the whole model are used.

4.2.4 Horizontal Seismic Load (DBE)

The stress distribution in the flywheel during an Operating Basis Earthquake (OBE) is determined by $\pm 3g$ horizontal acceleration.

The FE-mesh of the 3D horizontal seismic load model is shown in Fig.23. It consists of 3D solid elements for the shaft and the flywheel, which are rigidly connected to each other. Only half of the flywheel and a quarter of the shaft are modelled. Equivalent boundary conditions at the cutting planes are introduced. The constraints imposed on flywheel and shaft are shown in Fig.23. They are necessary to make the calculation possible.

To avoid an unnecessary increase of model size, the flywheel bore is simplified. Only the smaller shrink fit radius $R = 375$ mm is considered.

The maximum stress values are listed in the following table, the corresponding fringe plots are shown in Fig.26 to Fig.27.

Stresses under Seismic Load Horizontal (DBE)	Symbol	Unit	Value
Maximum Von Mises stress	$\sigma_{\text{Von Mises}}$	N/mm ²	3.6
Maximum radial stress	σ_{xx}	N/mm ²	0.7
Maximum shear stress	τ_{xy}	N/mm ²	1.6
Maximum axial stress	σ_{yy}	N/mm ²	1.3
Maximum tangential stress	σ_{zz}	N/mm ²	3.7

Due to conservatism the maximum calculated stresses for the whole model are used.

4.2.5 Synchronous Speed and OBE

To calculate the combined stress contribution in the flywheel under Upset Loading Conditions, the stresses under synchronous speed, vertical seismic load (OBE) and horizontal seismic load (OBE) will be superposed.

To get the maximum stresses, the maximum values of all stresses at the shrink fit are considered.

The stress-superposition of the maximum values lead to the following table:

Combined stresses under synchronous speed and OBE	Unit	Synchronous Speed Maximum Shrinkage	Seismic Load Vertical $\pm 3g$	Seismic Load Horizontal $\pm 2g$	Combined Stress Upset Loading Conditions
Maximum Von Mises stress	N/mm ²	192	17	2.4	200.4
Maximum radial stress	N/mm ²	-55	17	0.5	-37.5
Maximum shear stress	N/mm ²	13	-4	1.1	10.1
Maximum axial stress	N/mm ²	17	11	0.9	28.9
Maximum tangential stress	N/mm ²	171	15	2.5	188.5

The combined Von Mises stress under synchronous speed and OBE is calculated according to equation 1.

The maximum value of the Von Mises stress under Upset Loading Conditions is 200.4 N/mm². This is lower than the maximum admissible Von Mises stress of 526 N/mm².

4.2.6 Synchronous Speed and DBE

To calculate the combined stress contribution in the flywheel under Faulted Loading Conditions, the stresses under synchronous speed, vertical seismic load (DBE) and horizontal seismic load (DBE) will be superposed.

To get the maximum stresses, the maximum values of all stresses at the shrink fit are considered.

The stress-superposition of the maximum values lead to the following table:

Combined stresses under synchronous speed and DBE	Unit	Synchronous Speed Maximum Shrinkage	Seismic Load Vertical $\pm 3g$	Seismic Load Horizontal $\pm 3g$	Combined Stress Faulted Loading Conditions
Maximum Von Mises stress	N/mm ²	192	17	3.6	203.8
Maximum radial stress	N/mm ²	-55	17	0.7	-37.3
Maximum shear stress	N/mm ²	13	-4	1.6	10.6
Maximum axial stress	N/mm ²	17	11	1.3	19.3
Maximum tangential stress	N/mm ²	171	15	3.7	189.7

The combined Von Mises stress under synchronous speed and DBE is calculated according to equation 1.

The maximum value of the Von Mises stress under Faulted Loading Conditions is 203.8 N/mm². This is lower than the maximum admissible Von Mises stress of 526 N/mm².

4.3 Non-Ductile Fracture Analysis

Critical fracture speeds for non-ductile fracture will be calculated according to the calculation as reported in the paper of Riccardella & Bamford „Reactor Coolant Pump Flywheel Overspeed Evaluation“. The largest non-detectable single defect will be considered.

A Crack Growth Prediction Analysis which is attached in APPENDIX D shows that cycling the motor from zero to overspeed for more than 10000 times will not cause a crack to grow to its critical size.

The analysis should show that the critical fracture speed of the flywheel is higher than the predicted LOCA overspeed of 3697 rpm reported in ABB/CE Letter ST 95-0714 dated December 26, 1995.

Material Properties

Elastic modulus E, Poisson`s Ratio ν , mass density ρ are needed and given in 3.2.

Defect size

The largest defect in the region with the highest stress, e.g. the bore region of the flywheel, will be analysed. According to the ABB Ultrasonic Testing Specification HTAY 875-20-001.36 a maximum single defect with an area of 5 mm² is detectable in the r,z-plane of the flywheel. This defect is assumed to be semi-penny-shaped.

The defect size is:

$$A = \frac{1}{2} * \left(\frac{d^2 * \pi}{4} \right) = 5 \text{ mm}^2$$

this results in a defect-diameter d

$$d = \sqrt{\frac{8 * A}{\pi}} = 3.57 \text{ mm}$$

Due to conservatism a crack with double size will be analysed. The radius of this critical defect is given by:

$$c = a + 2d$$

An approximate solution for the stress intensity factor for a radial crack emanating from the bore of a rotating disk has been reported by Williams and Isherwood, referred to in the paper of Riccardella & Bamford „Reactor Coolant Pump Flywheel Overspeed Evaluation, and is given by the following expression:

$$K_I = \rho \omega^2 b^{2.5} \Phi \sqrt{\frac{\pi * \left(\frac{c * a}{b * b} \right)}{1 - \nu^2}}$$

$$\Phi = \left(\frac{3+\nu}{32}\right) \left[3\left(1+\frac{a^2}{b^2}\right) + 3\left(\frac{a}{b}\right)\left(\frac{b}{c}\right) + \left(1+\frac{a}{b}+\frac{a^2}{b^2}\right) \left(\frac{1-\frac{a}{b}}{1-\frac{c}{b}}\right) \right] - \left(\frac{1+3\nu}{32}\right) \left[\frac{\left(\frac{c}{b}\right)^3 - \left(\frac{a}{b}\right)^3}{\left(\frac{c}{b} - \frac{a}{b}\right)} + \frac{1}{3} \frac{\left(1-\frac{a}{b}\right)^3}{\left(1-\frac{c}{b}\right)} \right]$$

The stress rise factor α for the noddges at the inner bore diameter of the flywheel is calculated in a Finite Element Analysis using the same mesh as in the stress analysis. The analysis is made for a rotational speed of 2100 rpm because under these conditions the shrink fit is surely open. With the critical stress intensity factor K_{IC} the critical fracture speeds for non-ductile fracture of the flywheel can be calculated.

$$\frac{\alpha * K_I}{\omega^2} = \frac{K_{IC}}{\omega_c^2} = const.$$

$$\omega_c = \sqrt{\frac{K_{IC}}{\alpha * K_I} * \omega^2}$$

$$n_c = \frac{60\omega_c}{2\pi}$$

The calculations for both flywheel bore diameters are summarized in the following table:

Critical fracture speeds of non-ductile analysis				
	Variable	Unit	Ø 790 mm	Ø 750 mm
Input				
Inner radius	a	mm	395	375
Outer radius	b	mm	925	925
Crack position radius	c	mm	402.14	382.14
Poisson's ratio	ν	---	0.3	0.3
Mass density	ρ	kg/mm ³	7.85E-06	7.85E-06
Speed	n	rpm	2100	2100
Speed	n	rad/s	220	220
Stress rise factor	α	---	1.11	1.11
Critical stress intensity factor	K_{IC}	[N/mm ²]*mm ^{1/2}	7158.5	7158.5
Output				
Stress intensity factor	K_I	[N/mm ²]*mm ^{1/2}	1287.33	1275.48
Critical fracture speed	ω_c	rad/s	492.21	494.49
Critical fracture speed	n_c	rpm	4700	4722

The minimum critical fracture speed due to non-ductile fracture analysis is 4700 rpm. This is higher than the predicted LOCA overspeed of 3697 rpm .

4.4 Ductile Fracture Analysis

Critical fracture speeds will be calculated according to the calculation as reported in the paper of Riccardella & Bamford „Reactor Coolant Pump Flywheel Overspeed Evaluation“

Material Properties

Elastic constants E and ν and the ultimate tensile strength F_u are needed and given in 3.2.

Faulted Conditions Stress Limit

The capacity of a structure to resist ductile failure with sufficient margin of safety during faulted conditions can be demonstrated by meeting the faulted condition criteria of Section 3 of the ASME Boiler and Pressure Vessel Code (Appendix F). The faulted condition limits for elastic analysis are as follows:

- membrane stress $P_m < 0.7 F_u$
- membrane and bending stress: $P_m + P_b < 1.05 F_u$

where F_u is the minimum specified ultimate tensile strength of the material, P_m is the primary membran stress intensity under faulted condition loading, and P_b is the primary bending stress intensity.

In order to apply the stress limits to a non-linear stress distribution the actual stress distribution must be resolved into its membrane and bending components:

$$P_m := \frac{1}{b-a} * \int_a^b \sigma_{zz} dr \quad P_b := \frac{6}{(b-a)^2} * \int_a^b \sigma_{zz} * (r_m - r) dr \quad r_m := \frac{(a+b)}{2}$$

where r_m is the flywheel mean radius, a is the outer radius of the flywheel, b is the inner radius of the flywheel and σ_{zz} is the circumferential stress.

Substituting the circumferential stress term

$$\sigma_{zz} = \left(\frac{3+\nu}{8} \right) \rho \omega^2 \left[b^2 + a^2 + \frac{a^2 b^2}{r^2} - \left(\frac{1+3\nu}{3+\nu} \right) r^2 \right]$$

and carrying out the integrals yields

$$P_m = A_1 * \omega^2 \quad P_b = A_2 * \omega^2$$

with

$$A_1 = \left(\frac{3+v}{8}\right) \frac{\rho}{(b-a)} (b^2 - a^2) \left[1 - \frac{1}{3} \left(\frac{1+3v}{3+v}\right)\right]$$

$$A_2 = \left(\frac{3+v}{8}\right) \frac{6\rho}{(b-a)^2} \left\{ \frac{b^4(1+3v)}{12} + \frac{b^2 a}{2} \left[1 - \frac{1}{3} \left(\frac{1+3v}{3+v}\right)\right] - a^2 b^2 \ln\left(\frac{b}{a}\right) - \frac{ba^3}{2} \left[1 + \frac{1}{3} \left(\frac{1+3v}{3+v}\right)\right] - \frac{a^4(1+3v)}{12} \right\}$$

This equations will now be compared with the faulted condition limits in order to calculate the critical fracture speed of the flywheel.

$$\omega_c := \sqrt{0.7 \frac{F_u}{A_1}} \quad n_c := \frac{60\omega_c}{2\pi}$$

The calculations for both flywheel bore diameters are summarized in the following table:

Critical fracture speeds of ductile fracture analysis				
Input	Variable	Unit	Ø 790 mm	Ø 750 mm
Inner radius	a	mm	395	375
Outer radius	b	mm	925	925
Poisson's ratio	v		0.3	0.3
Measured tensile strength	F _u	N/mm ²	863	863
Output				
Primary membrane stress intensity per omega ²	A ₁	N/mm ²	0.0036032	0.0035145
Primary bending stress intensity per omega ²	A ₂	N/mm ²	0.0008784	0.0010525
Critical fracture speed (membrane stress)	ω _{c1}	rad/s	409.46	414.59
Critical fracture speed (membrane and bending stress)	ω _{c2}	rad/s	449.65	445.43
Critical fracture speed (membrane stress)	n _{c1}	rpm	3910	3959
Critical fracture speed (membrane and bending stress)	n _{c2}	rpm	4294	4254

The minimum critical fracture speed due to ductile fracture analysis is 3910 rpm. This is higher than the predicted LOCA overspeed of 3697 rpm .

5 References

The analysis is based on the following documents and specifications:

- Technical Specification Section H, Contract 1977
- Drawings HTAM 125306 and HTAM 125307
- The pre- and postprocessing and the calculations are performed on an Celebris XL590 computer using the finite element programm MECHANICA (Version 7.0) from RASNA CORPORATION, San Jose CA, USA.
- MECHANICA Reference Manuals Release 7.0 from RASNA CORPORATION, San Jose CA, USA, December 1994
- Riccardelli and W. H. Bamford, Reactor Coolant Pump Flywheel Overspeed Evaluation, Journal of Pressure Vessel Technology, Nov. 1974, pp279-285
- ABB-Specification HTAY 875-20-001.36 for Ultrasonic Testing
- J. A. Collins, Failure of Materials in Mechanical Design, John Wiley & Sons, 1981, (p.137)
- Robert C. Juvinall, Stress Strain and Strength, McGraw - Hill Book Company, 1967 (p.85)
- ABB/CE Letter ST-95-0714 dated December 26, 1995
- LADICIM, Informe Sobre Ensayos de Tenacidad a Fractura a Traves de la Integral Jo Santander, 17. May 1996

APPENDIX A: SYSTEM OF UNITS

System of Units

To Convert to		From		Divide by
Am. Unit	Symbol	SI Unit	Symbol	Am. Unit
inch	in	millimetre	mm	2.540E+01
foot	ft	metre	m	3.048E-01
foot	ft	millimetre	mm	3.048E+02
foot ²	sq ft	metre ²	m ²	9.290E-02
foot/second ²	ft/s ²	metre/second ²	m/s ²	3.048E-01
pound-mass	lb	kilogram	kg	4.536E-01
pound-force	lbf	Newton	N	4.448
kilopound-force/inch ²	ksl	Newton/millimetre ²	N/mm ²	6.895
kilopound-force inch	ksl in	Newton/millimetre	N/mm	1.751E+02
kilopound-force inch ^{1/2}	ksl in ^{1/2}	[Newton/millimetre ²] millimetre ^{1/2}	* [N/mm ²]*mm ^{1/2}	3.475E+01
pound-force/foot ²	psf	Newton/millimetre ²	N/mm ²	4.800E-05
foot pound-force	ft lbf	Newton millimetre	Nmm	1.356E+03

APPENDIX B: LIST OF SYMBOLS

List of Symbols

Symbol	SI-Unit	Am. Unit	Meaning
a	mm	in	Flywheel bore radius
b	mm	in	Outer flywheel radius
c	mm	in	Crack position radius
d	mm	in	Defect-Diameter
n	1/min	rpm	Rotational speed
n _c	1/min	rpm	Critical fracture speed
r	mm	in	Radius
A	mm	in ²	Crack area
E	N/mm ²	ksi	Young's modulus
F _u	N/mm ²	ksi	Ultimate tensile strength
G	N/mm ²	ksi	Shear modulus
K _I	[N/mm ²]*mm ^{1/2}	ksi * in ^{1/2}	Stress intensity factor
K _{IC}	[N/mm ²]*mm ^{1/2}	ksi * in ^{1/2}	Critical stress intensity factor
R _m	N/mm ²	ksi	Ultimate tensile strength
R _{p0.2}	N/mm ²	ksi	Yield strength
α	---	---	Stress rise factor
ν	---	---	Poisson's ratio
ω	rad/s	rad/s	Angular velocity
μ	---	---	Coefficient of friction
ρ	kg/mm ³	lb/in ³	Mass density
σ _{Von Mises}	N/mm ²	ksi	Von Mises stress
σ _{xx} , σ _{yy} , σ _{zz}	N/mm ²	ksi	Main tensions
τ _{xy} , τ _{xz} , τ _{yz}	N/mm ²	ksi	Shear tensions

APPENDIX C: FIGURES

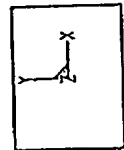
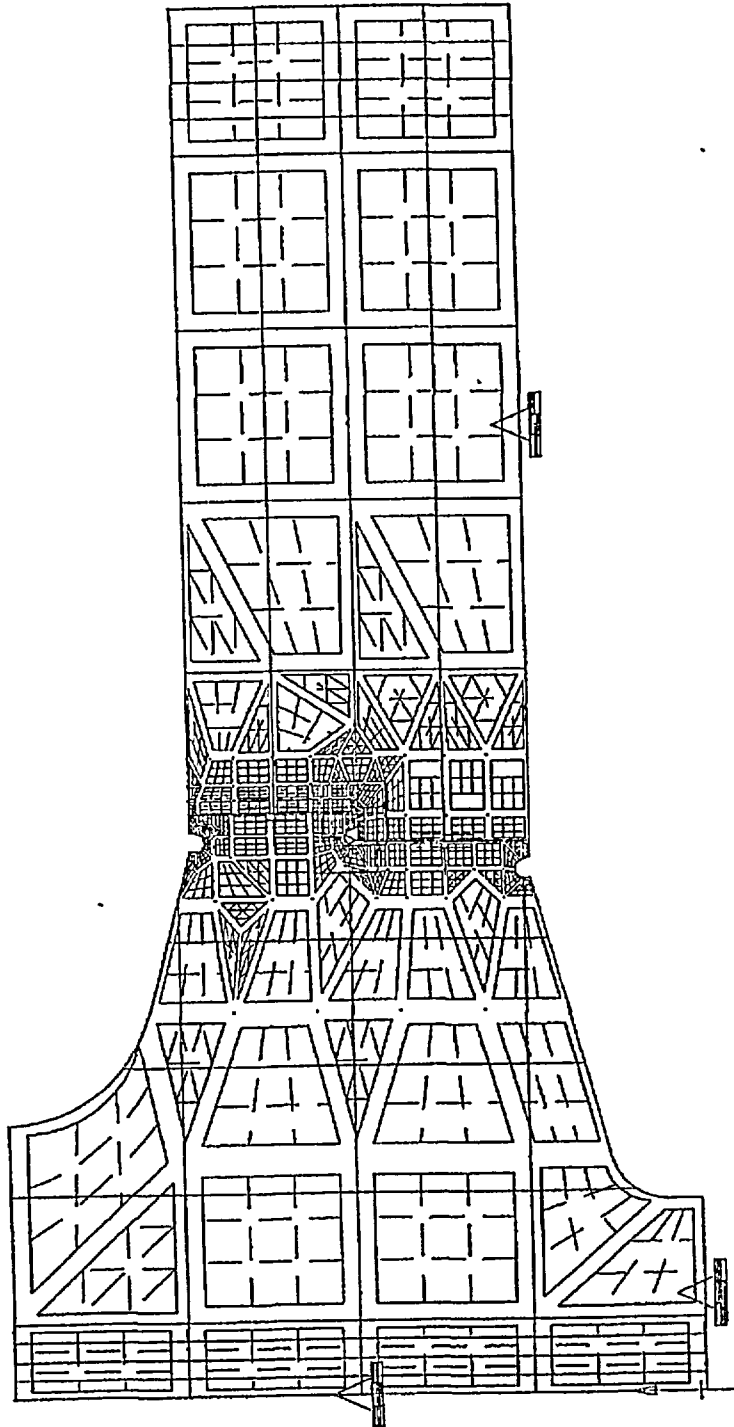
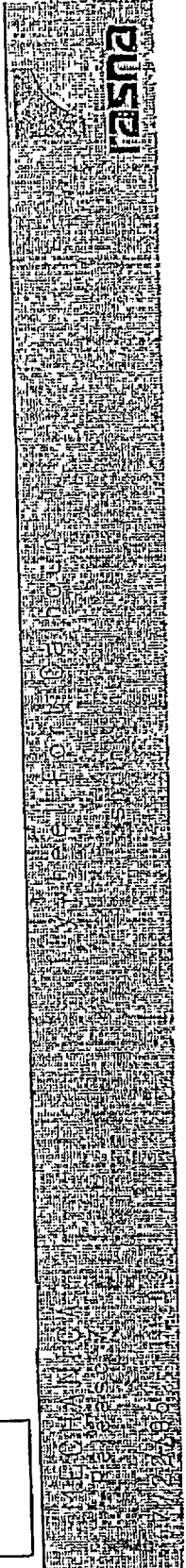
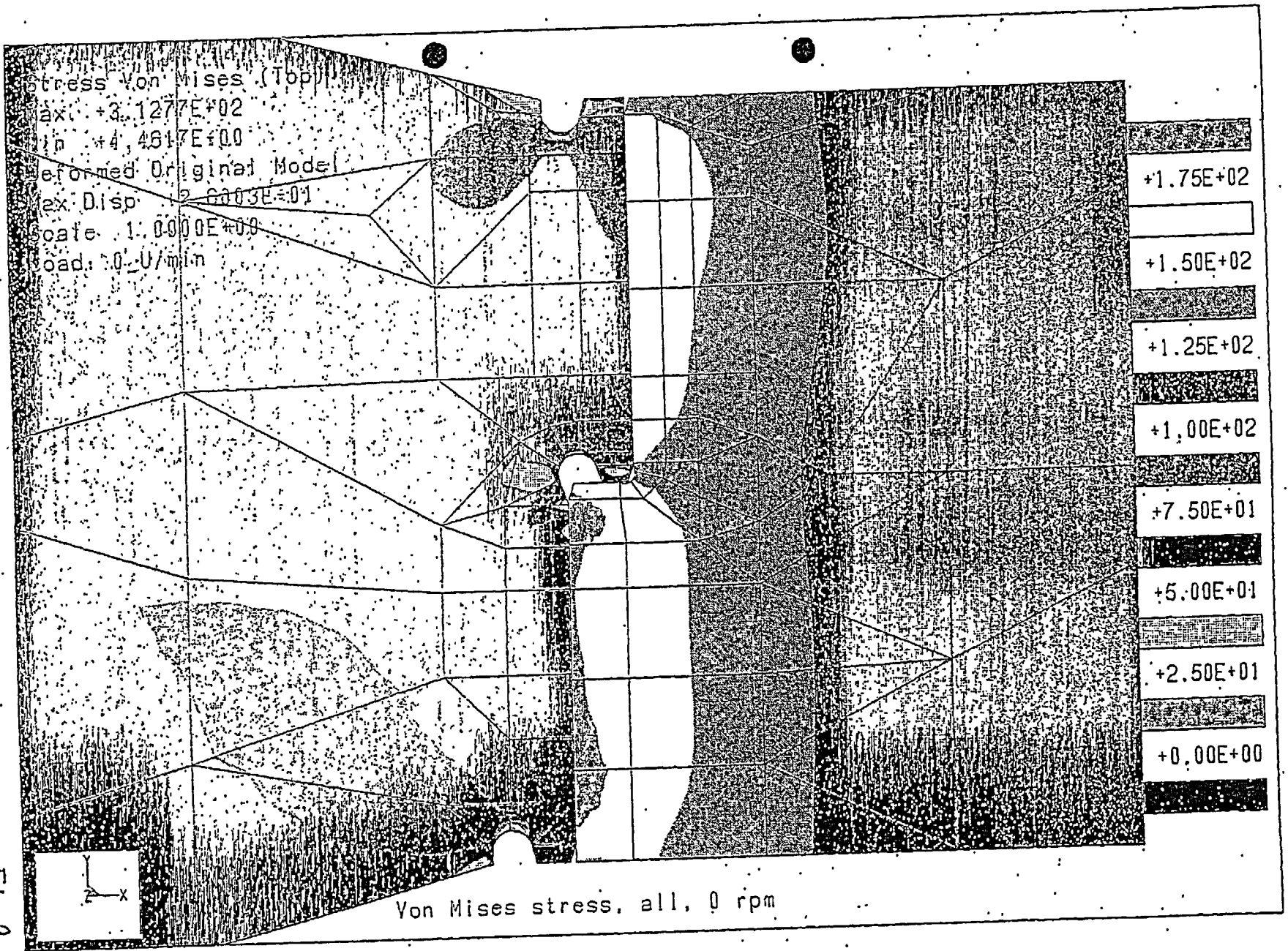


Fig. 1



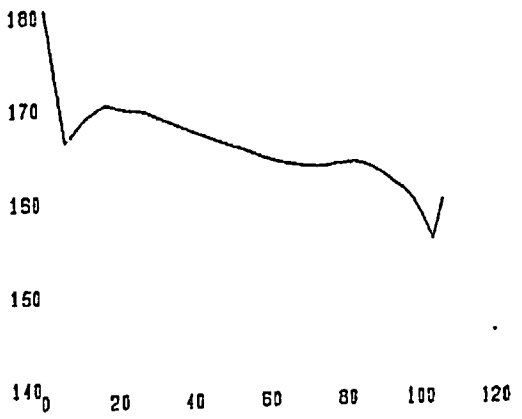
The original document is of questionable quality but what follows is the best available image.

Color Graph



Stress Von Mises (Top)
Curves
Load: 0_U/min

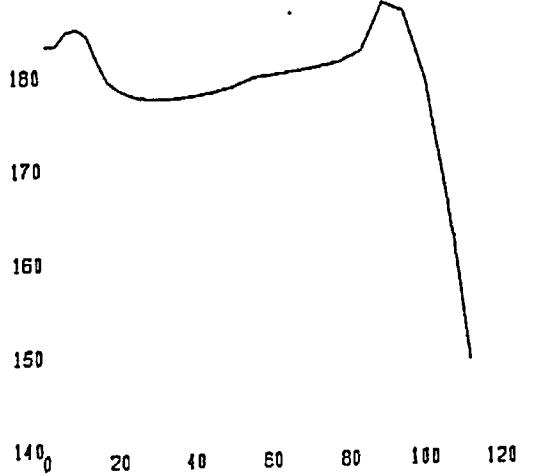
Stress Von Mises



Von Mises stress, shrink fit 790 mm, 0 rpm

Stress Von Mises (Top)
Curves
Load: 0_U/min

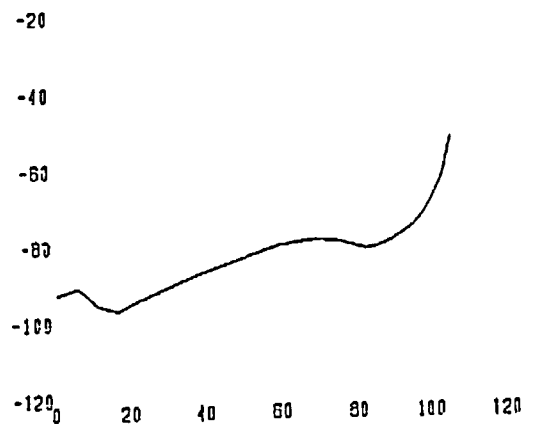
Stress Von Mises



Von Mises stress, shrink fit 750 mm, 0 rpm

Stress XX (Top)
Curves
Load: 0_U/min

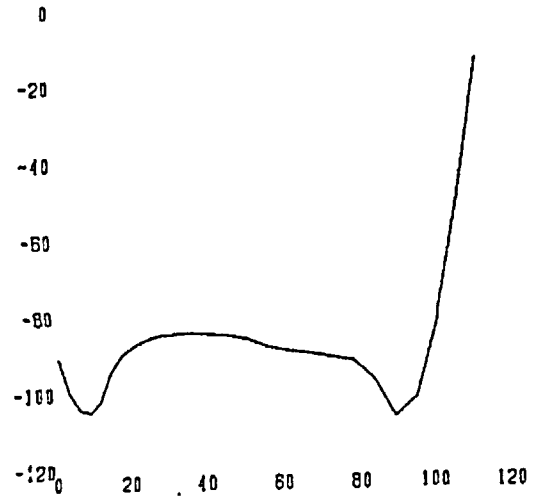
Stress Stress XX



radial stress, shrink fit 790 mm, 0 rpm

Stress XX (Top)
Curves
Load: 0_U/min

Stress Stress XX

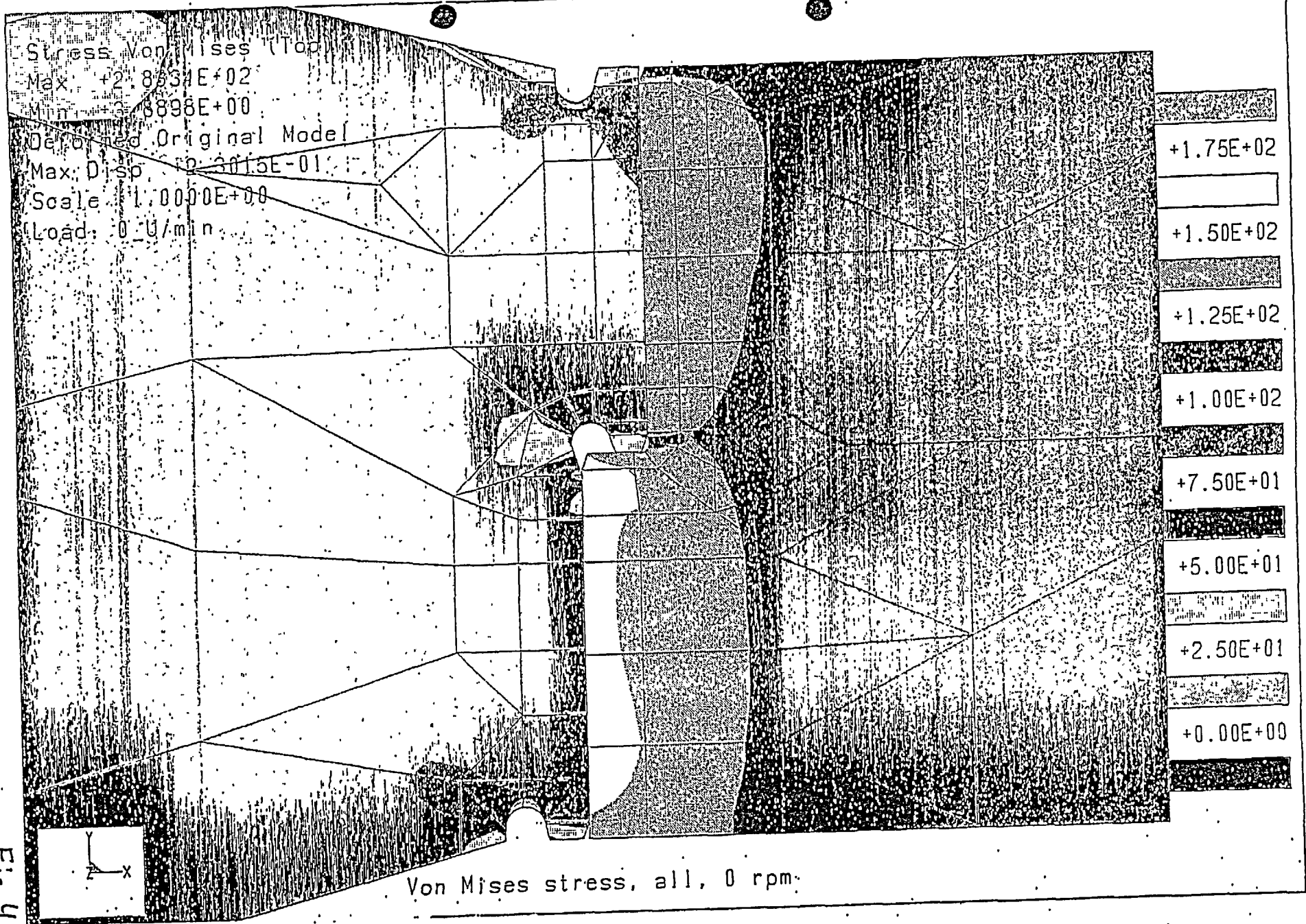


radial stress, shrink fit 750 mm, 0 rpm

Fig. 3

The original document is of questionable quality but what follows is the best available image.

Color Graph

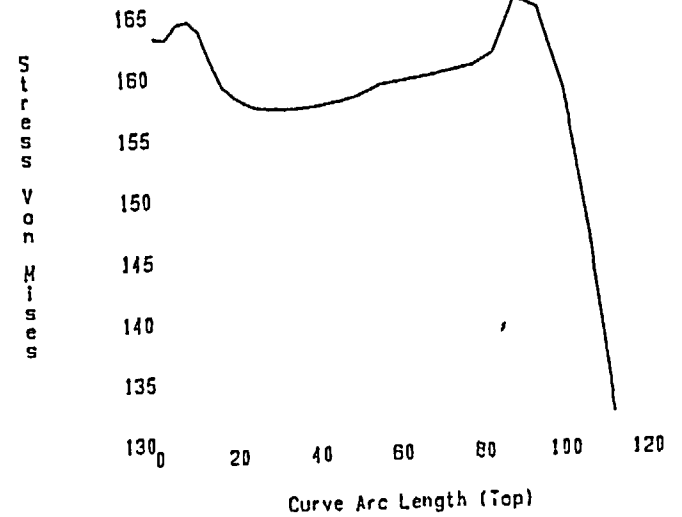


Stress Von Mises (Top)
Curves
Load: 0_U/min



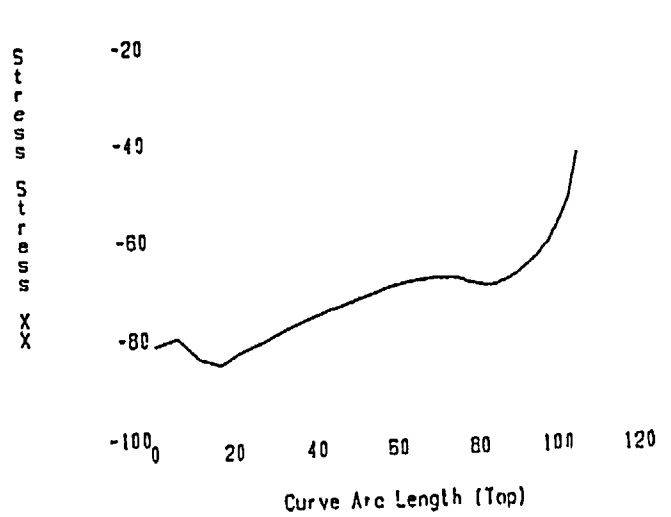
Von Mises stress, shrink fit 0.780 mm, 0 rpm

Stress Von Mises (Top)
Curves
Load: 8_U/min



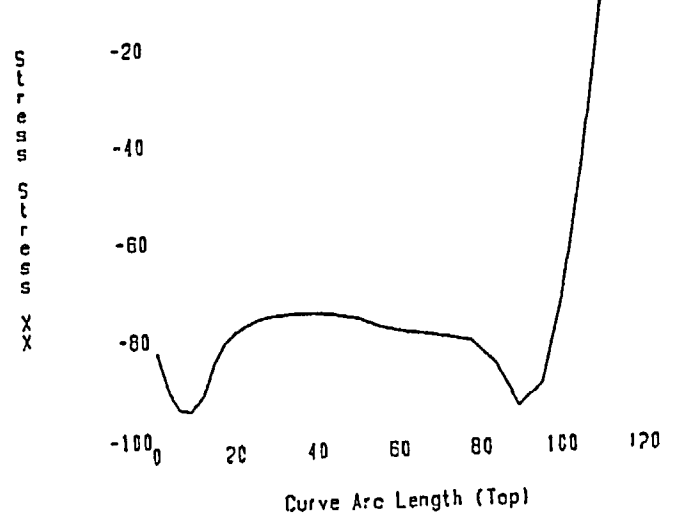
Von Mises stress, shrink fit 0.750 mm, 8 rpm

Stress XX (Top)
Curves
Load: 0_U/min



radial stress, shrink fit 0.780 mm, 0 rpm

Stress XX (Top)
Curves
Load: 0_U/min



radial stress, shrink fit 0.750 mm, 8 rpm

Fig. 5

The original document is of questionable quality but what follows is the best available image.

Color Graph

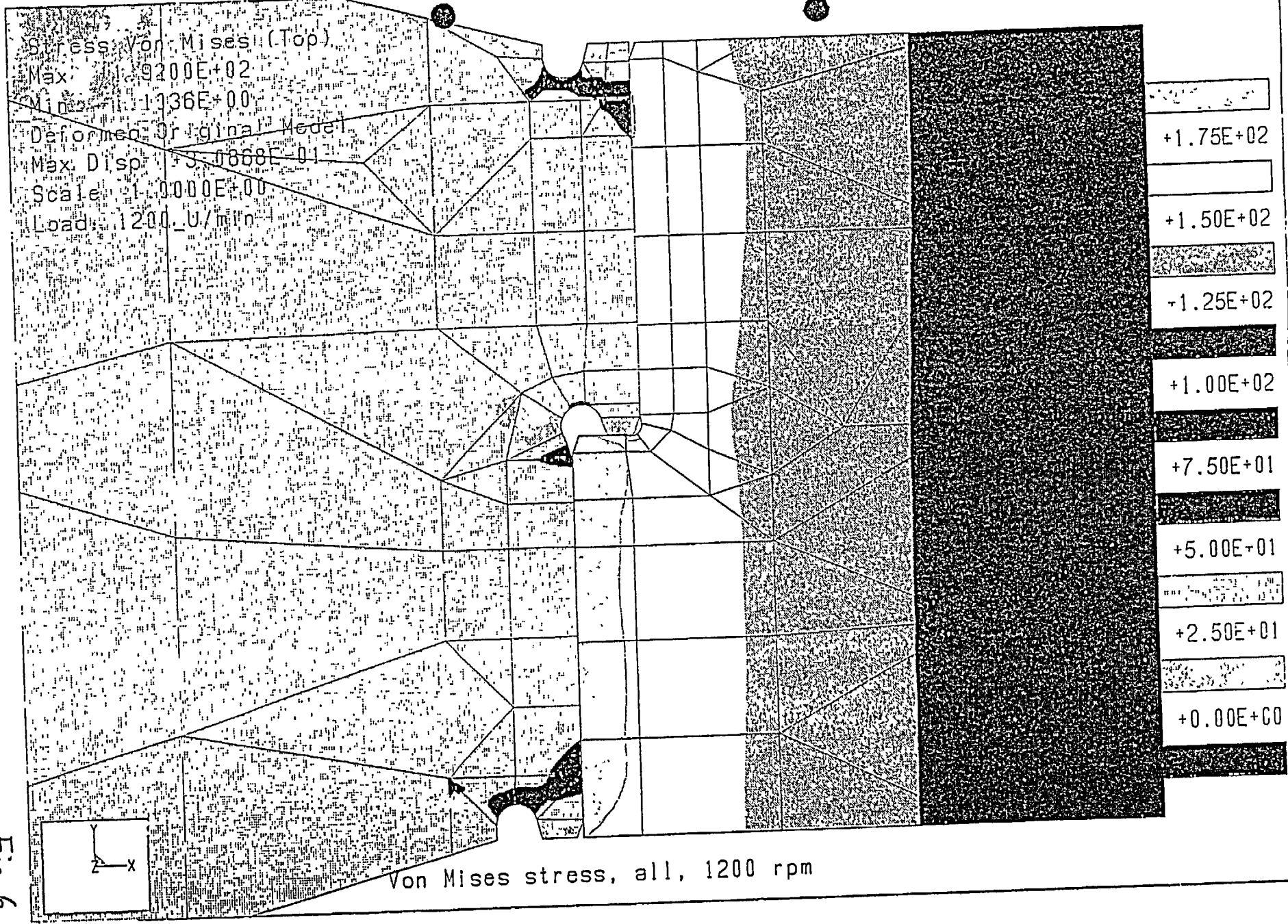
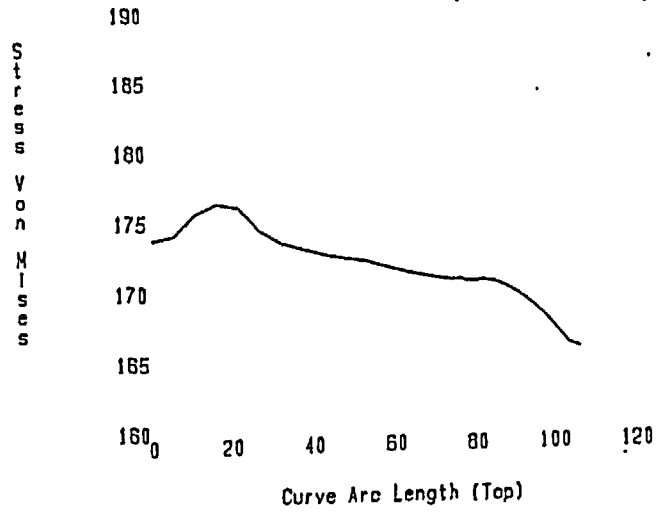


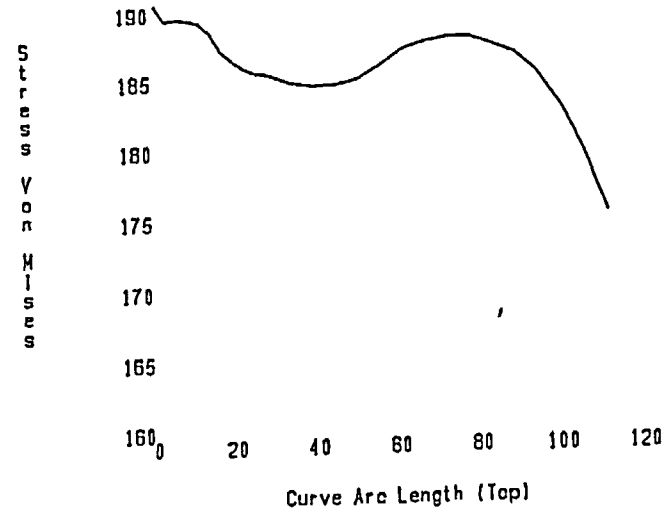
Fig. 6

Stress Von Mises (Top)
Curves
Load: 1200_U/min



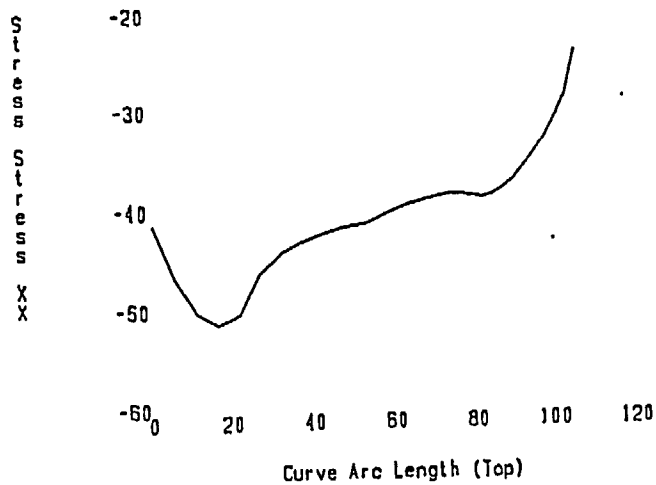
Von Mises stress, shrink fit Ø 790 mm, 1200 rpm

Stress Von Mises (Top)
Curves
Load: 1200_U/min



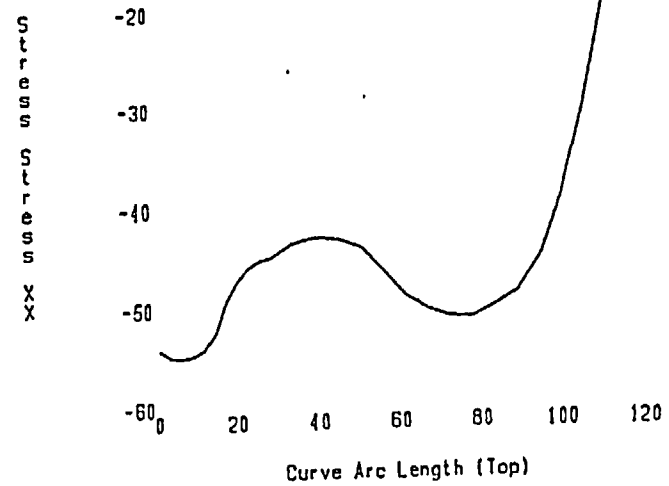
Von Mises stress, shrink fit Ø 750 mm, 1200 rpm

Stress XX (Top)
Curves
Load: 1200_U/min



radial stress, shrink fit Ø 790 mm, 1200 rpm

Stress XX (Top)
Curves
Load: 1200_U/min



radial stress, shrink fit Ø 750 mm, 1200 rpm

Fig. 7

The original document is of questionable quality but what follows is the best available image.

Color Graph

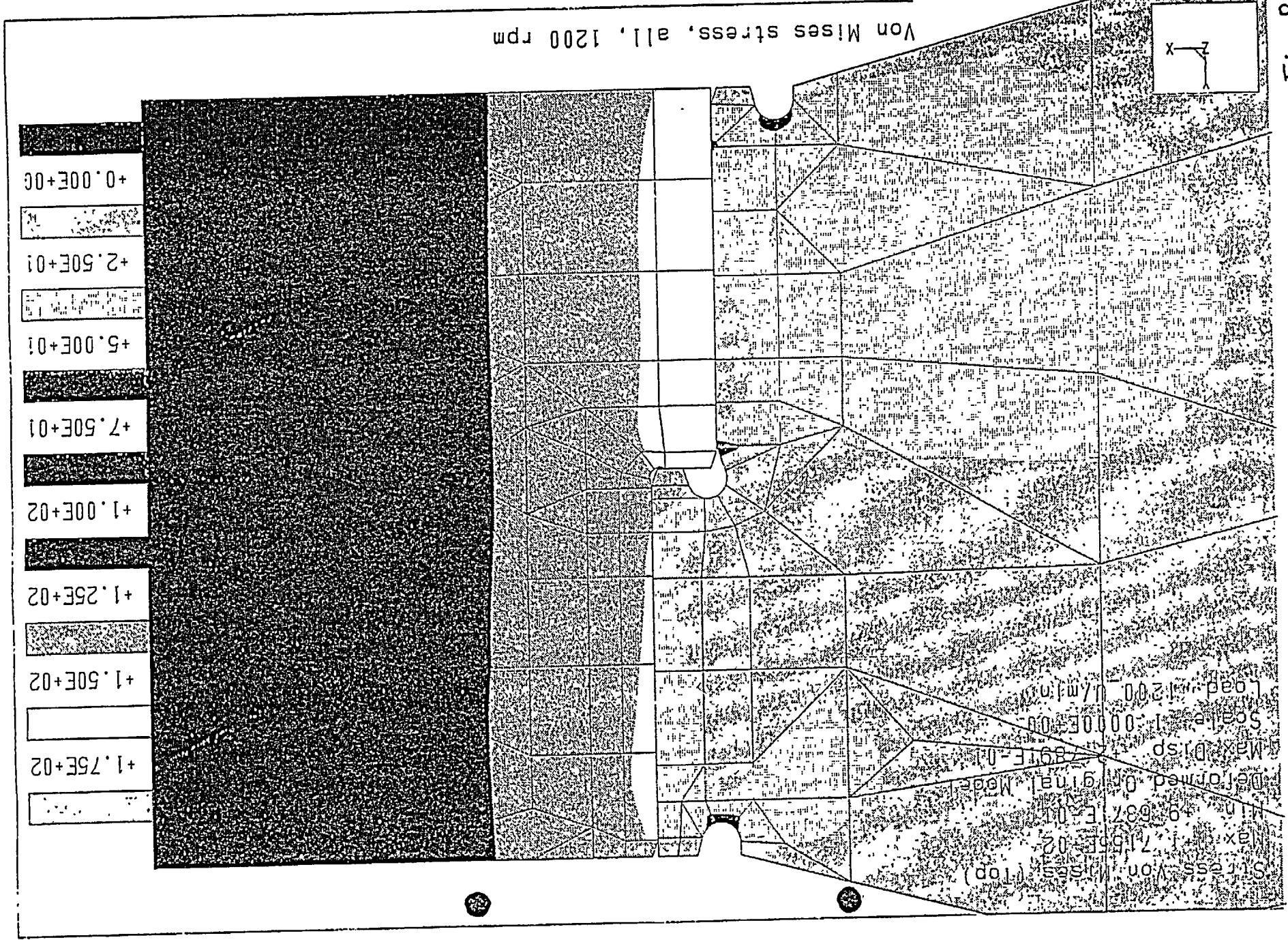


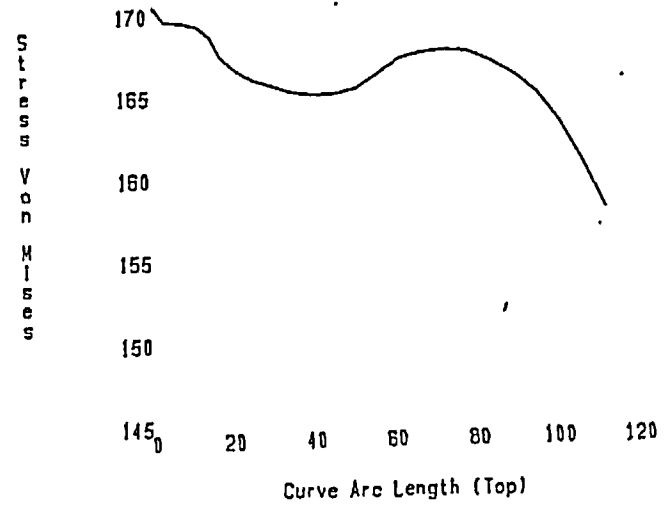
Fig. 8

Stress Von Mises (Top)
Curves
Load: 1200_U/min



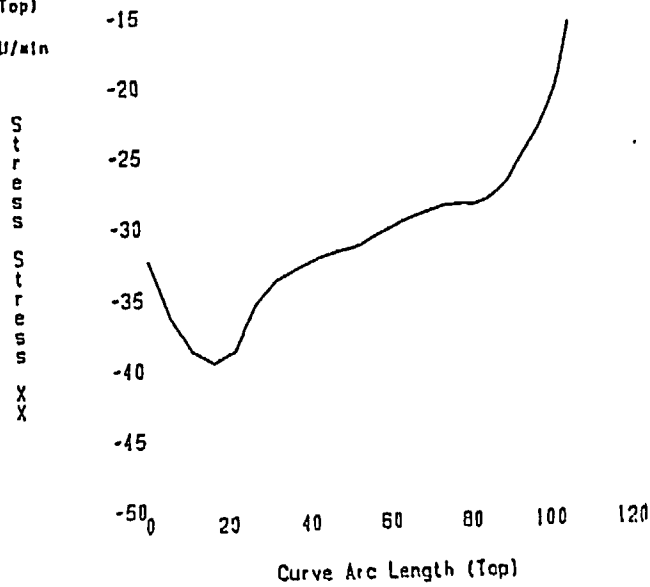
Von Mises stress, shrink fit Ø 790 mm, 1200 rpm

Stress Von Mises (Top)
Curves
Load: 1200_U/min



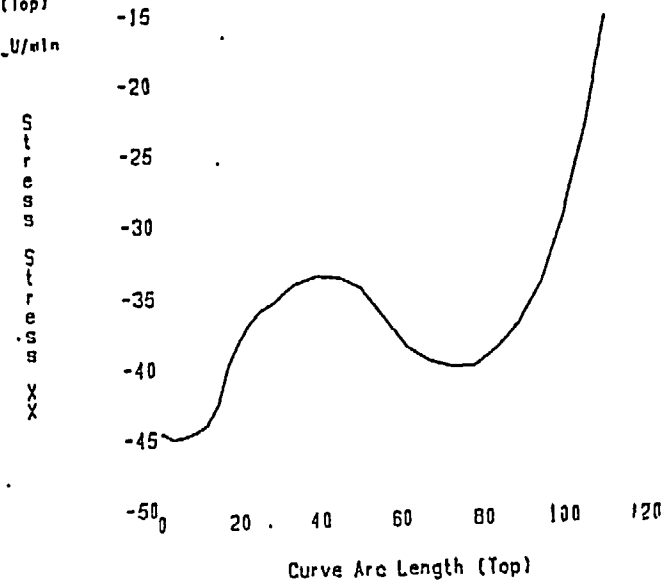
Von Mises stress, shrink fit Ø 750 mm, 1200 rpm

Stress XX (Top)
Curves
Load: 1200_U/min



radial stress, shrink fit Ø 790 mm, 1200 rpm

Stress XX (Top)
Curves
Load: 1200_U/min



radial stress, shrink fit Ø 750 mm, 1200 rpm

Fig. 9

The original document is of questionable quality but what follows is the best available image.

Color Graph

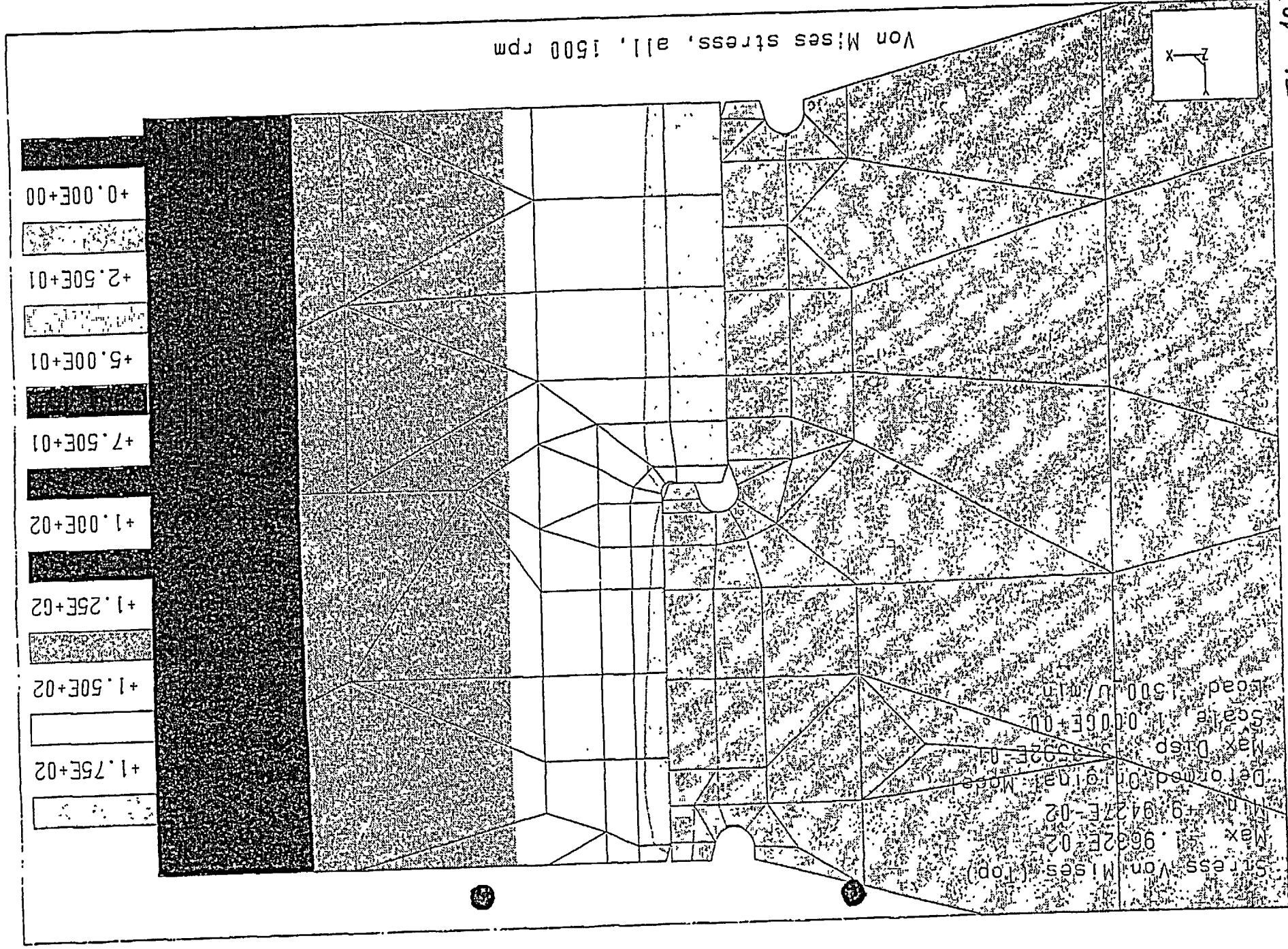
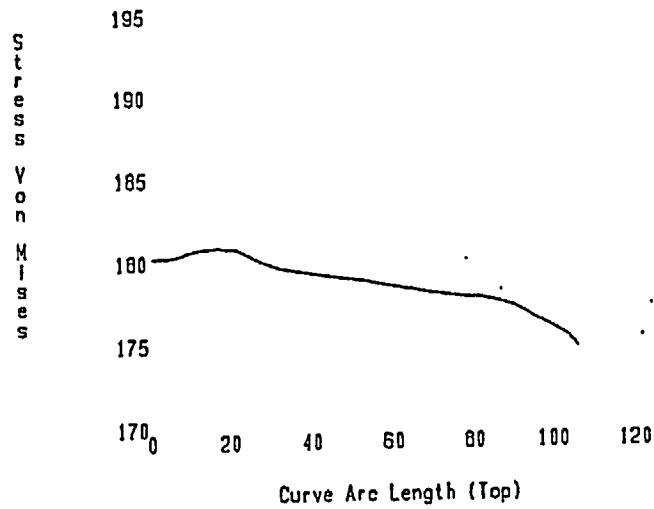


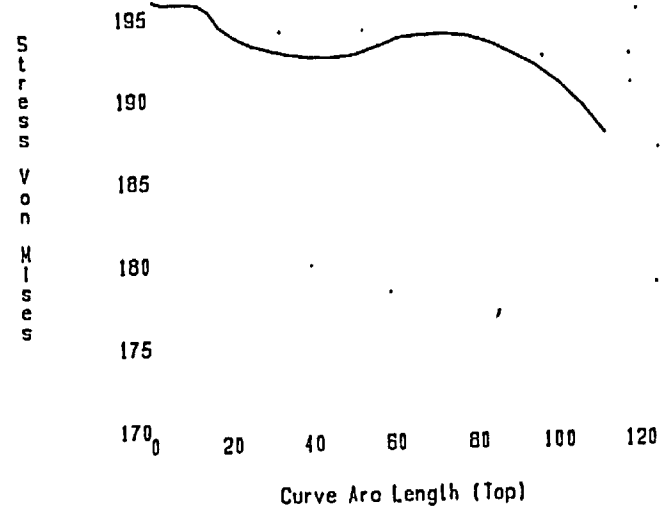
Fig. 10

Stress Von Mises (Top)
Curves
Load: 1500_U/min



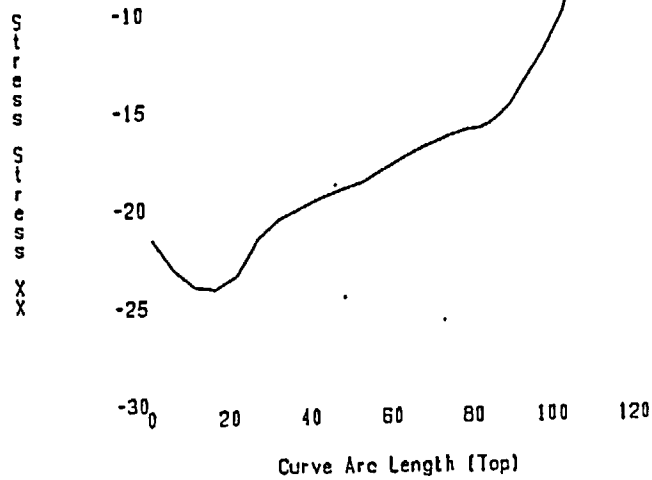
Von Mises stress, shrink fit Ø 780 mm, 1500 rpm

Stress Von Mises (Top)
Curves
Load: 1500_U/min



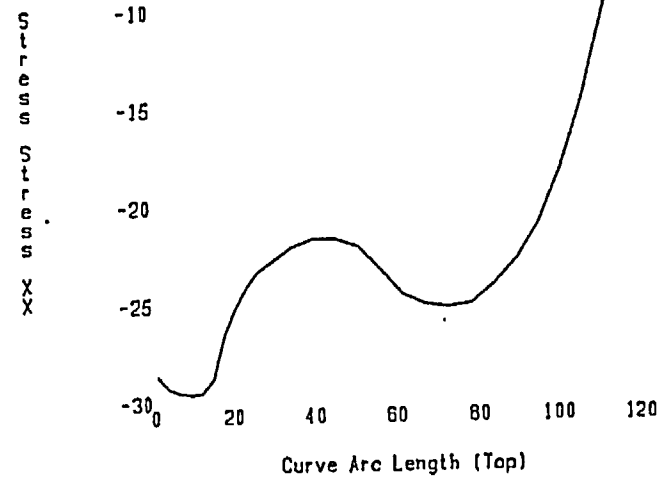
Von Mises stress, shrink fit Ø 750 mm, 1500 rpm

Stress XX (Top)
Curves
Load: 1500_U/min



radial stress, shrink fit Ø 780 mm, 1500 rpm

Stress XX (Top)
Curves
Load: 1500_U/min



radial stress, shrink fit Ø 750 mm, 1500 rpm

Fig. 11

The original document is of questionable quality but what follows is the best available image.

Color Graph

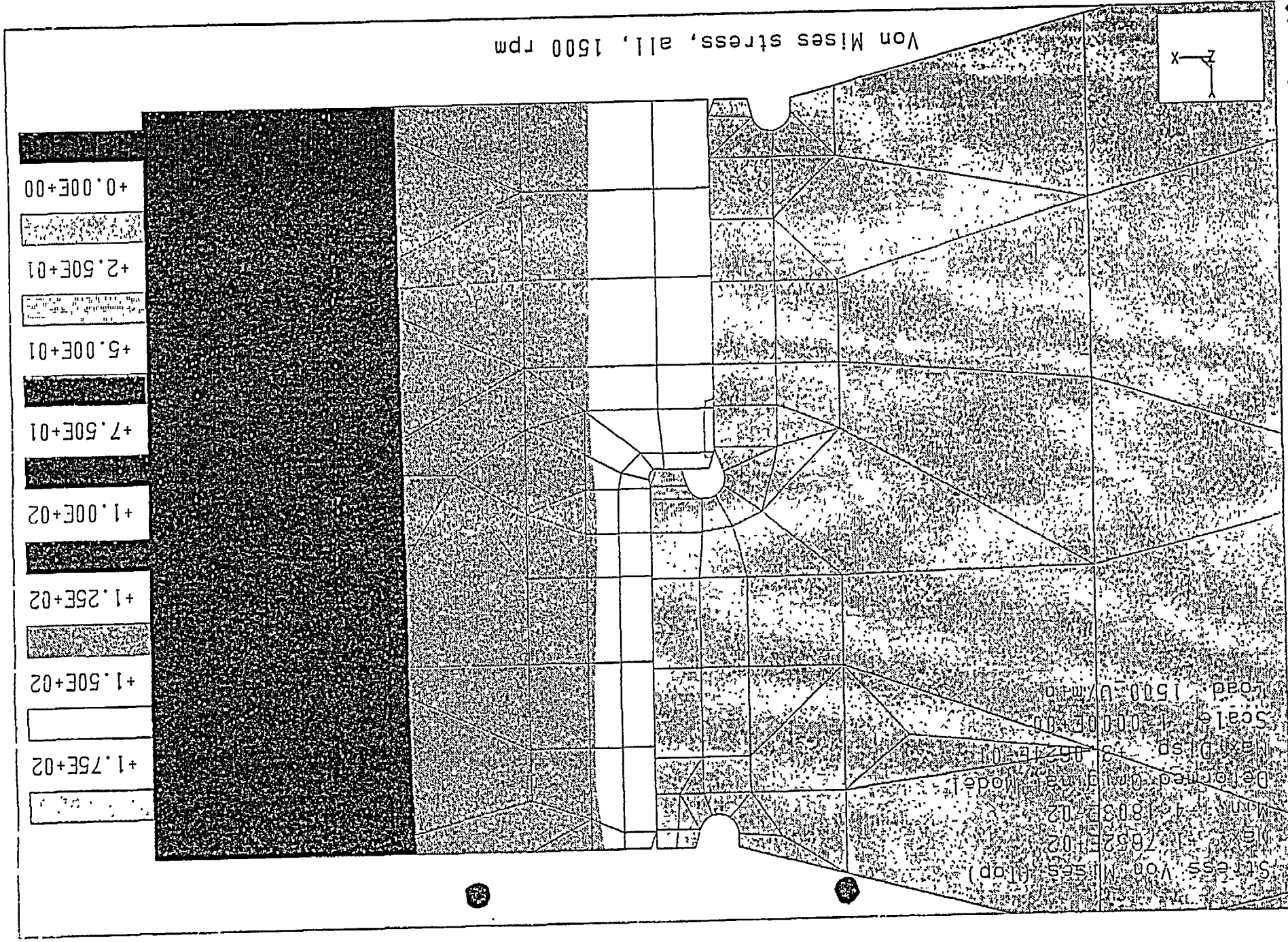
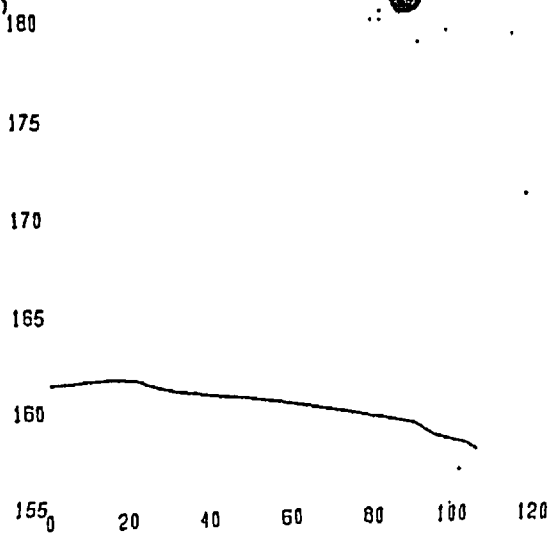


Fig. 12

Stress Von Mises (Top)
Curves
Load: 1500_U/min

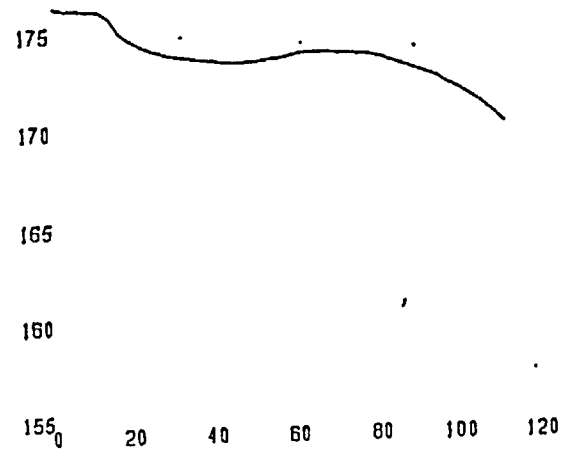
Stress Von Mises



Von Mises stress, shrink fit Ø 790 mm, 1500 rpm

Stress Von Mises (Top)
Curves
Load: 1500_U/min

Stress Von Mises



Von Mises stress, shrink fit Ø 750 mm, 1500 rpm

Stress XX (Top)
Curves
Load: 1500_U/min

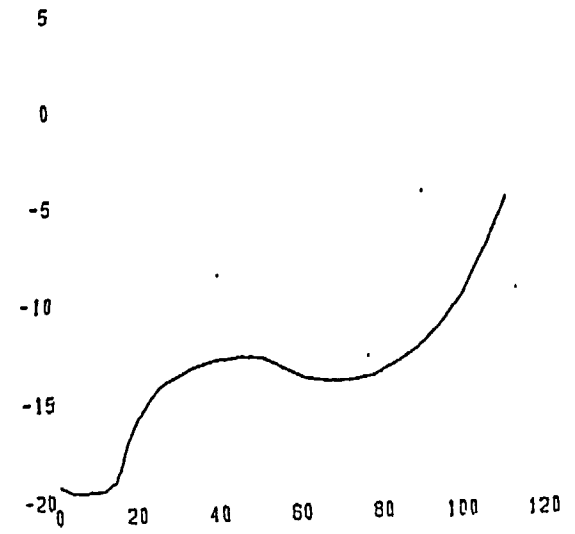
Stress XX



radial stress, shrink fit Ø 790 mm, 1500 rpm

Stress XX (Top)
Curves
Load: 1500_U/min

Stress XX



radial stress, shrink fit Ø 750 mm, 1500 rpm

Fig. 13

The original document is of questionable quality but what follows is the best available image.

Color Graph

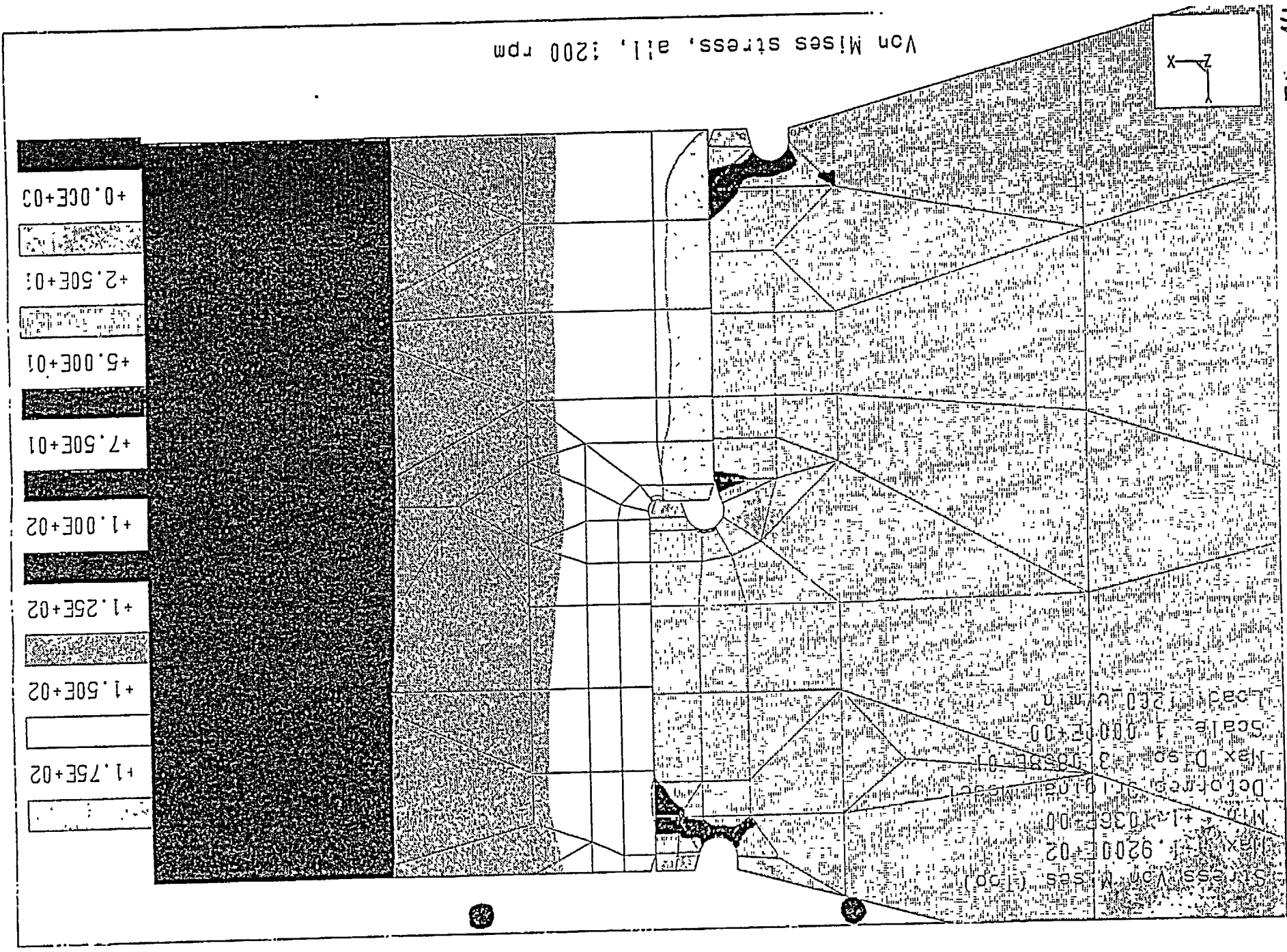
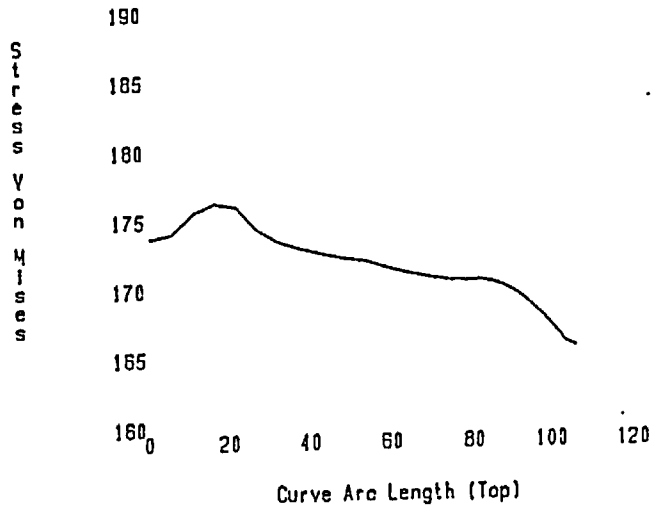


Fig. 14

Stress Von Mises (Top)
Curves
Load: 1200_U/min



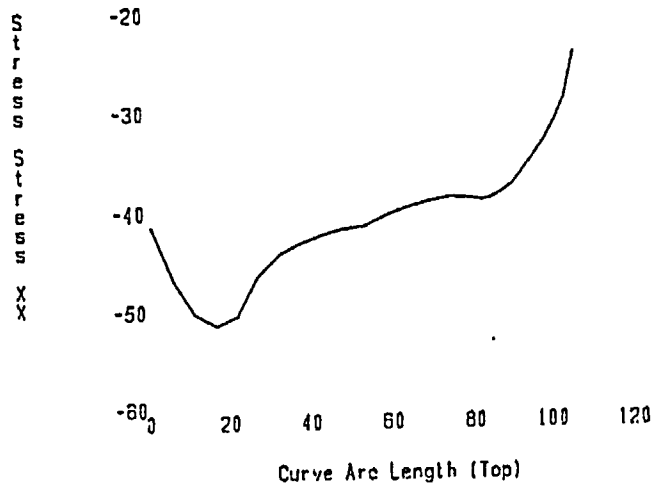
Von Mises stress, shrink fit 790 mm, 1200 rpm

Stress Von Mises (Top)
Curves
Load: 1200_U/min



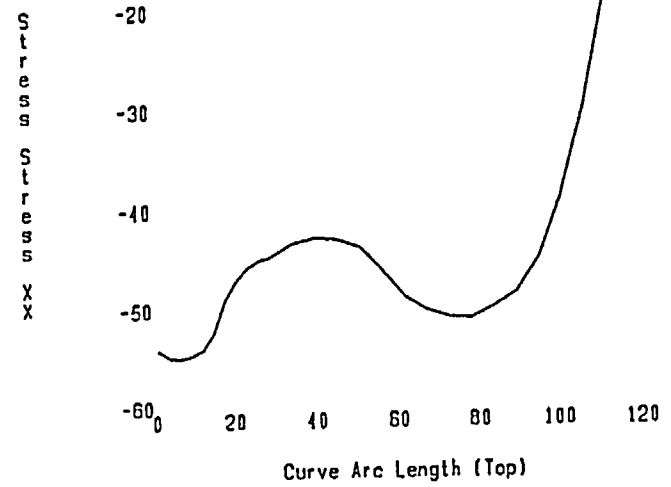
Von Mises stress, shrink fit 750 mm, 1200 rpm

Stress XX (Top)
Curves
Load: 1200_U/min



radial stress, shrink fit 790 mm, 1200 rpm

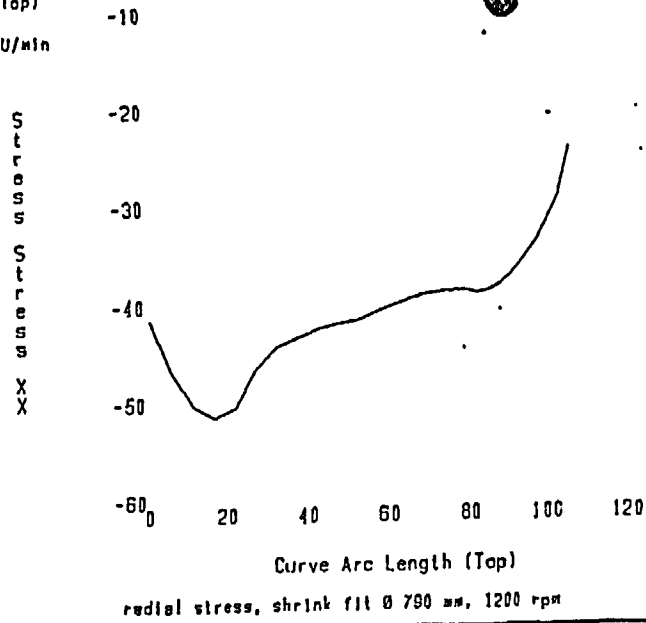
Stress XX (Top)
Curves
Load: 1200_U/min



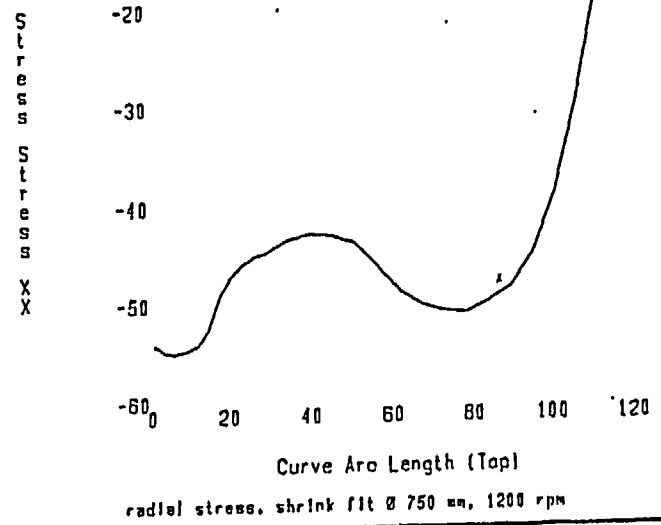
radial stress, shrink fit 750 mm, 1200 rpm

Fig. 15

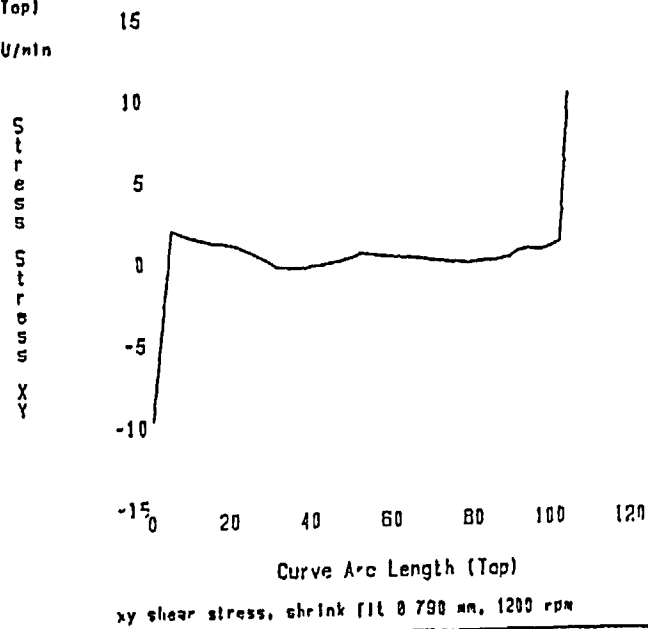
Stress XX (Top)
Curves
Load: 1200_U/min



Stress XX (Top)
Curves
Load: 1200_U/min



Stress XY (Top)
Curves
Load: 1200_U/min



Stress XY (Top)
Curves
Load: 1200_U/min

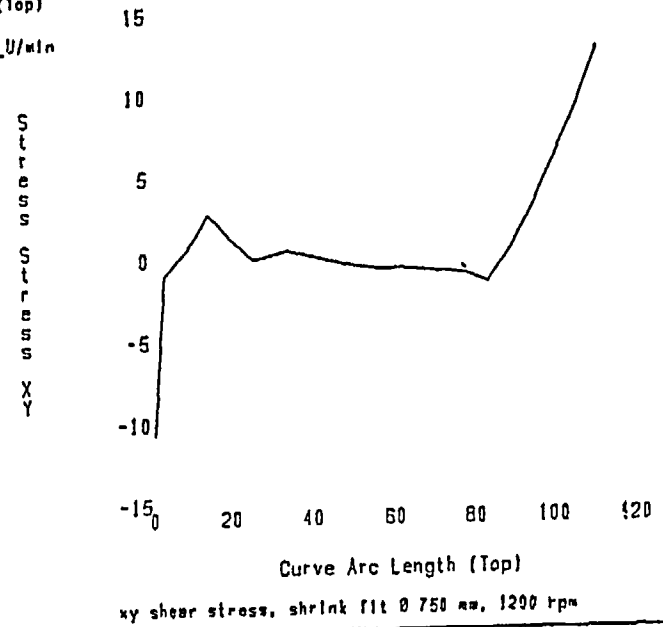
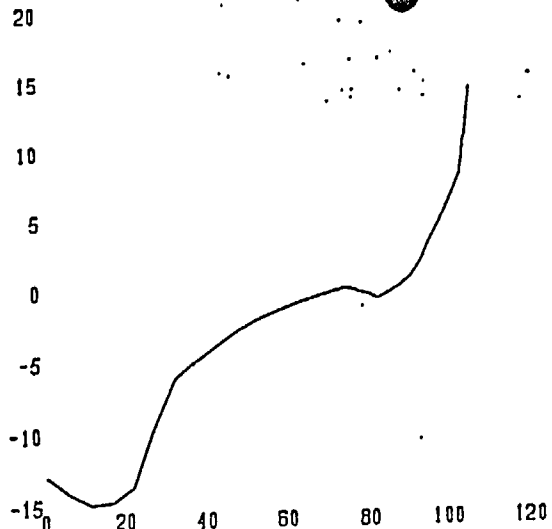


Fig. 16

Stress YY (Top)
Curves
Load: 1200_U/min

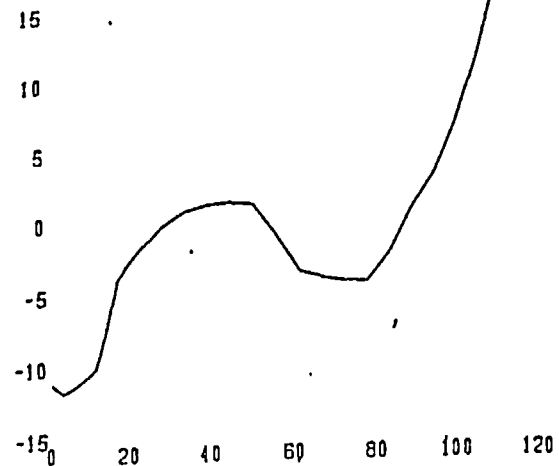
S
t
r
e
s
s
S
t
r
e
s
s
Y
Y



axial stress, shrink fit \varnothing 790 mm, 1200 rpm

Stress YY (Top)
Curves
Load: 1200_U/min

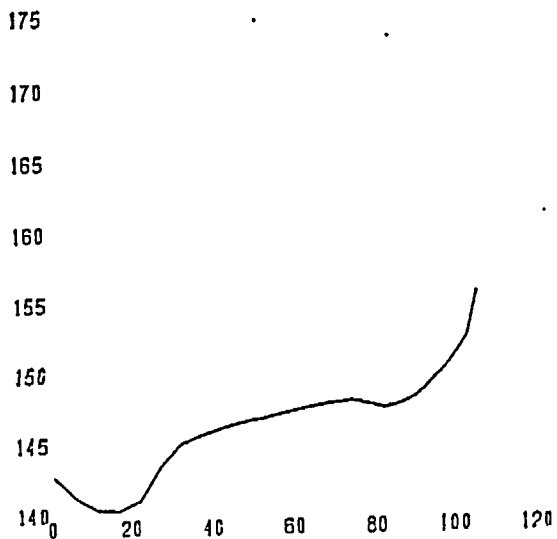
S
t
r
e
s
s
S
t
r
e
s
s
Y
Y



axial stress, shrink fit \varnothing 750 mm, 1200 rpm

Stress ZZ (Top)
Curves
Load: 1200_U/min

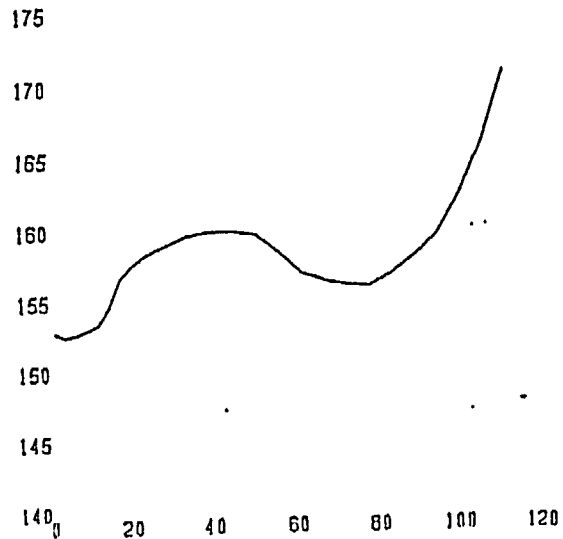
S
t
r
e
s
s
S
t
r
e
s
s
Z
Z



tangential stress, shrink fit \varnothing 790 mm, 1200 rpm

Stress ZZ (Top)
Curves
Load: 1200_U/min

S
t
r
e
s
s
S
t
r
e
s
s
Z
Z



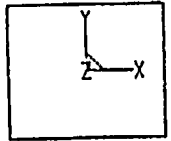
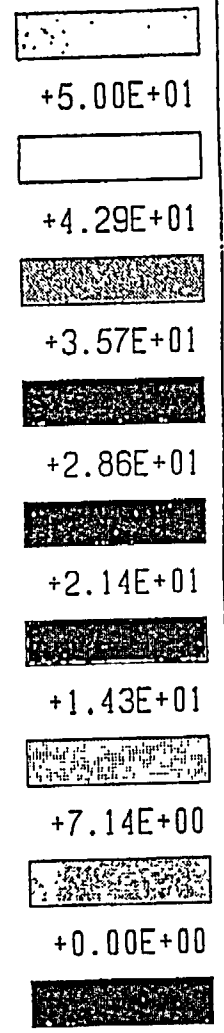
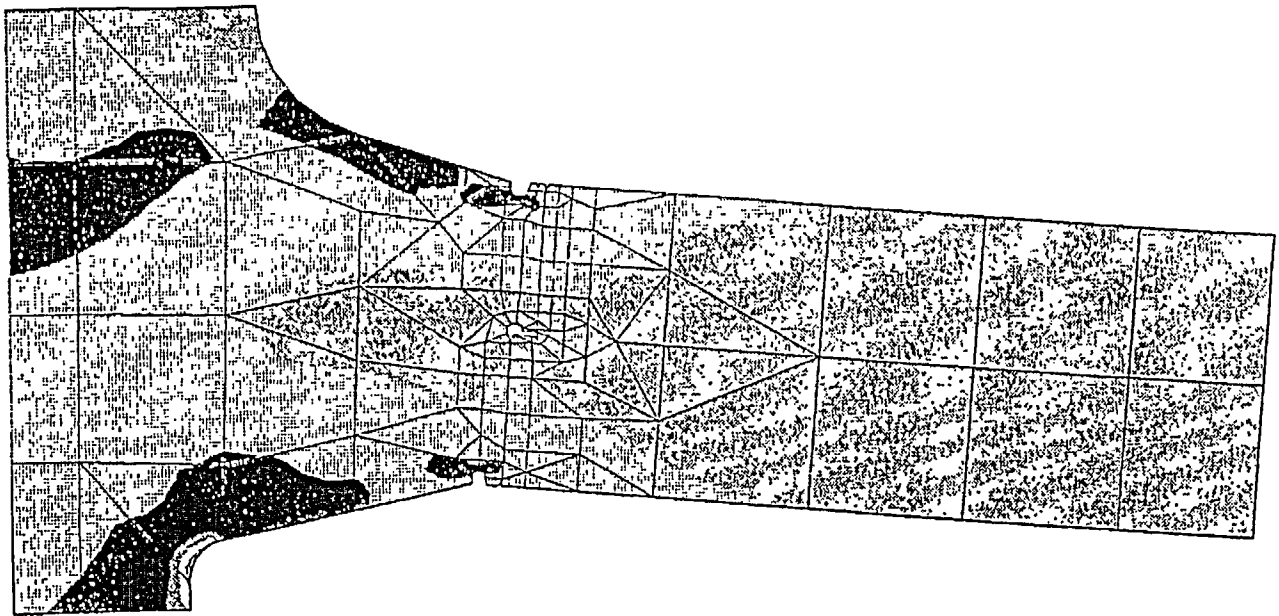
tangential stress, shrink fit \varnothing 750 mm, 1200 rpm

Fig. 17

The original document is of questionable quality but what follows is the best available image.

Color Graph

Stress Von Mises (Top)
Max +5.9233E+01
Min +.0289E-01
Deformed Original Model
Max Disp +1.5563E-01
Scale 5.0000E+02
Load: G4_vertical

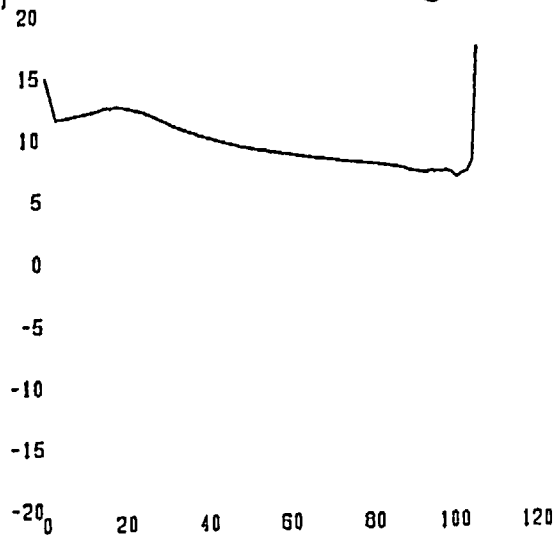


Von Mises stress, all, 0 rpm, 4g_vertical

Fig. 19

Stress Von Mises (Top)
Curves
Load: G4_vertical

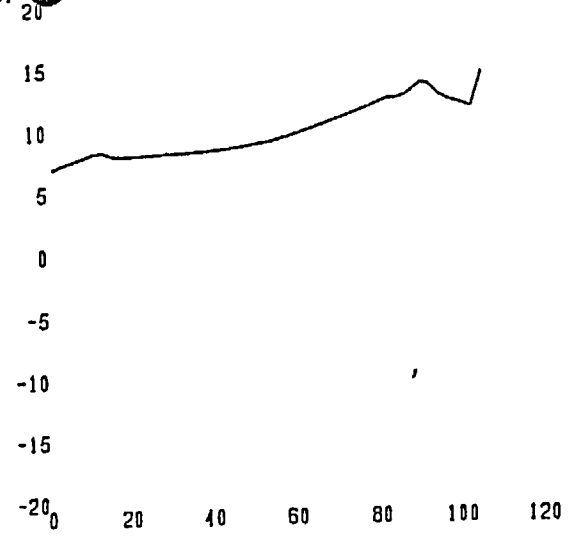
Stress
Von
Mises



Von Mises stress, Ø 790 mm, 0 rpm, 4g_vertical

Stress Von Mises (Top)
Curves
Load: G4_vertical

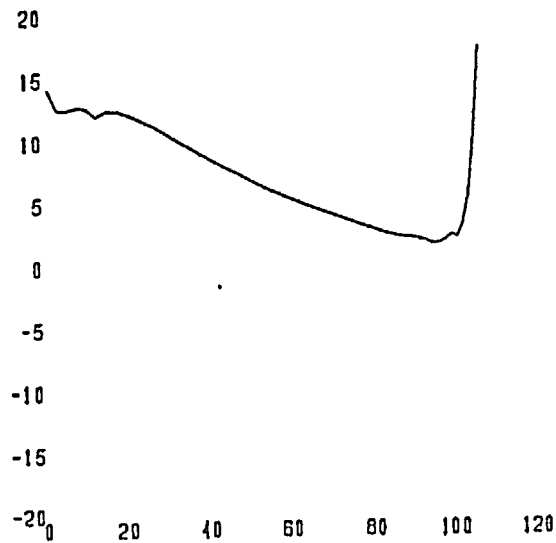
Stress
Von
Mises



Von Mises stress, Ø 750 mm, 0 rpm, 4g_vertical

Stress XX (Top)
Curves
Load: G4_vertical

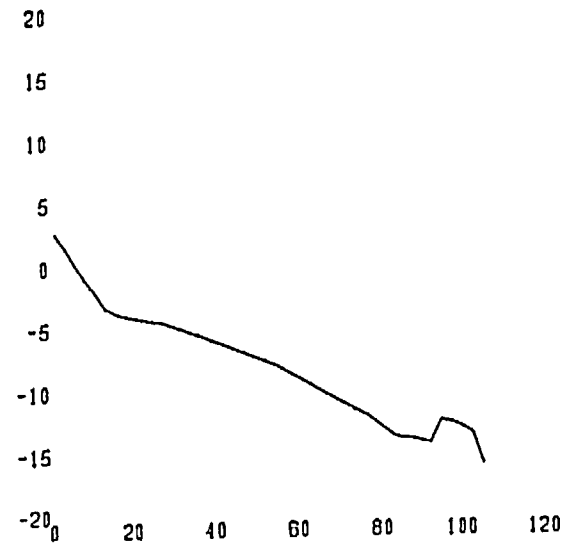
Stress
Stress
XX



radial stress, Ø 790 mm, 0 rpm, 4g_vertical

Stress XX (Top)
Curves
Load: G4_vertical

Stress
Stress
XX

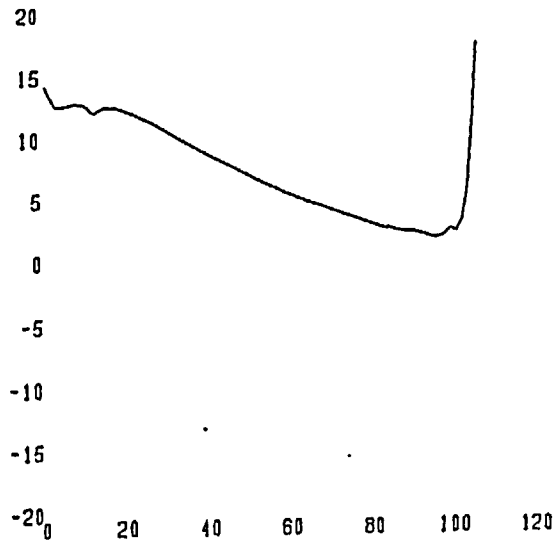


radial stress, Ø 750 mm, 0 rpm, 4g_vertical

Fig. 20

Stress XX (Top)
Curves
Load: G4_vertical

S
t
r
e
s
s
S
t
r
e
s
s
X
X

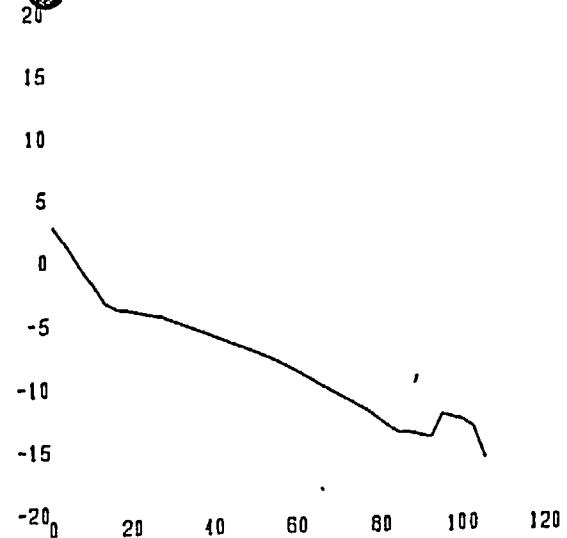


Curve Arc Length (Top)

radial stress, Ø 790 mm, 0 rpm, 4g_vertical

Stress XX (Top)
Curves
Load: G4_vertical

S
t
r
e
s
s
S
t
r
e
s
s
X
X

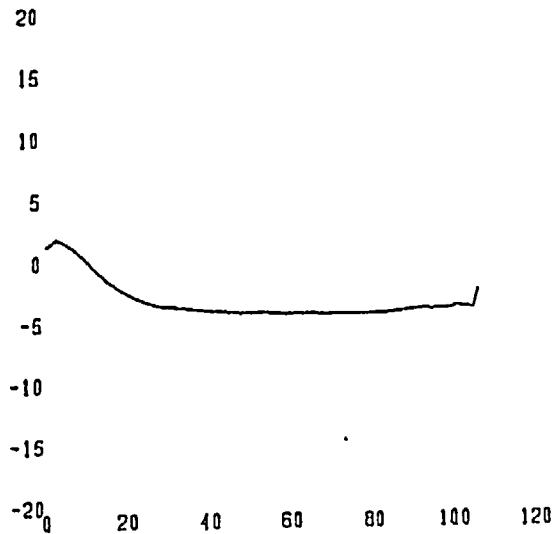


Curve Arc Length (Top)

radial stress, Ø 750 mm, 0 rpm, 4g_vertical

Stress XY (Top)
Curves
Load: G4_vertical

S
t
r
e
s
s
S
t
r
e
s
s
X
Y

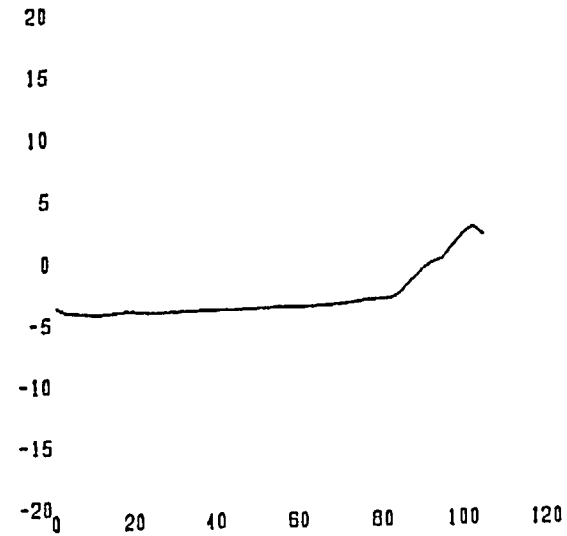


Curve Arc Length (Top)

xy shear stress, Ø 790 mm, 0 rpm, 4g_vertical

Stress XY (Top)
Curves
Load: G4_vertical

S
t
r
e
s
s
S
t
r
e
s
s
X
Y

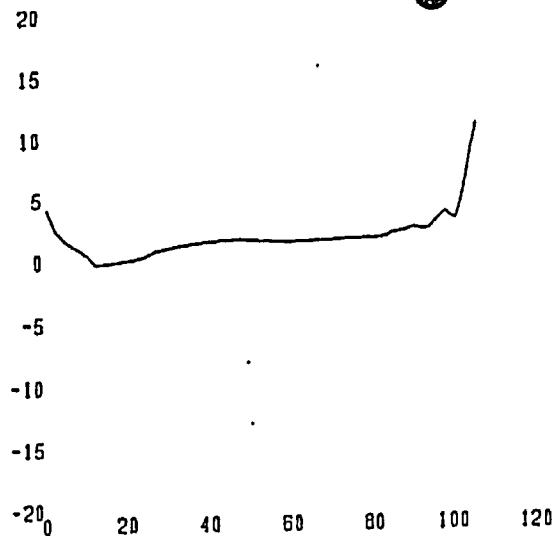


Curve Arc Length (Top)

xy shear stress, Ø 750 mm, 0 rpm, 4g_vertical

Stress YY (Top)
Curves
Load: G4_vertical

Stress
Stress
Y

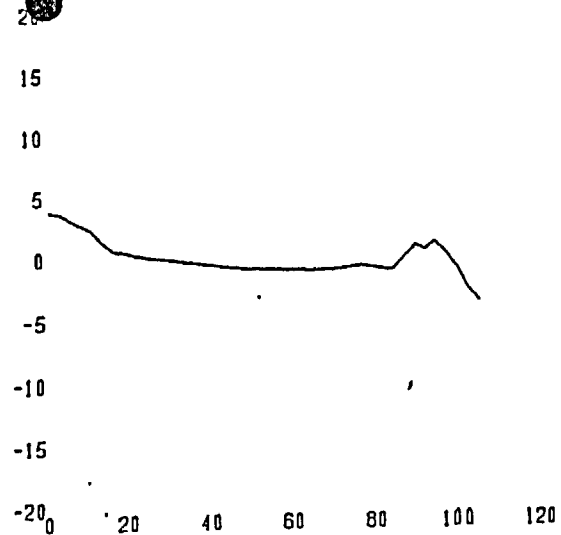


Curve Arc Length (Top)

axial stress, Ø 790 mm, 0 rpm, 4g_vertical

Stress YY (Top)
Curves
Load: G4_vertical

Stress
Stress
Y

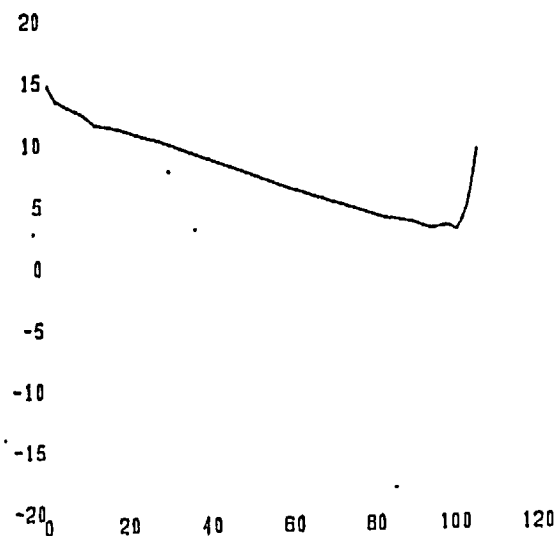


Curve Arc Length (Top)

axial stress, Ø 750 mm, 0 rpm, 4g_vertical

Stress ZZ (Top)
Curves
Load: G4_vertical

Stress
Stress
Z

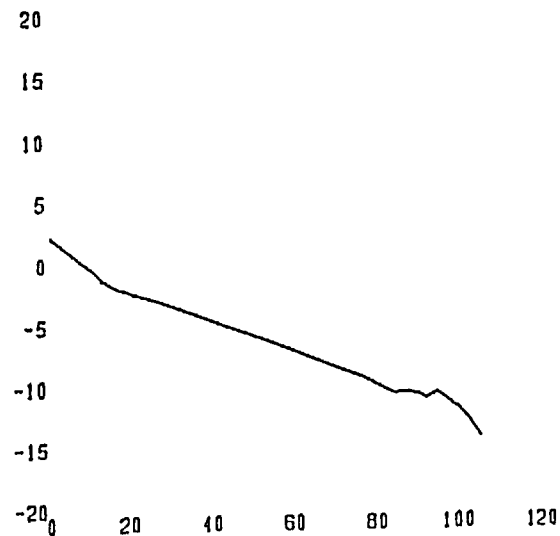


Curve Arc Length (Top)

tangential stress, Ø 790 mm, 0 rpm, 4g_vertical

Stress ZZ (Top)
Curves
Load: G4_vertical

Stress
Stress
Z



Curve Arc Length (Top)

tangential stress, Ø 750 mm, 0 rpm, 4g_vertical

Fig. 22

The original document is of questionable quality but what follows is the best available image.

*Pertains to the next
4 color graphs*

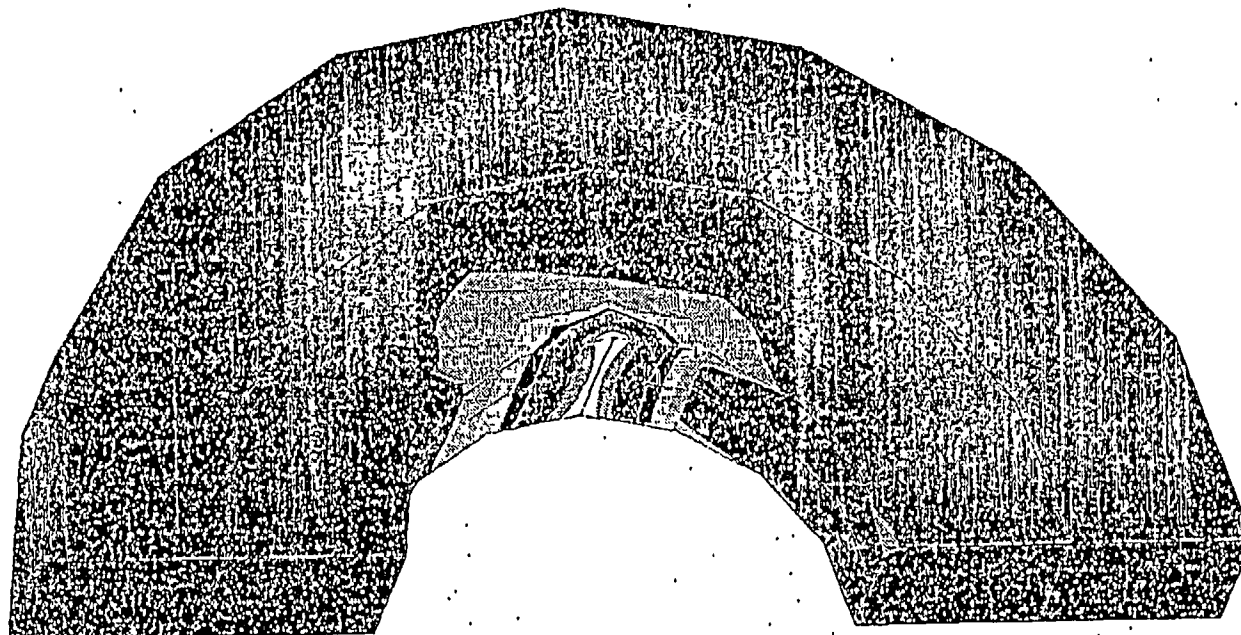
Stress Von Mises (Top)

Max +2.3893E+00

Min +7.2303E-03

Groups

Load: GX_2



+2.12E+00



+1.86E+00



+1.60E+00



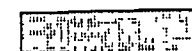
+1.33E+00



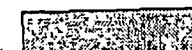
+1.07E+00



+8.03E-01



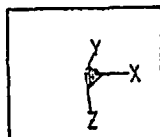
+5.38E-01



+2.74E-01

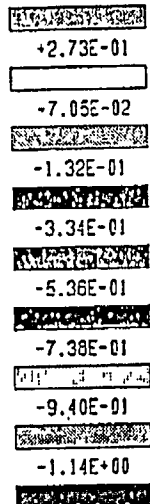
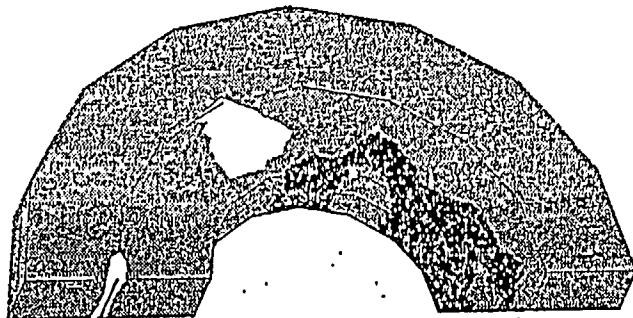


Fig: 24



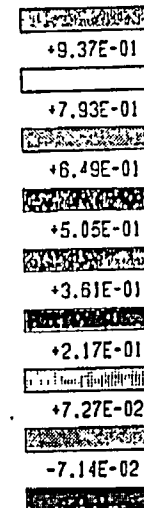
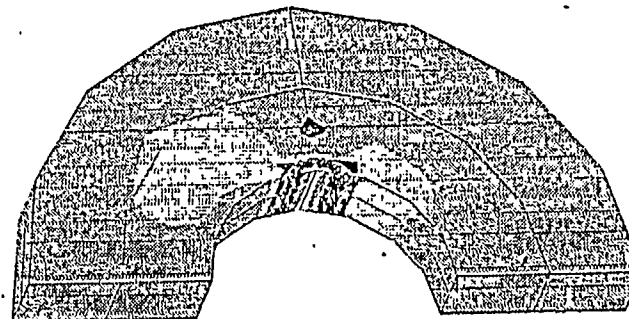
Von Mises stress, flywheel, 2g_horizontal

Stress RR (Top)
 Max +4.7462E-01
 Min -1.3441E+00
 Groups
 Load: GX_2



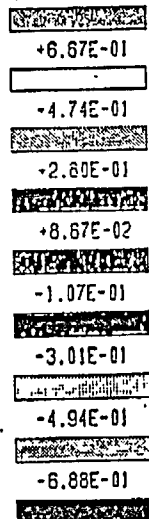
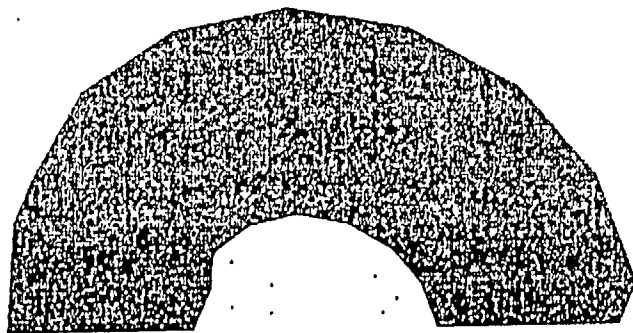
radial stress, flywheel, 2g_horizontal

Stress RT (Top)
 Max +1.0618E+00
 Min -2.1554E-01
 Groups
 Load: GX_2



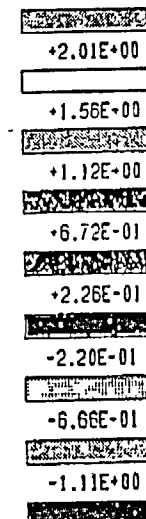
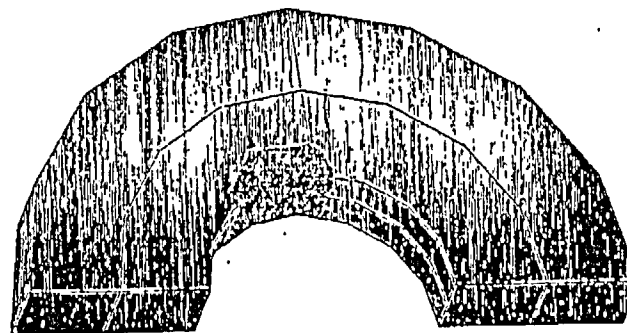
shear stress, flywheel, 2g_horizontal

Stress ZZ (Top)
 Max +8.6109E-01
 Min -8.8136E-01
 Groups
 Load: GX_2



axial stress, flywheel, 2g_horizontal

Stress TT (Top)
 Max +2.4569E+00
 Min -1.5586E+00
 Groups
 Load: GX_2



tangential stress, flywheel, 2g_horizontal

Fig. 25

Stress Von Mises. (Top)

Max +3.5840E+00

Min +1.0845E-02

Groups

Load: GX_3

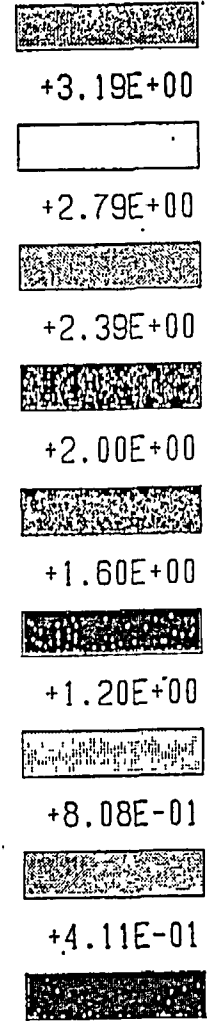
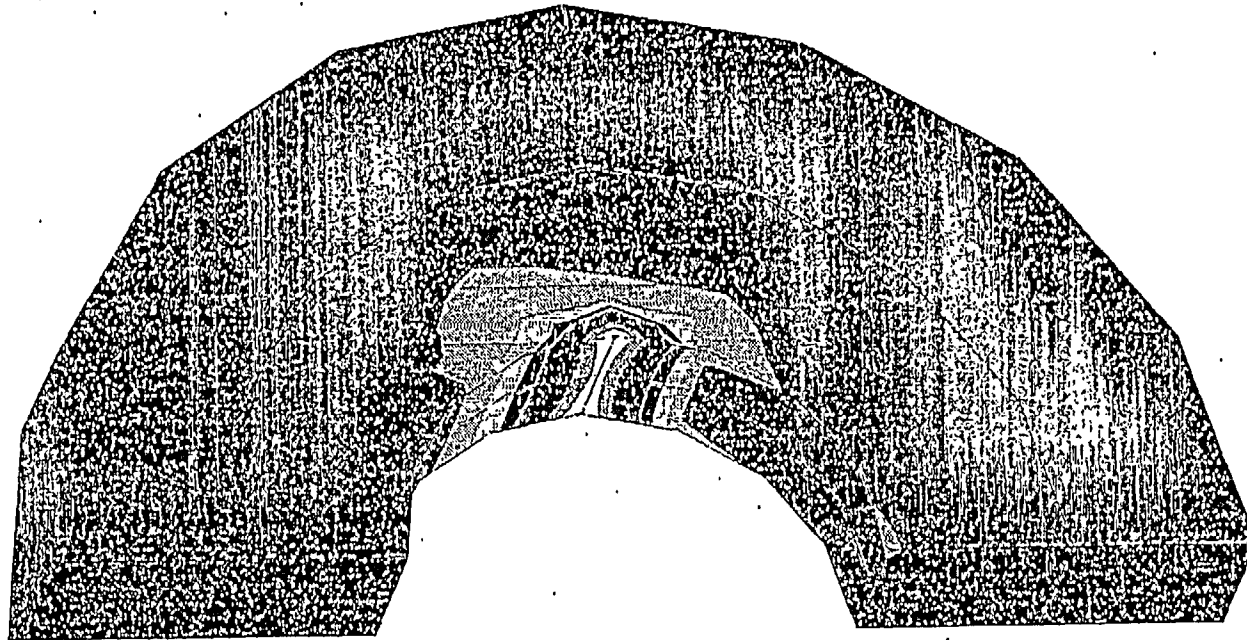
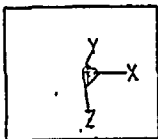
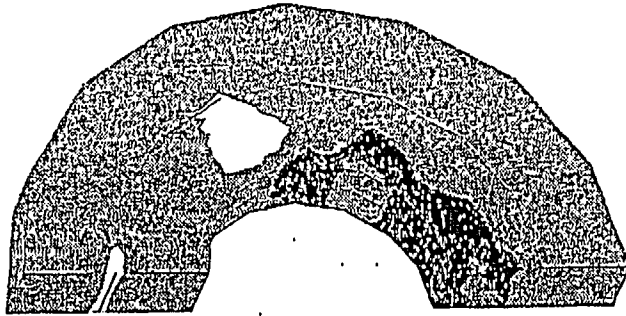


Fig. 26

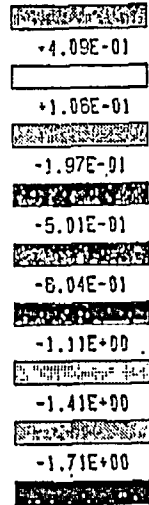


Von Mises stress, flywheel, 3g_horizontal

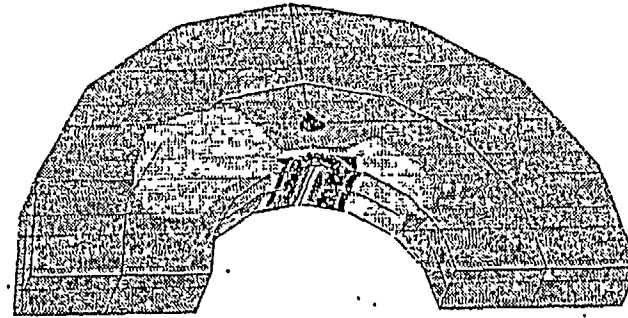
Stress RR (Top)
 Max +7.1193E-01
 Min -2.0162E+00
 Groups
 Load: GX_3



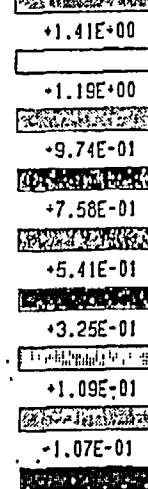
radial stress, flywheel, 3g_horizontal



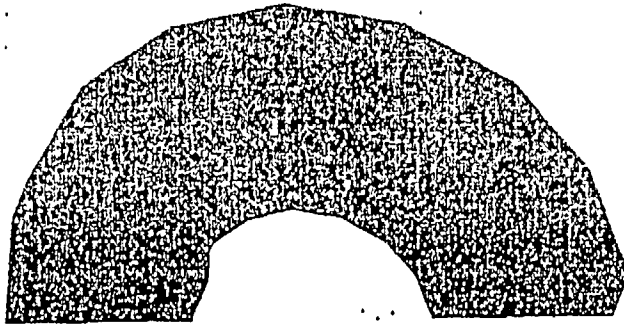
Stress RT (Top)
 Max +1.6224E+00
 Min -3.2332E-01
 Groups
 Load: GX_3



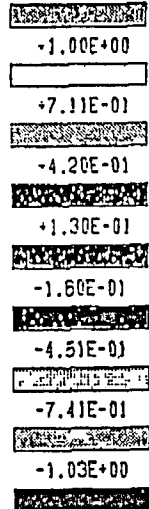
shear stress, flywheel, 3g_horizontal



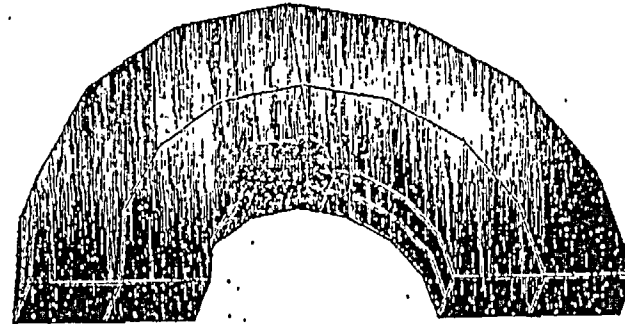
Stress ZZ (Top)
 Max +1.2816E+00
 Min -1.3220E+00
 Groups
 Load: GX_3



axial stress, flywheel, 3g_horizontal



Stress TT (Top)
 Max +3.6853E+00
 Min -2.3379E+00
 Groups
 Load: GX_3



tangential stress, flywheel, 3g_horizontal

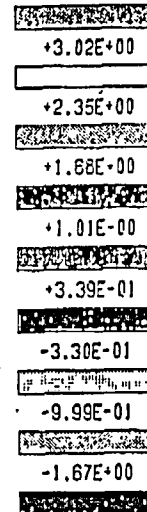


Fig. 29

APPENDIX D: CRACK GROWTH CALCULATION

The fracture analysis is made with a material similar in strength to the flywheel material but with lower fracture toughness. This calculation shows that the critical crack size is not reached inside a range of 10000 cycles running up the motor from zero to overspeed. The calculation input and output is shown on the following two pages.

BRUCHMECHANISCHE BEURTEILUNG VON ULTRASCHALL-EINZELANZEIGEN 16-10-96

Name der Anlage: Fort Calhoun
Schmiedestück: Flywheel

Bemerkung: sigma = tangential stress
theoretical defect diameter
single display

Ersatzreflektorgrösse: 3.6 mm
Anfangsrisslänge a0: 2.28 mm
Anfangsrisslänge c0: 5.69 mm
Achsenverhältnis $\epsilon_0 = a0/c0$: 0.40
Max. zulässige Risslänge cmax: 7.0 mm

BELASTUNGSWERTE ZUR ERMITTLUNG DES ERMÜDUNGSRISSWACHSTUMS:

Spannungsschwingbreite $\Delta\sigma$: 210 MPa
Temperatur Terw: 20 °C
Vorgegebene Lastspielzahl Nvor: 10000
Ausgabeintervall Ndiff: 500

BELASTUNGSWERTE ZUR BERECHNUNG DES SPRÖDBRUCHRISIKOS:

Spannung σ_∞ : 210 MPa
Temperatur Tc: 20 °C

MATERIALWERTE:

Material: ST572
Elastizitätsmodul bei 20°C: 211000 MPa
Elastizitätsmodul bei Terw = 20°C: 211000 MPa
Streckgrenze bei Terw = 20°C: 700 MPa
Bruchzähigkeit K1c bei Terw = 20°C: 155.0 MPa√m

Rissfortschrittsgesetz bei Terw = 20°C: $da/dN = 0.10E-10 * (\Delta K/MPa\sqrt{m})^{3.00}$ * m/LS

Streckgrenze bei Tc = 20°C: 700 MPa
Bruchzähigkeit K1c bei Tc = 20°C: 155.0 MPa√m

EVALUATION OF ULTRASONIC FLAW READINGS ACCORDING TO FRACTURE MECHANICS

Plant name	Fort Calhoun	
Forged piece	Flywheel	
Comments	Sigma = tangential stress Theoretical defect diameter Single display	
Substitution for reflector size	3.6	mm
Crack length a0 at begin	2.28	mm
Crack length c0 at begin	5.69	mm
Aspect ratio $\epsilon_0 = a_0/c_0$	0.40	
Allowed crack length	7.0	mm

LOADS FOR DETERMINATION OF THE FATIGUE CRACK GROWTH

Stress p-p value $\Delta\sigma$	210	Mpa
Temperature Terw	20	°C
Given number of load cycles Nvor	10000	
Output interval for load cycles Ndiff	500	

LOADS FOR DETERMINATION OF THE BRITTLE FRACTURE RISC

Stress σ_∞	210	Mpa
Temperature Tc	20	°C

MATERIAL DATA

Material name	ST572	
Modulus of elasticity at 20°C	211000	Mpa
Modulus of elasticity at Terw = 20°C	211000	Mpa
Yield stress at Terw = 20°C	700	MPa
Fracture toughness K _{Ic} at Terw = 20°C	155	MPa√m
Crack growth rate at Terw = 20°C	$da/dN = 0.10E-10 * (\Delta K / [MPa\sqrt{m}])^3$ m/cycle	
Yield stress at Tc = 20°C	700	MPa
Fracture toughness K _{Ic} at Tc = 20°C	155	MPa√m

RESULTS

given Table

CALCULATION TERMINATED AFTER 52610 LOADCYCLES BECAUSE THE NEXT LOAD CYCLE VIOLATES THE REQUIREMENT $c(N) < 0.7 * \text{MIN.BORDER DISTANCE} = 7.0 \text{ mm} !!!$

ABR ADD.	Revision:	Language	Page	HTAM 622595
	D 96-10-18	en	56 / 56	

ERGEBNISSE:

N	a(N)	c(N)	Ya(N)	Yc(N)	SΔK(N)	ac(N)	Sa(N)
-	mm	mm	-	-	-	mm	-
0	2.277	5.692	1.55	0.62	9.98	226.83	99.62
500	2.296	5.697	1.55	0.62	9.96	227.52	99.11
1000	2.315	5.702	1.55	0.63	9.93	228.21	98.60
1500	2.334	5.707	1.54	0.63	9.90	228.92	98.09
2000	2.353	5.712	1.54	0.63	9.88	229.63	97.59
2500	2.372	5.717	1.54	0.64	9.85	230.35	97.10
3000	2.392	5.722	1.54	0.64	9.83	231.07	96.61
3500	2.412	5.728	1.53	0.65	9.80	231.80	96.12
4000	2.431	5.733	1.53	0.65	9.78	232.54	95.64
4500	2.451	5.739	1.53	0.65	9.76	233.28	95.17
5000	2.471	5.744	1.53	0.66	9.73	234.03	94.69
5500	2.492	5.750	1.52	0.66	9.71	234.79	94.23
6000	2.512	5.756	1.52	0.66	9.68	235.55	93.76
6500	2.533	5.762	1.52	0.67	9.66	236.32	93.31
7000	2.553	5.768	1.52	0.67	9.64	237.10	92.85
7500	2.574	5.774	1.51	0.67	9.61	237.88	92.40
8000	2.595	5.780	1.51	0.68	9.59	238.66	91.96
8500	2.617	5.787	1.51	0.68	9.57	239.46	91.52
9000	2.638	5.793	1.51	0.69	9.54	240.26	91.08
9500	2.659	5.800	1.50	0.69	9.52	241.07	90.65
10000	2.681	5.807	1.50	0.69	9.50	241.88	90.22
52610	5.149	7.000	1.30	0.95	0.74	324.16	62.95

ABBRUCH DER BERECHNUNG NACH 52610 LASTSPIELEN, DA BEIM NÄCHSTEN LASTSPIEL
DIE BEDINGUNG $c(N) < 0.7 * \text{MIN. RANDABSTAND} = 7.0 \text{ MM}$ VERLETZT WIRD !!!

PRODUCTION ENGINEERING DIVISION
 QUALITY PROCEDURE FORM

PED-QP-3.6
 R4

REVIEWER'S CHECKLIST COMPUTER CALCULATIONS

Flywheel Strength Analysis HTAM 622592

* - *ABB Seismic Qualification Cooling Water Piping HTAM 622599*

CALC NUMBER:

	Yes	No	N/A
* 1. Does the computer run have title, date and page number and alphanumeric program number on every sheet?		X	
* 2. Is the listing of computer input provided?		X	
3. Is the machine generated program name and version on each run or is indicated in the calculation?	X		
4. Is the identification number (Ref. PED-MEI-23, Section 5.3.1) on the cover sheet as part of the calculation's description. NOTE: Only applies to DEN Mechanical and Electrical/I&C Departments.			
* 5. Is the computer software validated and verified?	X		
5.a IF NO: Is the computer code developed for one-time-use on a programmable calculator or microcomputer.			
5.b If yes, has a functional description of the program, identification of the equations, identification of the code (title, revision, manufacturer), identification of the software and brief user's instructions been provided in the calculation?			
6. If the computer software has been loaded on an in-house computer, have the changes made by OPPD been properly reviewed (verified and validated) for their impact on the accuracy of the code and have been found satisfactory, or is the in-house computer software validated?			
* 7. Is the computer program appropriate to do the intended calculation?	X		
* 8. Was an alternate calculation or model utilized to verify results? If so, is it attached to this calculation?		X	
* 9. Is the modeling correct in terms of geometry input and initial conditions?	X		
* 10. Are the results reasonable when compared to the inputs?	X		
Reviewer Comments:			
Reviewer	Date		

ABB	ABB Industrie AG			HTAM 622595	
Responsible department: CH-IMWPV2	Take over department:	Revision: A '96-06-03	Doc.-type: Report	File no.: 622595_A.DOC	
Prepared: 96-06-03 Meckel <i>Meckel</i>	Checked: 96-06-03 Grgic	Approved: 96-06-03 Seldler <i>Seld</i>	Language	Page:	
Valid for:	Derived from:	Replaces:	Classify no:	Data set:	

Fort Calhoun

REACTOR COOLANT PUMP MOTOR

QOVG 900 fa6

Fort Calhoun Power Station

Omaha Public Power District
Omaha, Nebraska

FLYWHEEL STRENGTH ANALYSIS

OPERATING, SEISMIC AND FRACTURE CONDITIONS

Supplement 1

P.O. 1977

Supplement 1

This report is a supplement to the report HTAM 622595 from 96-01-20.

Occasion

After delivery of the flywheel it was recognized, that the shrink fit diameter of the flywheel $\varnothing A$ was not inside the range of specification. (see Att. 1)

	Shaft Diameter		Bore Diameter of the Flywheel	
	$\varnothing a$	$\varnothing b$	$\varnothing A$	$\varnothing B$
specified	790.680 ⁰ _{-0.030}	750.700 ⁰ _{-0.030}	790.000 ^{+0.050} ₀	750.000 ^{+0.050} ₀
measured	790.670	750.690	790.100 790.060	750.030

Additional FE-calculations were made to check, if the manufactured shrink fit can be accepted.

Stress Calculation

The calculation with maximum shrink fit showed the following stresses as compared to the former calculations (see Att. 2):

	former calculation		new calculation	
	Calculated Von Mises Stress	Admissible Stress	Calculated Von Mises Stress	Admissible Stress
Synchronous speed (1200 rpm)	192.0 N/mm ²	195 N/mm ²	208.5 N/mm ²	245 N/mm ²
Test overspeed (1500 rpm)	196.3 N/mm ²	390 N/mm ²	210.6 N/mm ²	490 N/mm ²

Admissible Stresses

The admissible stress of the former calculation was calculated based on the specified yield strength of 585 N/mm² [85 ksi]. The yield strength as measured by the purchaser (see Att. 3) is given with 735 N/mm² [106.6 ksi]. That is why the admissible stress in the flywheel can be raised

- from 195 N/mm² to 245 N/mm² for normal operating speed
- from 390 N/mm² to 490 N/mm² for test overspeed
- from 526 N/mm² to 661 N/mm² for synchronous speed with OBE or DBE

Transmissible Torque

The calculation showed the following transmissible torques as compared to the former calculations :

Transmissible torque	Former Calculations minimum transmissible torque Nmm (ft lbf)	New Calculations real transmissible torque Nmm (ft lbf)	Rated motor torque Nmm (ft lbf)	New Safty margin
Synchronous speed (1200 rpm)	7.936E+08 (5.853E+05)	8.098E+08 (5.972E+05)	2.166E+07 (1.597E+04)	37.4
Test overspeed (1500 rpm)	2.547E+08 (1.878E+05)	5.627E+08 (4.149E+05)	2.166E+07 (1.597E+04)	26.0

Conclusion

Compared to the former calculation the maximum Von Mises stress is about 15 N/mm² higher. The admissible stress has increased for about 50 N/mm² for 1200 rpm and for about 100 N/mm² for 1500 rpm due to the higher yield point of the manufactured material. The recalculated stresses are well acceptable and there is even a higher safety margin. The transmissible torque of the manufactured shrink fit is also higher than the minimum transmissible torque calculated in the former report.

The stresses due to seismic load are superposed to the stresses at normal operating speed. This means that all seismic stresses will be raised for the same amount of about 17 N/mm². This results in a calculated Von Mises stresses of about 218 N/mm² for synchronous speed and OBE and 221 N/mm² for synchronous speed and DBE. The admissible stress for these cases is 661 N/mm². The recalculated stresses are well acceptable.

Final result

The stresses in the flywheel calculated with the given dimensions and material properties are admissible for all load cases prescribed and in all these cases the flywheel will maintain ist structural integrity.

Attachment 1: Inspection Protocol

The inspection protocols are displayed on the following three pages.



Int.-Best. 1-364043-763-42000 Anlage FORT CALHOUN

Masch.-Typ 00VR 900 FAG Fabr.-Nr./Laut.-Nr. HM 1005400

Eink.-Nr. Lieferant Name:

Gegenstand Schwungrad (Protokoll) Ident.Nr. HTAM 431 660

Ausgangsmaterial Ident.Nr.

Herstellmenge 1 Geprüft 1 Fehlerh. 1 Fertig b. Op Prod.Unterbr. JA X Nein

Fehler Innendurchmesser (Bohrung) 790,000 +0,050 ist zu gross!

Soll = 790,000 +0,050
Ist = 790,060 - 790,100

≅ 5% weniger Schwungrad!

Ursache

Antrag zum ⇒ Werkstoff: Verfahren gemäss Plan!

Entscheid ⇒ Erlaubt: Lieferant informieren / Preisreduktion

Fehlerbehebungsentscheid (Reibungslager austauschen lassen)

Verhütungsmassnahmen

Entscheid Sonderfreigabe Konzession Erledigt für diesen Auftrag

Abt. Datum Name Abt. Datum Name

Fehlerursache(n) nachhaltig beseitigt

(auch bei allen laufenden Aufträgen und Lagerrollen)

Kurztext der Verbesserung:

Laufweg

Table with columns: Abt., Datum, Name / Vis erledigt. Includes entries for IMW, IMM, and IMFO with dates and names like Rieck, Roller, and Weber Ch/DleUker K.

Auswertung

Table for evaluation: Verursacher, Fehlerort, Fehlerart, Fertigung, Fehlerursache, Technik, Fehlerkategorie. Includes a grid for error location and type.

FM in DV erfasst Dat. Name FM-Lauf.-Nr.

Fehlermeldung Kopf / Kosten / Verrechnung - die Rückseite

Ergänzung Fehlermeldungsformular Rückseite (UM-WS 0104) und IM-AB 002 Detail zu Pkt. 3.1 (SAP Innenauftrag gültig ab 1.1.1996 bis 31.12.1996 / Teilprojekt vorgezogenes Rechnungswesen)

ABB ABB Industrie AG Bereich Elektrische Maschinen **Fehlermeldung**

Ausgibt. Dat. **30.5.96** Aussteller **Marrenz** Insel/Abt. **760** z **1** FM-Nr. **605622**

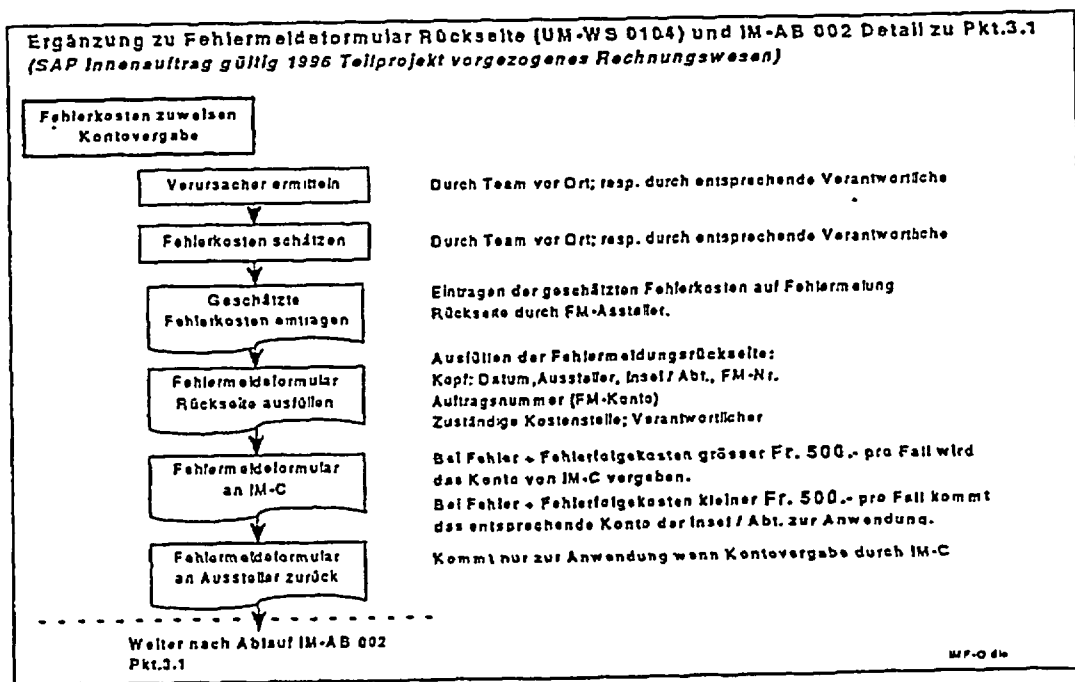
Auftragswert: **7850** Auftragsbezeichnung: **Fehler/Verluste** Auftragsnummer

Geschätzte Fehlerkosten (Fehlerbehebungs- + Folgekosten) Fr.

Produkt- / Prozessverantwortliche für die Fehlerbehebung

Technik					Fremdmaterial				
Betroffene Produkte / PG	Abteilg.	Kostenstelle	Verantwortliche		Betroffene Produkte / PG	Abteilg.	Kostenstelle	Verantwortliche	
			Verantwortlicher	Teil.Nr.				Verantwortlicher	Teil.Nr.
<input type="checkbox"/> DNA / DMB 760 / 761 / 762 / 763	ING	09400	Sacher R.	66460	<input type="checkbox"/> DNA / DMB 760 bis 763	IM-B1	78010	Luchstener A.	66363
<input type="checkbox"/> ANA / ANB / ANK / ANL 750 bis 752 und 734 / 773	IM-P1	94511	Eichenberger K.	66369	<input type="checkbox"/> Trak. / Erreger 741-744 // 732	IM-B1	78010	Luchstener A.	66363
<input checked="" type="checkbox"/> Alle AC; (inkl. ANA, ANB, ANK) 735 / 736 / 737 / 738 / 739	IM-FE2	94512	Frick E.	66465	<input type="checkbox"/> ANA / ANB / ANK / ANL 750 bis 752	IM-E3	78010	Harzner VC	66366
<input type="checkbox"/> Traktion 741 bis 744	IM-WT (IM-FE1)	94580	Decker F.	66366	<input type="checkbox"/> Alle AC (inkl. ANA / ANB / ANK) 734 bis 738 / 773	IM-B4	78010	Folter J.	66438
<input type="checkbox"/> Erreger 732	IM-P1 (IM-FE1)	94580	Decker F.	66366	<input type="checkbox"/> 787 bis 788 und restliche Produkte	IM-B4	78010	Folter J.	66438
<input type="checkbox"/> 787 bis 788 (inkl. alle IM-Produkte)	IM-F1	94202	Schwenberger W.	66145					
<input type="checkbox"/> Alle Produkte	IME	95280							

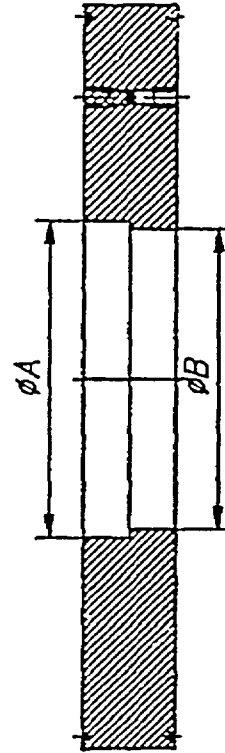
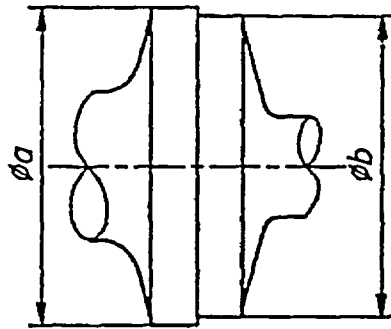
Fertigung				
Betroffene Produkte	Abteilg.	Kostenstelle	Verantwortliche	
			Verantwortlicher	Teil.Nr.
<input type="checkbox"/> Alle Produkte	IM-F10	71000	Lucht A.	66562
<input type="checkbox"/> Alle Produkte	IM-F20	72000	Wienackner H.	66005
<input type="checkbox"/> Alle Produkte	IM-F30	73000	Ehm S.	66406
<input type="checkbox"/> Alle Produkte	IM-F30	75000	Gerzer W.	66134
<input type="checkbox"/> Alle Produkte	IM-F80	76000	Verzaflo D.	66407
<input type="checkbox"/> Alle Produkte	IM-F70	77000	Schmitt B.	66057



Schwungrad montiert
dwg. HTAM 242841

Die Abmassprotokollierung erfolgt vor der
Aufschrumpfoperation.

Welle bearbeitet
dwg. HTAM 125307



Abteilung:	IMF - 760
Datum:	30.5.96
Pruefer:	Mascher

	Welle		Bohrung	
	φ a	φ b	φ A	φ B
Soll [mm]	790.680 ⁰ / _{-0.030}	750.700 ⁰ / _{-0.030}	790.000 ^{+0.050} / ₀	750.000 ^{+0.050} / ₀
nominal [°]	31.1291 ⁰ / _{-0.0012}	29.5551 ⁰ / _{-0.0012}	31.1024 ⁰ / _{-0.0020}	29.5276 ⁰ / _{-0.0020}
Ist [mm]			790,380 790,060	750,030
actual [°]				
Oberfl. Guete				

fuer dieses Dokument und den darin dargestellten Gegenstand
 behalten wir uns (i.S. Rech.-s vor. Verwirklichung, Bekanntheit an
 Dritte oder Verwertung seines Inhalts sind ohne unsere ausdrueckliche
 Zustimmung verboten. © ABB INDUSTRIE AG, Baden 1994

Rauheits-Symbole nach GZN 020007
 entsprechend DIN ISO 1302

Allgemeine Toleranzen fuer spondbare und umformende Bearbeitung
 Laengen- und Winkelmaesse "mittel" "grob"
 nach HZN 401638, DIN 7168 T.1, ISO 2768 DIN 7168 T.2...

Datum	Gezeichnet	Freig.

Erstellt:	95-12-12 Frances VF	Sep. SL gleicher Nr.	<input type="checkbox"/>
Geprueft:	95-12-12 Rieck	Sep. SL anderer Nr.	<input type="checkbox"/>
Freigegeben:	95-12-12 Seidler	Zuständige Stelle:	CHIND-IMW
Ersatz fuer:		Entstand aus:	
		MRZ:	1-364043-736-42000

Titel	Pruefprotokoll-Blatt
	Asynchronmaschine: Schwungrad
Typ:	QOVG 900 FA 6
Ident-Nr.:	HTAM431660

Maassstab	1
Sprache	D/E
Format	A4
Blatt-Nr.	1/1

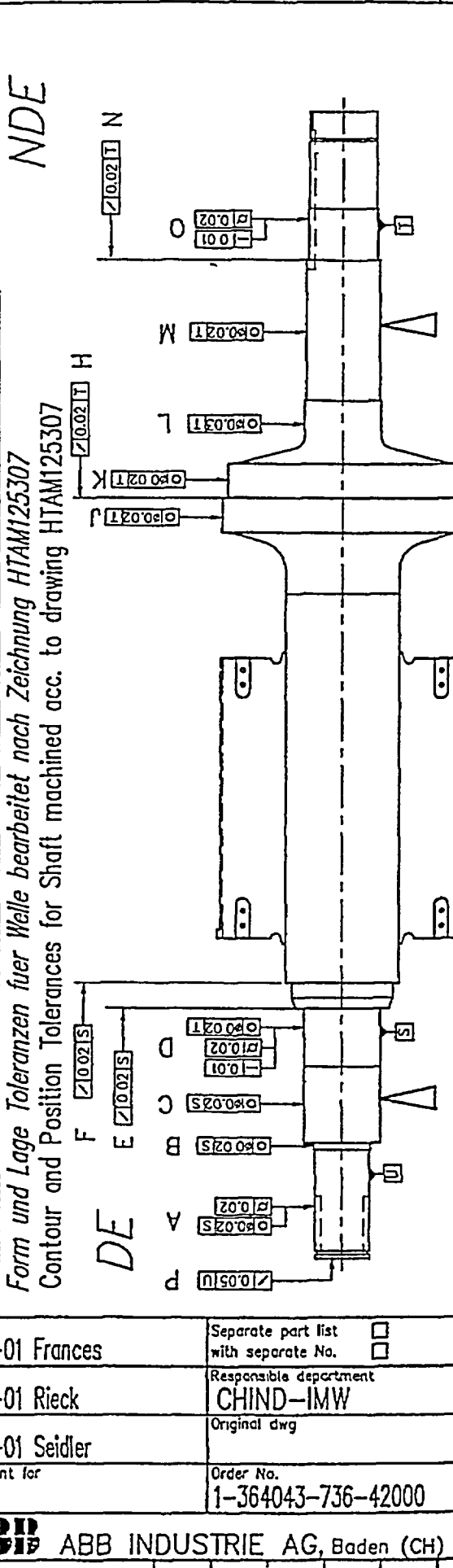
ABBIMAGE

AutoCAD

1-364 043-736-42000
 HTAM 431660

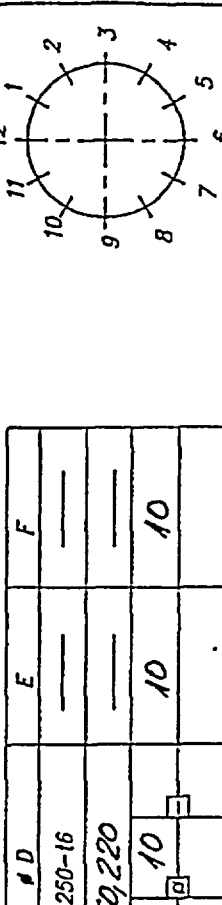
General tolerances for cutting and non-cutting machining: linear and angular dimensions ISO 2768, SADA 422, DIN 7168T.1
 "medium" "coarse" DIN 7168 T.2...
 Symbols for roughness according to ISO 1302, 9ADA 431
 We reserve all rights in this document and in the information contained therein. Reproduction, use or disclosure to third parties without express authority is strictly forbidden.
 © ABB INDUSTRIE AG, Duden 1994

Rev	Change	Date	Changed	Appr.



NDE
 Form und Lage Toleranzen fuer Welle bearbeitet nach Zeichnung HTAM125307
 Contour and Position Tolerances for Shaft machined acc. to drawing HTAM125307

DE
 F $\sqrt{0.025}$ S
 E $\sqrt{0.025}$ S
 D $\sqrt{0.025}$ S
 C $\sqrt{0.025}$ S
 B $\sqrt{0.025}$ S
 A $\sqrt{0.025}$ S
 P $\sqrt{0.05}$ U
 U
 V
 W
 X
 Y
 Z
 AA
 AB
 AC
 AD
 AE
 AF
 AG
 AH
 AI
 AJ
 AK
 AL
 AM
 AN
 AO
 AP
 AQ
 AR
 AS
 AT
 AU
 AV
 AW
 AX
 AY
 AZ
 BA
 BB
 BC
 BD
 BE
 BF
 BG
 BH
 BI
 BJ
 BK
 BL
 BM
 BN
 BO
 BP
 BQ
 BR
 BS
 BT
 BU
 BV
 BW
 BX
 BY
 BZ
 CA
 CB
 CC
 CD
 CE
 CF
 CG
 CH
 CI
 CJ
 CK
 CL
 CM
 CN
 CO
 CP
 CQ
 CR
 CS
 CT
 CU
 CV
 CW
 CX
 CY
 CZ
 DA
 DB
 DC
 DD
 DE
 DF
 DG
 DH
 DI
 DJ
 DK
 DL
 DM
 DN
 DO
 DP
 DQ
 DR
 DS
 DT
 DU
 DV
 DW
 DX
 DY
 DZ
 EA
 EB
 EC
 ED
 EE
 EF
 EG
 EH
 EI
 EJ
 EK
 EL
 EM
 EN
 EO
 EP
 EQ
 ER
 ES
 ET
 EU
 EV
 EW
 EX
 EY
 EZ
 FA
 FB
 FC
 FD
 FE
 FF
 FG
 FH
 FI
 FJ
 FK
 FL
 FM
 FN
 FO
 FP
 FQ
 FR
 FS
 FT
 FU
 FV
 FW
 FX
 FY
 FZ
 GA
 GB
 GC
 GD
 GE
 GF
 GG
 GH
 GI
 GJ
 GK
 GL
 GM
 GN
 GO
 GP
 GQ
 GR
 GS
 GT
 GU
 GV
 GW
 GX
 GY
 GZ
 HA
 HB
 HC
 HD
 HE
 HF
 HG
 HH
 HI
 HJ
 HK
 HL
 HM
 HN
 HO
 HP
 HQ
 HR
 HS
 HT
 HU
 HV
 HW
 HX
 HY
 HZ
 IA
 IB
 IC
 ID
 IE
 IF
 IG
 IH
 II
 IJ
 IK
 IL
 IM
 IN
 IO
 IP
 IQ
 IR
 IS
 IT
 IU
 IV
 IW
 IX
 IY
 IZ
 JA
 JB
 JC
 JD
 JE
 JF
 JG
 JH
 JI
 JJ
 JK
 JL
 JM
 JN
 JO
 JP
 JQ
 JR
 JS
 JT
 JU
 JV
 JW
 JX
 JY
 JZ
 KA
 KB
 KC
 KD
 KE
 KF
 KG
 KH
 KI
 KJ
 KK
 KL
 KM
 KN
 KO
 KP
 KQ
 KR
 KS
 KT
 KU
 KV
 KW
 KX
 KY
 KZ
 LA
 LB
 LC
 LD
 LE
 LF
 LG
 LH
 LI
 LJ
 LK
 LL
 LM
 LN
 LO
 LP
 LQ
 LR
 LS
 LT
 LU
 LV
 LW
 LX
 LY
 LZ
 MA
 MB
 MC
 MD
 ME
 MF
 MG
 MH
 MI
 MJ
 MK
 ML
 MN
 MO
 MP
 MQ
 MR
 MS
 MT
 MU
 MV
 MW
 MX
 MY
 MZ
 NA
 NB
 NC
 ND
 NE
 NF
 NG
 NH
 NI
 NJ
 NK
 NL
 NM
 NO
 NP
 NQ
 NR
 NS
 NT
 NU
 NV
 NW
 NX
 NY
 NZ
 OA
 OB
 OC
 OD
 OE
 OF
 OG
 OH
 OI
 OJ
 OK
 OL
 OM
 ON
 OO
 OP
 OQ
 OR
 OS
 OT
 OU
 OV
 OW
 OX
 OY
 OZ
 PA
 PB
 PC
 PD
 PE
 PF
 PG
 PH
 PI
 PJ
 PK
 PL
 PM
 PN
 PO
 PP
 PQ
 PR
 PS
 PT
 PU
 PV
 PW
 PX
 PY
 PZ
 QA
 QB
 QC
 QD
 QE
 QF
 QG
 QH
 QI
 QJ
 QK
 QL
 QM
 QN
 QO
 QP
 QQ
 QR
 QS
 QT
 QU
 QV
 QW
 QX
 QY
 QZ
 RA
 RB
 RC
 RD
 RE
 RF
 RG
 RH
 RI
 RJ
 RK
 RL
 RM
 RN
 RO
 RP
 RQ
 RR
 RS
 RT
 RU
 RV
 RW
 RX
 RY
 RZ
 SA
 SB
 SC
 SD
 SE
 SF
 SG
 SH
 SI
 SJ
 SK
 SL
 SM
 SN
 SO
 SP
 SQ
 SR
 SS
 ST
 SU
 SV
 SW
 SX
 SY
 SZ
 TA
 TB
 TC
 TD
 TE
 TF
 TG
 TH
 TI
 TJ
 TK
 TL
 TM
 TN
 TO
 TP
 TQ
 TR
 TS
 TT
 TU
 TV
 TW
 TX
 TY
 TZ
 UA
 UB
 UC
 UD
 UE
 UF
 UG
 UH
 UI
 UJ
 UK
 UL
 UM
 UN
 UO
 UP
 UQ
 UR
 US
 UT
 UU
 UV
 UW
 UX
 UY
 UZ
 VA
 VB
 VC
 VD
 VE
 VF
 VG
 VH
 VI
 VJ
 VK
 VL
 VM
 VN
 VO
 VP
 VQ
 VR
 VS
 VT
 VU
 VV
 VW
 VX
 VY
 VZ
 WA
 WB
 WC
 WD
 WE
 WF
 WG
 WH
 WI
 WJ
 WK
 WL
 WM
 WN
 WO
 WP
 WQ
 WR
 WS
 WT
 WU
 WV
 WW
 WX
 WY
 WZ
 XA
 XB
 XC
 XD
 XE
 XF
 XG
 XH
 XI
 XJ
 XK
 XL
 XM
 XN
 XO
 XP
 XQ
 XR
 XS
 XT
 XU
 XV
 XW
 XX
 XY
 XZ
 YA
 YB
 YC
 YD
 YE
 YF
 YG
 YH
 YI
 YJ
 YK
 YL
 YM
 YN
 YO
 YP
 YQ
 YR
 YS
 YT
 YU
 YV
 YW
 YX
 YZ
 ZA
 ZB
 ZC
 ZD
 ZE
 ZF
 ZG
 ZH
 ZI
 ZJ
 ZK
 ZL
 ZM
 ZN
 ZO
 ZP
 ZQ
 ZR
 ZS
 ZT
 ZU
 ZV
 ZW
 ZX
 ZY
 ZZ



Position *
 Ansicht DE (view from DE)
 * Angabe der Positionen-Nr nur wenn Schlag > 10 µm
 (record Position-No. only if total indicator reading > 10 µm)

Department	IMF-777
Date	16.04.96
Checked	T. Adje

SOl [mm]	Nominal [mm]	Actuel [mm]	Rundlauf [µm]	Conaxiale runby [µm]	Position *
177.77 $^{+0.025}$	185-16	185,180	10	10	
	250-16	250,220	10	10	
	250-16	250,220	10	10	
	250-16	250,220	10	10	

SOl [mm]	Nominal [mm]	Actuel [mm]	Rundlauf [µm]	Conaxiale runby [µm]	Position *
790.68 $^{+0.03}$	750.70 $^{+0.03}$	750,690	10	10	
790,670	750,030	750,100	10	10	
20	10	10	10	10	
2	4	4	4	4	

Prepared 95-12-01 Frances	Separate part list with separate No. <input type="checkbox"/>
Reviewed 95-12-01 Rieck	Responsible department CHIND-IMW
Approved 94-12-01 Seidler	Original dwg
Replacement for	Order No. 1-364043-736-42000

Title Pruefprotokoll-Blatt Form- & Lage- Tol. WELLE Test Certificate Contour and Position Tol. SHAFT	Scale 1
Type QOVG 900 FA 6	Language D/E
Document No. HTAM431662	Size A4
Revision	Sheet 1/1

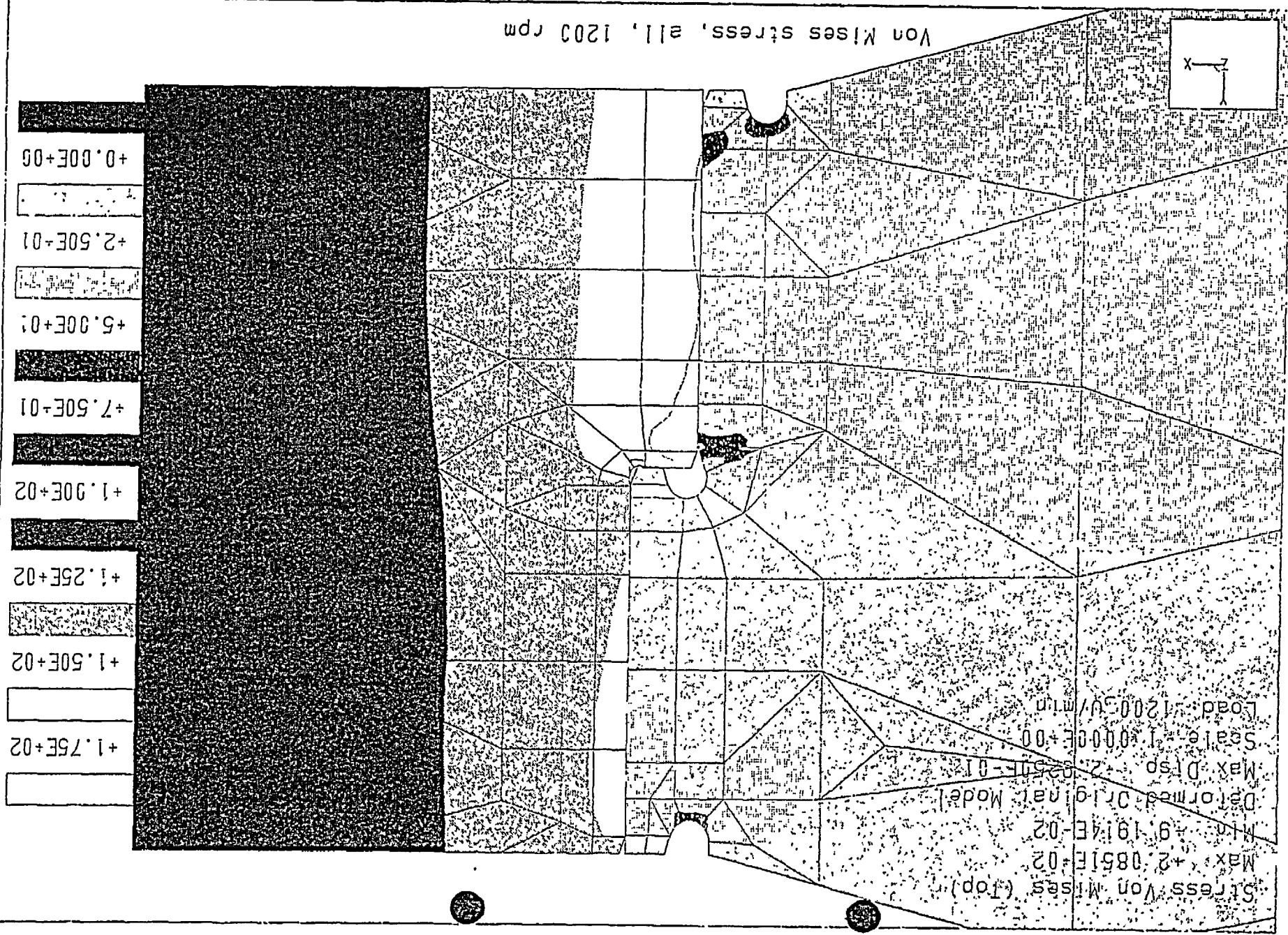
ABB INDUSTRIE AG, Baden (CH)

Attachment 2: Calculations

The results of the FE-calculation is shown on the following four pages. These plots are comparable to Fig. 6, Fig. 7, Fig. 10 and Fig. 11 in the former report.

The original document is of questionable quality but what follows is the best available image.

Color Graph

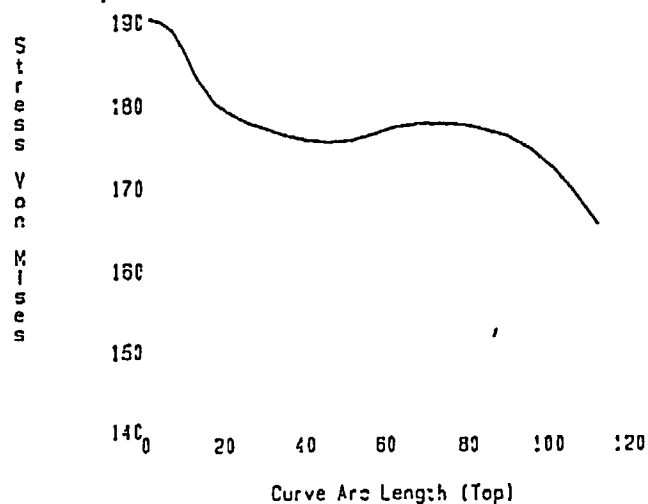


Stress Von Mises (Top)
Curves
Load: 1200_U/min



Von Mises stress, shrink fit Ø 790 mm, 1200 rpm

Stress Von Mises (Top)
Curves
Load: 1200_U/min



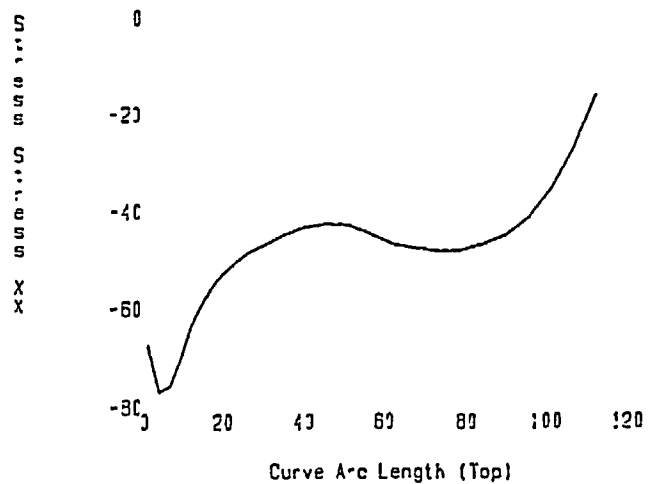
Von Mises stress, shrink fit Ø 750 mm, 1200 rpm

Stress XX (Top)
Curves
Load: 1200_U/min



radial stress, shrink fit Ø 790 mm, 1200 rpm

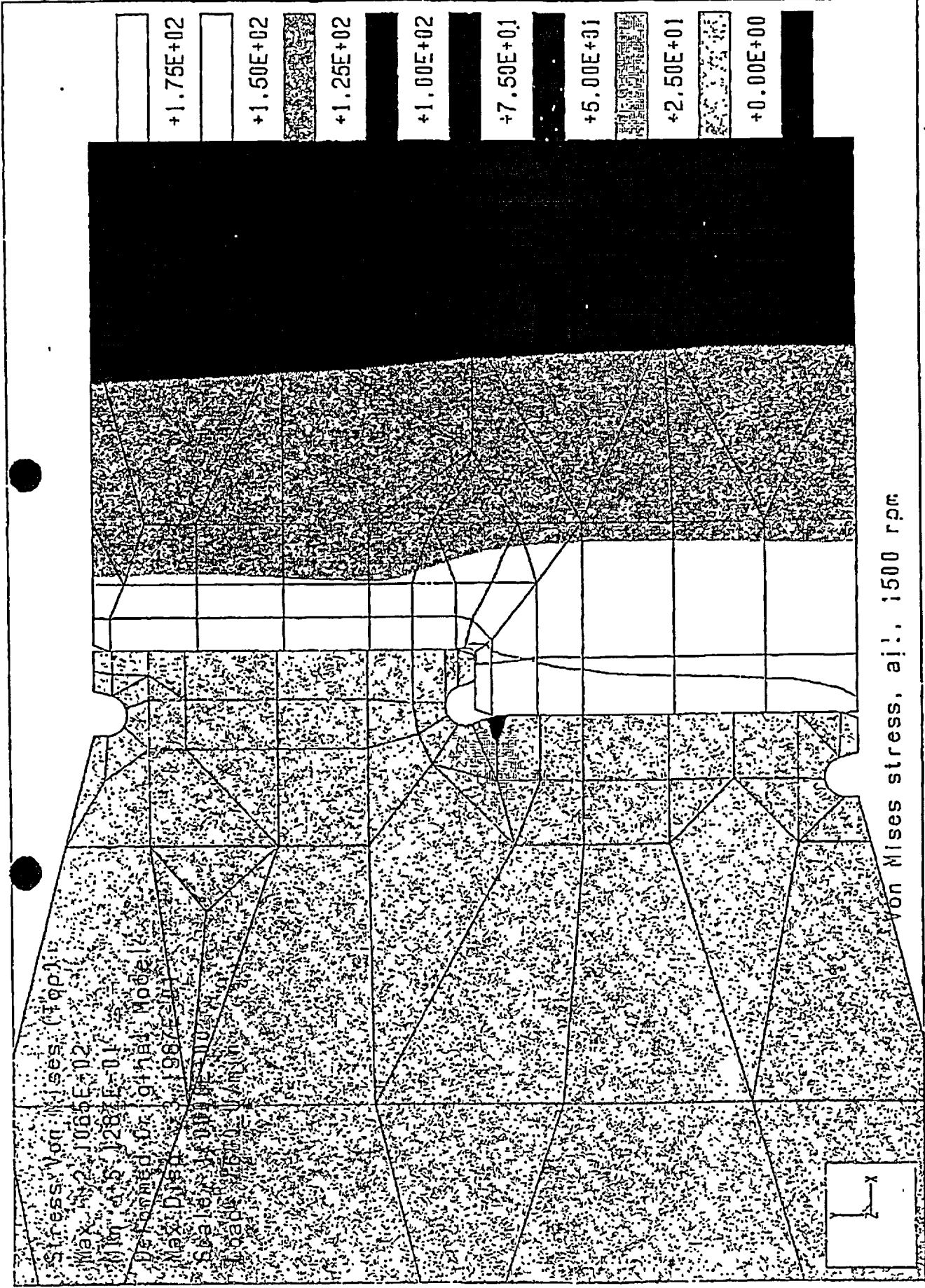
Stress XX (Top)
Curves
Load: 1200_U/min



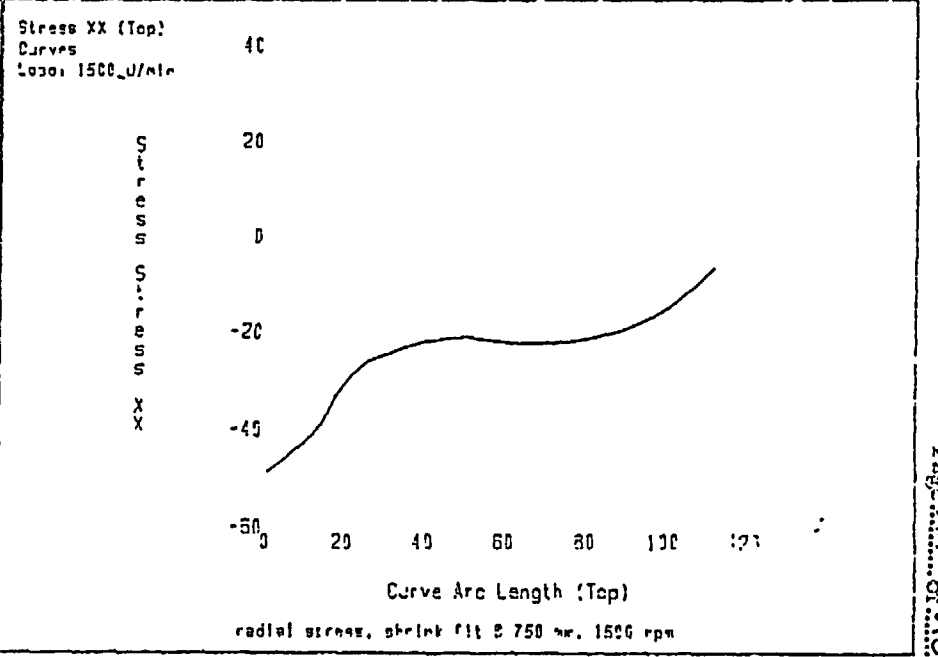
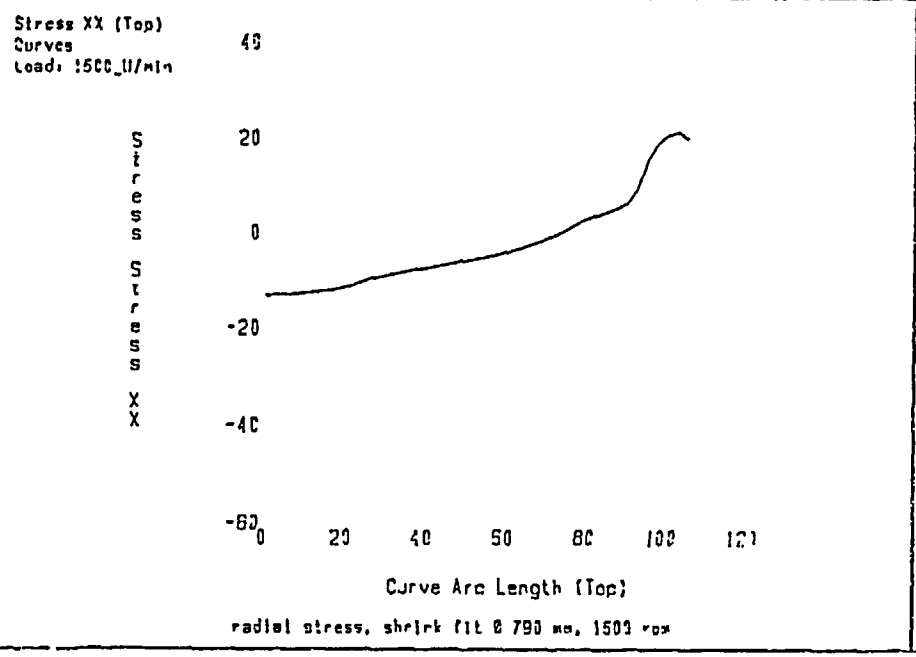
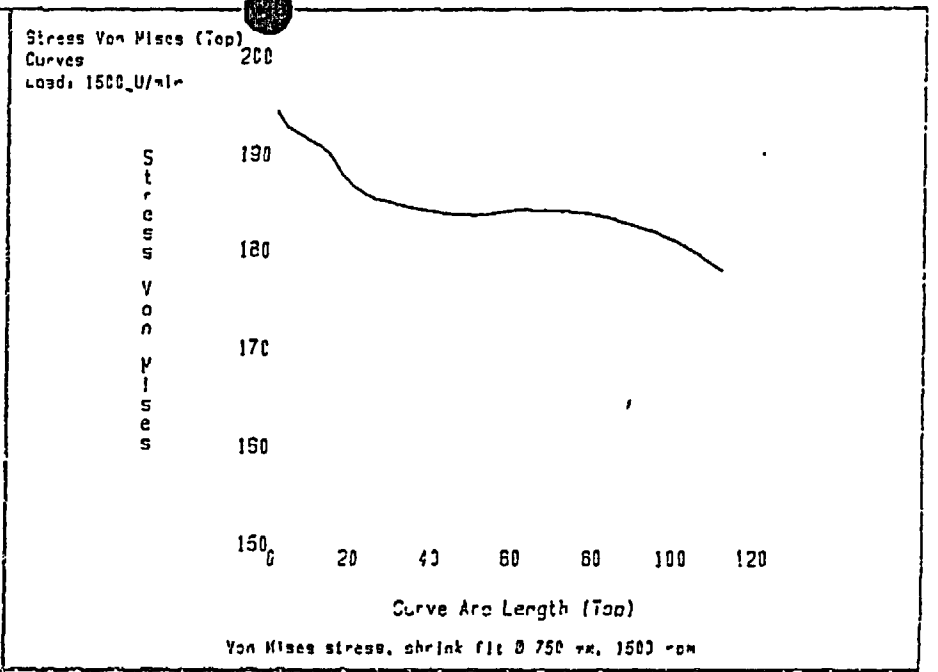
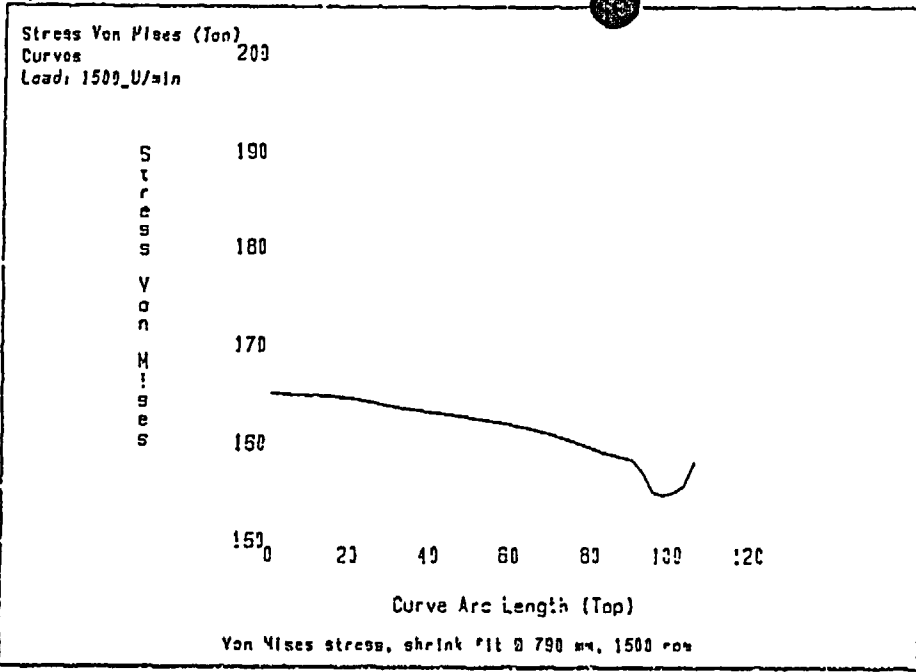
radial stress, shrink fit Ø 750 mm, 1200 rpm

The original document is of questionable quality but what follows is the best available image.

Color Graph



+1.75E+02
 +1.50E+02
 +1.25E+02
 +1.00E+02
 +7.50E+01
 +5.00E+01
 +2.50E+01
 +0.00E+00



Attachment 3: Material Specification

The material specification by SIDENOR is given on the following page.

ABB Industrie AG

Telefax-Facsimile



an / to:

SIDENOR
Fabrica de Reinosa
Mr. V. Rodriguez
Paseo Alejandro Galonje, 1
39200 Reinosa-Cantabria-Espagna
Fax-No.: 0034 942 77 52 85

von / from:

Herbert Husl
Abt. / Dept. IMW
CH-5242 Birr
Switzerland
Tel. No.: +41 58 466 50 65
Fax-No.: +41 58 466 51 20

Copies to:

Anz. Seiten inkl. Deckblatt / Total no of pages incl. cover sheet
1

Ihre / Your Ref.:
38810

Project: Fort Calhoun
Subject: Flywheel

SIDENOR DIRECCION COMERCIAL	CONTROL DOCUMENTOS
	Recibido 5.7.91

Datum / Date
08.05.98

Unsere / Our Ref.:
67-50874-2

George

Dear Mr. Rodriguez,

AT. MR. HERBERT HUSL

Final Inspection

ABB is going to witness the final tests on friday, Mai 10, 1998.
The responsible person contacts you directly.

Q-Manual

We need the english Q-Manual till Mai 17, 1998.

Revised

Material (probes) for the US-Customer

Herbert Husl
080596

You have to send the probes directly to our customer OPPD.
Mr. Roller gave you the adress a View weeks ago.
Choose the most common way for sending the probes.

Material data

Please provide a.s.a.p. the measured material data as these are:
Yield point: ? RE 735 N/mm²
Tensile strength: ? RM 863 N/mm²

Please let me the answers till this evening. Thank you.

With kind regards,

Herbert Husl, Project Manager